ADVANCES IN APPLIED MECHANICS, VOLUME 33

Motions of Microscopic Surfaces in Materials

Z. SUO

Mechanical and Environmental Engineering Department,
Materials Department
University of California,
Santa Barbara, CA

I. Introduction 194

II. Interface Migration: Formulation 196
A. Nonequilibrium Thermodynamic Process 197
B. Equation of Motion When Surface Tension Is Isotropic 201
C. Weak Statement and Galerkin Method 202
D. Geometric View 204
E. Variational Principle 205
F. Triple Junction; Equilibrium or Nonequilibrium 206

III. Interface Migration Driven by Surface Tension and Phase Difference . 209
A. Spherical Particle in a Large Mass of Vapor 209
B. Anisotropic Surface Tension: Rod- or Plate-Shaped Particles 211
C. Self-Similar Profile: Thermal Grooving 212
D. Steady-State Profile 215
E. Grain-Boundary Migration in a Thin Film; Effect of Surface Evaporation 217
F. Steady-Moving Interface Driven by Surface Tension and Phase Difference 221

IV. Interface Migration in the Presence of Stress and Electric Fields 222
A. Free Energy 223
B. Ellipsoidal Transformation Particle in Infinite Matrix under Remote Loading 227
C. Growth of a Spherical Particle of Dilation 229
D. Growth of a 180° Domain in Barium Titanate 230
E. Explicit Formula for the Driving Pressure 234

V. Diffusion on Interface: Formulation 235
A. General Considerations 235
B. Differential Equations 238
C. Weak Statements 241
D. Multiple Kinetic Processes 244

0065-2165/97 $25.00

VI. Shape Change due to Surface Diffusion under Surface Tension 245
A. Rayleigh Instability 245
B. A Row of Grains—A Model with Two Degrees of Freedom 250
C. Grooving and Pitting 255
D. Grain-Boundary Migration in Thin Film; Effect of Surface Diffusion 257
E. Steady Surface Motion 259

VII. Diffusion on an Interface between Two Materials 261
A. Rigid Inclusion Moving in a Matrix 262
B. Diffusion-Controlled Interfacial Sliding 264
C. Grain-Boundary Migration in Thin Film; Effect of Inclusion 266

VIII. Surface Diffusion Driven by Surface- and Elastic-Energy Variation . . . 267
A. Instability of a Flat Surface 268
B. Pore-Shape Change 271
C. Nosing, Cusping, and Subcritical Cracking 278

IX. Electromigration on Surface 279
A. Surface Diffusion Driven by the Electron Wind 280
B. Pore Drifting in the Electron Wind 283
C. Pore Breaking Away from Trap 284
D. Transgranular Slits 286

Acknowledgments 289

References 289

I. Introduction

Soap bubbles show up in kitchens, science museums, and popular books (e.g., Isenberg, 1978). There has long been a tradition of drawing analogies between soap films and microscopic surfaces in solids. The analogy, however, can be misleading. The air pressure in each bubble is uniform and relates to the bubble volume. The shapes of an assemblage of bubbles minimize the total film area for the given volume of every bubble. The shapes change when air is blown into the bubbles or diffuses across the films.

In solids, there exist phase boundaries, grain boundaries, domain walls, and bi-material interfaces. The stress in each solid grain is usually nonuniform, and the total surface area need not be minimal for given grain volumes. In addition to surface tension, the free energy results from stress,

electric field, and composition gradient, etc. Kinetic processes include diffusion, creep, and reaction.

The motion of the microscopic surfaces affects material processing and performance. For a bulk material, an overall knowledge of the structure, such as the grain size distribution and pore volume fraction, is often adequate. For a film or a line, where the grain size is comparable to the film thickness and linewidth, an overall knowledge of structure is inadequate; for example, in submicron aluminum interconnects, the electromigration damage relates to structural details, e.g., crystalline texture, individual grain-boundary orientation (Thompson and Lloyd, 1993). In cases like this, the internal surfaces are better viewed as components of one single structure.

We can now analyze deformation in complex structures using general-purpose computer codes. It would help many technical innovations if we could do the same for the evolving structures in materials. With this in mind, this article reviews the recent development of an approach that treats surface motion in a way that resembles the finite element analysis of deformation. Attention is focused on two mass transport mechanisms: migration of, and diffusion on, an interface. Examples are also given for other mass transport mechanisms.

At the heart of the approach is a weak statement that combines the kinetic laws and the free energy variation associated with virtual surface motion. On one hand, this weak statement reproduces the differential equations of Herring (1951) and Mullins (1957). On the other hand, this weak statement forms the basis for various Galerkin-type methods. In the latter, a surface is described with a finite number of generalized coordinates, and the Galerkin procedure reduces the weak statement to a set of ordinary differential equations that evolve into the generalized coordinates.

Depending on one's purpose, one may describe a surface with either a few or many degrees of freedom. To study certain global aspects of the surface motion, one may describe the surface with a few degrees of freedom. Ideas in low-dimensional nonlinear dynamics apply. Even with a linear kinetic law, surface evolution is highly nonlinear because of large shape and topology changes. The surface may undergo instabilities and bifurcations.

Rigorously, a surface has infinitely many degrees of freedom. To resolve local details, one must describe the surface with many degrees of freedom. A systematic approach is to divide the surface into many small, but finite,

elements and follow the motion of the nodes of the elements. The Galerkin procedure gives a viscosity matrix that connects the generalized forces and the generalized velocities. The procedure is analogous to the finite element analysis of deformation.

Most sections of this article may be read independently. The main exceptions are Sections II and V, which formulate, respectively, interface migration and interface diffusion. The subjects of all sections should be clear from the Table of Contents. Free energy is used throughout the article to study isothermal processes. (An entropy-based formulation is necessary if heat transfer plays a part.) The treatment is phenomenological with few references to the underlying atomic processes. Such continuum models are indispensable because a microstructural feature often contains a huge number of atoms. Technical processes are used to motivate the discussion, but the emphasis is on basic principles and simple demonstrations. Analytical solutions of several idealized models are included; they shed light on more complex phenomena, and may also serve as benchmark problems for general-purpose codes in the future. No attempt, however, has been made to review the literature exhaustively. By focusing on the principles and demonstrations, the reader should grasp what this line of thinking has to offer, and integrate it to his or her own way of thinking.

II. Interface Migration: Formulation

This section demonstrates the basic principles by examining a classical model with very few ingredients. An interface separates either two materials, or two phases of the same atomic composition, or two grains of the same crystalline structure. The free energy that drives the interface migration has contributions from many origins. This section includes only the interface tension, and the free-energy difference between the two phases in bulk.

Many kinetic processes may determine the velocity of the interface motion. If a phase transition generates a large amount of heat, such as during freezing, heat diffusion often limits the interface velocity. If the two phases have different compositions, such as in solution precipitation, mass diffusion in the phases often limits the interface velocity. In addition to diffusing over long range, atoms must leave one phase, cross the interface, and join the other phase. This last process will be referred to as interface migration. This section analyzes the situations in which long-range heat

and mass diffusion are absent or rapid, so that the interface process limits its velocity.

This model arises from many phenomena; see Taylor *et al.* (1992) for a literature survey. The presentation here focuses on the free energy variation associated with the virtual motion of the interface, leading to a weak statement. The weak statement, much like its counterparts in continuum mechanics, is the basis for finite element methods. It has been used, for example, by Sun *et al.* (1994) to study void shape change in an elastic crystal via surface reaction, and by Cocks and Gill (1995) to study grain growth.

A. Nonequilibrium Thermodynamic Process

To be definite, here we will visualize the model in terms of one of its many applications: a solid particle in contact with its vapor. Atoms either condense from the vapor, or evaporate from the solid, both causing the interface to move. Imagine a situation in which atoms diffuse rapidly in the vapor, but react slowly on the interface, so that the vapor maintains a uniform composition and pressure. The vapor phase is in one equilibrium state, and the solid phase is in another equilibrium state. The two phases, however, are *not* in equilibrium with each other, so that one phase grows at the expense of the other. The ingredients of this nonequilibrium thermodynamic model follow.

1. *Free Energy*

Let γ be the surface tension (i.e., the free energy per area of the interface), which may depend on crystalline orientation. Let g be the difference in the free energy density of the two phases (i.e., the free energy increase associated with the condensation of unit volume of the solid). The introduction of the solid particle into the vapor changes the free energy of the entire system by

$$G = \int \gamma dA + gV. \tag{2.1}$$

The integral extends over the interface area A, and V is the volume of the solid particle. We will assume that the particle is immersed in a large mass of the vapor, so that g is constant as the reaction proceeds.

When the surface tension is isotropic (i.e., independent of crystalline orientation), $G = \gamma A + gV$. Thermodynamics requires that the reaction proceed to decrease the free energy. The surface tension is positive and therefore strives to decrease the surface area. When the solid surface is concave, such as a dent on a flat surface, γ favors condensation. When the solid surface is convex, such as a hillock on the surface, γ favors vaporization. The free energy density difference between the two phases, g, can be either positive or negative. When $g > 0$, it favors vaporization and reduces the particle volume. When $g < 0$, it favors condensation and increases the particle volume. In general, both γ and g affect interface motion.

2. *Virtual Migration and Driving Pressure*

Free energy by itself is insufficient to determine the particle shape change, because countless ways of shape change would reduce the free energy. To evolve the particle shape, the model needs more ingredients.

Figure 1 illustrates the motion of an interface by mass exchange between the solid and the vapor. A *virtual migration* of the interface is a small movement in the direction normal to the interface that need not

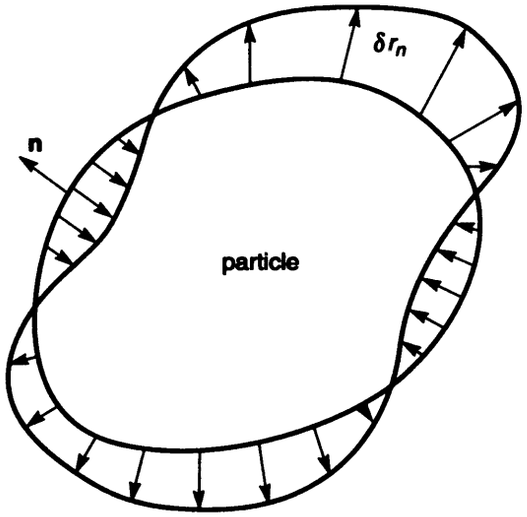

FIG. 1. An interface between a solid and a vapor undergoes a virtual motion. The magnitude of the virtual migration, δr_n, should be small, and may vary over the interface.

obey any kinetic law. The amount of the motion, δr_n, can differ from point to point over the interface. Associated with the virtual migration, the free energy varies by δG. Define a thermodynamic force, $\mathscr{P}$, as the free energy decrease associated with adding unit volume of atoms to the particle, namely,

$$\int \mathscr{P} \delta r_n \, dA = -\delta G. \tag{2.2}$$

The integral extends over the interface area. The virtual motion, δr_n, is an arbitrary function of the position on the interface, and (2.2) uniquely defines the quantity $\mathscr{P}$ at every point on the surface; an explicit formula is given later. The quantity has a unit of pressure (force/area or energy/volume), and has been variably called driving pressure, driving stress, or driving traction.

3. *Kinetic Law*

Let v_n be the *actual velocity* of the interface in the direction normal to the interface (i.e., the volume of atoms added to the particle per area per time). The actual velocity is taken to be a function of the driving pressure. Specifically, the velocity is taken to be linearly proportional to the driving pressure:

$$v_n = L\mathscr{P}. \tag{2.3}$$

Here L is the mobility of the interface. This quantity will be used as a phenomenological parameter of the model, to be determined by comparing model predictions with experimental observations. Thermodynamics requires that the interface move in the direction that reduces the free energy G, so that $L > 0$. Extension to nonlinear kinetic relations can be made (e.g., Loge and Suo, 1996).

The considerations above define the dynamics of surface motion. At a given time, the free energy variation determines the driving pressure, and the kinetic law updates the particle shape for a small time step. The process repeats for many time steps to evolve the surface.

The driving force is defined at every point on the surface, which is then used to specify the kinetic law. Such a kinetic law is local in that the rate at a point only depends on the force at this point. By no means is such a law

universally correct. For example, crystal may grow at a step around a screw dislocation. The present approach is subject to the common restriction of a continuum theory: the theory applies when the length scale of interest is much larger than the length scale characteristic of defects.

4. *Atomic Origin of Interface Migration Mobility*

Before continuing with the phenomenological treatment, we make a digression and consider briefly the atomistic origin of L. One can obtain L from an atomistic picture of the reaction process. Formulas obtained this way may give approximately correct dependence on variables such as temperature, with parameters such as activation energy fitted to experimental data.

Consider, for example, an interface of two phases of the same composition, e.g., a grain boundary. The interface moves as atoms leave one phase, cross the interface, and attach to the other phase. Turnbull (1956) showed that the interface velocity is linear in the driving pressure if $\Omega\mathscr{P} \ll kT$, where Ω is the atomic volume, k Boltzmann's constant, and T the absolute temperature. The interface motion involves the same atomic process as self-diffusion on the interface. The interface mobility L relates to the self-diffusivity on the interface D by $L = \Omega^{2/3}D/kT$. The self-diffusivity is given approximately by $D = \nu b^2 \exp(-q/kT)$, where ν is the frequency of atomic vibration, b the atomic spacing, and q the activation energy for one atom to jump from one position to another.

This connection between L and D, however, is an oversimplification. For example, impurity atoms segregated to a grain boundary can affect L and D disproportionally. This empirical fact has long been used in ceramic sintering; impurities are added to inhibit grain growth without retarding densification.

As another example, consider a single-element crystal in contact with its vapor. Atoms in the two phases exchange at the interface by evaporation and condensation. Mullins (1957) showed for this case $L = p_0\Omega^2(2\pi m)^{-1/2}(kT)^{-3/2}$, where p_0 is the vapor pressure in equilibrium with the flat solid surface, and m the mass per atom. The process considered by Mullins involves the rate of the atoms of the vapor hitting the surface, and the atoms of the solid emitting to the vapor. The reaction on the surface is instantaneous, with no activation barrier. In general, however, a multielement crystal and a vapor of several molecular species react on the interface with activation barriers.

B. Equation of Motion When Surface Tension is Isotropic

When surface tension is isotropic, the solid-vapor interface at a given time is usually a smooth surface in three dimensions. The surface has the properties commonly studied in differential geometry: the area of a surface element dA; the unit vector normal to the surface $\mathbf{n}$, taken to direct the vapor phase; and the principal radii of curvature R_1 and R_2, taken to be positive for a convex particle. Of particular interest is the sum of the principal curvatures,

$$K = \frac{1}{R_1} + \frac{1}{R_2}.$$

Associated with the virtual migration δr_n, the interface area varies by

$$\delta A = \int K \delta r_n \, dA$$

and the particle volume varies by

$$\delta V = \int \delta r_n \, dA.$$

The integrals extend over the interface.

When the surface tension is isotropic, the free energy is $G = \gamma A + gV$. Consequently, associated with the virtual motion of the surface, the free energy varies by

$$\delta G = \int (\gamma K + g) \, \delta r_n \, dA. \tag{2.4}$$

A comparison of (2.4) and (2.2) gives

$$\mathscr{P} = -\gamma K - g. \tag{2.5}$$

This equation expresses the driving pressure in terms of the geometric parameter, K, and the energetic quantities, γ and g. As expected, γ tends to drive the surface in the direction toward the center of curvature, and g tends to cause the solid to shrink if $g > 0$.

A combination of (2.3) and (2.5) leads to

$$v_n = -L(\gamma K + g). \tag{2.6}$$

This partial differential equation governs the interface motion.

Equation (2.5) contains the special case $\mathscr{P} = -\gamma K$, known as the Laplace-Young relation for liquid films (e.g., Isenberg, 1978), where $\mathscr{P}$ is the pressure difference between the two neighboring bubbles. This relation results from the equilibrium of a liquid film under the pressure difference and the surface tension. Such interpretations are misleading for a phase boundary in solid state.

C. Weak Statement and Galerkin Method

The partial differential equation (2.6) is not a good way to look at the general problem for several reasons. First, (2.6) is incorrect when surface tension is anisotropic. Second, because the problem in general has to be analyzed approximately, a partial differential equation need not be a good starting point. The following weak statement circumvents the difficulties of anisotropy, and leads to the Galerkin method in numerical analysis. Other merits of the weak statement will become evident as the subject develops.

Completely ignore Section B, and start from Section A again. Replace the driving pressure $\mathscr{P}$ in (2.2) with the interface velocity v_n by using the kinetic law (2.3), giving

$$\int \frac{v_n}{L}\,\delta r_n\,dA = -\delta G. \tag{2.7}$$

Make the following statement: the actual velocity, v_n, must satisfy (2.7) for virtual migration δr_n of *arbitrary* distribution on the interface. Following the terminology of variational calculus, we refer to this as the *weak statement* of the problem.

One may find an approximate interface velocity that satisfies (2.7) for a family of virtual motions (instead of *arbitrary* virtual motions). Obviously, the larger the family, the more accurate the approximation. This consideration leads to the Galerkin method, a formal presentation of which follows.

Model the surface with n degrees of freedom, writing $q_1, \ldots q_n$ for the generalized coordinates, and $\dot{q}_1, \ldots \dot{q}_n$ for the generalized velocities. For example, a sphere has one degree of freedom, its radius; a rod has two degrees of freedom, its radius and height; a general surface may be modeled by an assembly of triangles, with the positions of the vertexes being the generalized coordinates. Describe a surface by expressing the position vector on the surface, $\mathbf{x}$, as a function of two surface coordinates, s_1 and s_2, and the time t. Using the generalized coordinates, we express the position vector as $\mathbf{x}(s_1, s_2; q_1, \ldots, q_n)$, with the time implicitly contained in the generalized coordinates.

The free energy is a function of the generalized coordinates, $G(q_1, q_2, q_3, \ldots)$. The generalized forces, $f_1, \ldots, f_n$, are the differential coefficients of the free energy, namely

$$\delta G = -f_1\,\delta q_1 - f_2\,\delta q_2 - \cdots - f_n\,\delta q_n. \tag{2.8}$$

Once the free energy function is known, the generalized forces are calculated from $f_i = -\partial G/\partial q_i$.

The virtual motion of the surface, δr_n, is linear in the variations of the generalized coordinates:

$$\delta r_n = \sum \left(\mathbf{n} \cdot \frac{\partial \mathbf{x}}{\partial q_i}\right) \delta q_i \equiv \sum N_i \delta q_i. \tag{2.9}$$

The shape functions N_i depend on the generalized coordinates. The interface velocity is linear in the generalized velocities:

$$v_n = \sum N_i \dot{q}_i. \tag{2.10}$$

Substituting the above into the weak statement, (2.7), we obtain

$$\sum_{i,j} H_{ij}\dot{q}_j\,\delta q_i = \sum_i f_i \delta q_i, \tag{2.11}$$

where

$$H_{ij} = \int \frac{N_i N_j}{L}\,dA. \tag{2.12}$$

Equation (2.11) holds for arbitrary virtual changes δq_i, so that the coefficient for each δq_i must equal. Thus,

$$\sum_j H_{ij}\dot{q}_j = f_i. \tag{2.13}$$

Equation (2.13) is a set of linear algebraic equations for the generalized velocities. Once solved, they update the generalized coordinates for a small time step. The process is repeated for many steps to evolve into the surface. Because the matrix H and the force column f depend on the generalized coordinate column q, (2.13) is a nonlinear dynamical system.

The physical interpretation of the matrix H is evident from (2.13): the element of the matrix, H_{ij}, is the resistant force in the q_i-direction when the state moves at unit velocity in q_j-direction. We will call H the viscosity matrix. From (2.12), H depends on the generalized coordinates but is independent of the generalized velocities or the positions on the interface. The viscosity matrix is symmetric and positive-definite.

D. Geometric View

One can visualize the above formulation in geometric terms (Sun *et al.*, 1996, Yang and Suo, 1996). Imagine a hyperspace with the free energy as the vertical axis, and the generalized coordinates as the horizontal axes. The free-energy function, $G(q_1, q_2, q_3, \ldots)$, is a surface in this space, to be called the energy landscape. A point on the landscape represents in general a nonequilibrium state of the system, described with a set of values of the generalized coordinates and a value of the free energy. The bottoms of valleys on the landscape represent equilibrium states of the system.

A curve on the landscape represents an evolution path of the system. Thermodynamics requires that the system evolve to reduce the free energy, and therefore the evolution path be a descending curve on the landscape. Starting from any point other than a valley bottom on the landscape, infinite descending curves exist. Consequently, thermodynamics by itself does not set the evolution path. Nor does thermodynamics select one valley as a final equilibrium state among several valleys. The evolution path is set by thermodynamics and kinetics acting together.

At a point on the landscape, the slopes of the landscape represent the generalized forces. The Galerkin procedure assigns a viscosity matrix H at every point on the landscape. The generalized velocities are determined by $\dot{q} = H^{-1}f$, which gives the direction and magnitude of the incremental motion on the landscape. The evolution path is thus determined incrementally.

This global, geometric view does not add any new information to the problem, but does give an intuitive feel for a complex system. If the energy landscape contains several valleys, the one that will be reached by the system as the final equilibrium state will also depend on kinetics. A change in the kinetic parameters, without changing the energy landscape, may shift the system from moving to one valley to another. An example is given in Section VI.B. In the language of nonlinear dynamics, we say that the change of kinetic parameters changes the basins of attraction. Clearly, this is a universal theme of material processing.

E. Variational Principle

The following variational principle is equivalent to the weak statement in Section C. In numerical analysis, these two forms lead to an identical set of ordinary differential equations. In the remainder of the article, we will use the weak statement exclusively. The variational principle is included here for completeness.

Let $\overline{\omega}$ be a virtual interface velocity distribution, which need not satisfy any kinetic law. Associated with the virtual velocity, the free energy changes at rate $\dot{G}$. Introduce a functional

$$\Pi = \dot{G} + \int \frac{\overline{\omega}^2}{2L}\, dA, \tag{2.14}$$

which is a combination of the virtual free-energy rate and a term associated with the virtual rate. The functional is purely a mathematical construct, and has no clear physical meaning. Given an arbitrary virtual velocity distribution $\overline{\omega}$, one can compute a value of Π.

The variational principle is now stated: Of all the virtual velocity distribution $\overline{\omega}$, the actual distribution v_n minimizes Π.

The proof of the principle follows. According to (2.2), the virtual free energy rate is

$$\dot{G}(\overline{\omega}) = -\int \mathscr{P}\overline{\omega}\, dA,$$

which is linear in the virtual velocity. Consequently, the difference in Π is

$$\Pi(\overline{\omega} + v_n) - \Pi(v_n) = \dot{G}(\overline{\omega}) + \int \frac{v_n}{L}\,\overline{\omega}\, dA + \int \frac{\overline{\omega}^2}{2L}\, dA.$$

The actual velocity satisfies the kinetic relation $v_n/L = \mathscr{P}$. According to (2.2), the sum of the first two terms vanishes. Thus,

$$\Pi(\overline{\omega} + v_n) - \Pi(v_n) = \int \frac{\overline{\omega}^2}{2L}\, dA.$$

This is nonnegative for any virtual velocity distribution, hence the proof.

F. Triple Junction; Equilibrium or Nonequilibrium

1. *Force on Triple Junction*

If the solid particle is polycrystalline, the free energy becomes

$$G = \gamma_S A_S + \gamma_b A_b + gV. \tag{2.15}$$

Here γ_S is the surface tension of the solid-vapor interface, γ_b the surface tension of the grain boundaries, A_S the area of the interface, and A_b the area of the grain boundaries. For simplicity, both surface tensions are taken to be isotropic.

As an example, Figure 2 shows that a grain boundary and two surfaces form a triple junction, i.e., a line in the third dimension. The length of the junction is l, and the two surfaces meet at angle Ψ (i.e., the dihedral angle). Move the junction by δy and the surfaces by δr_n, resulting in a virtual change in the free energy, δG. Define the driving force on the triple junction, f, and the driving force on the surface, $\mathscr{P}$, simultaneously by

$$fl\delta y + \int \mathscr{P}\delta r_n \, dA = -\delta G. \tag{2.16}$$

This is an extension of (2.2).

We may postulate separate kinetic laws for the junction and surface motion:

$$\dot{y} = L_t f, \, v_n = L\mathscr{P}, \tag{2.17}$$

where $\dot{y}$ is the velocity of the triple junction, L_t the junction mobility, and L the surface mobility. Equations (2.16) and (2.17) complete the modification.

One can find an explicit expression for the force on the triple junction. When the junction moves by distance δy, the area of the grain boundary

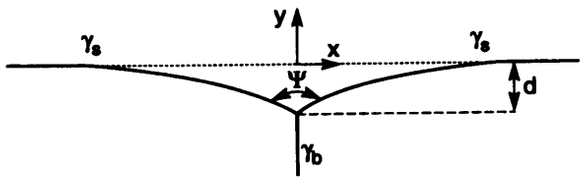

FIG. 2. A triple junction formed by a grain boundary and two free surfaces.

changes by $l\delta y$, and the area of the two surfaces changes by $-2\cos(\Psi/2)l\delta y$. Consequently, associated with the virtual motion of the junction and the surfaces, the free energy changes by

$$\delta G = \left(-2\gamma_S \cos\frac{\Psi}{2} + \gamma_b\right) l\delta y + \int (\gamma_S K + g)\, \delta r_n \, dA. \tag{2.18}$$

A comparison of (2.16) and (2.18) gives the expressions for the two driving forces:

$$f = 2\gamma_S \cos\frac{\Psi}{2} - \gamma_b, \, \mathscr{P} = -\gamma_S K - g. \tag{2.19}$$

The driving force on the junction, f, has a clear interpretation: it is the sum of the surface tensions projected along the y-axis. In this example, because of symmetry, we only need to consider the motion in the y direction. If the junction can move in both x and y directions, there are driving forces in both directions.

One can also include junction motion into the weak statement. Replace the forces in (2.16) with the velocities by using the kinetic laws (2.17), giving

$$\frac{\dot{y}}{L_t} l\delta y + \int \frac{v_n}{L} \delta r_n \, dA = -\delta G. \tag{2.20}$$

The actual velocities, $\dot{y}$ and v_n, satisfy (2.20) for arbitrary virtual motions, δy and δr_n. In this weak statement, the surface tension for both the grain boundary and the surfaces can be anisotropic, provided the free energy G is evaluated by a surface integral of the surface tension.

2. *Equilibrium Triple Junction*

The triple junction is commonly assumed to be in equilibrium at all times, even when the surfaces still move. That is, the driving forces on the triple junction vanish at all times. For the present example, setting $f = 0$ in (2.19) results in the well-known expression for the equilibrium dihedral angle Ψ_e:

$$\cos\frac{\Psi_e}{2} = \frac{\gamma_b}{2\gamma_S}. \tag{2.21}$$

This relation fixes the slope of the surfaces at the junction.

The assumption of equilibrium junction is justified by the relative rate of the junction motion and surface motion. It only takes a small number of atomic adjustments to reach the equilibrium angle, so that the time needed for the overall grain shape change is limited by the surface motion. The idea can be made definite as follows. Let d be a length scale that one likes to resolve from the model, e.g., the depth of the surface groove caused by the grain boundary underneath. The effect of the junction mobility is negligible if $L_t d/L \gg 1$.

Assume equilibrium junction is equivalent to prescribing an infinitely large junction mobility. Consequently, the first term in the weak statement (2.20) drops, which then becomes identical to (2.7). The weak statement (2.7) simultaneously determines the surface velocity and enforces the triple junction equilibrium. In applying the Galerkin procedure to the weak statement (2.7), one need not fix the dihedral angle to the equilibrium value. Rather, the equilibrium dihedral angle comes out as a part of the solution, approximately in a short time, consistent with the level of approximation of the entire surfaces.

In the terminology of variational calculus, the equilibrium dihedral angle is a *natural boundary condition*, which is enforced by the weak statement itself. The position of the end of the surface is an *essential boundary condition*, which must be enforced in addition to the weak statement.

3. *Nonequilibrium Triple Junction*

Situations exist where the junction mobility plays a role. For example, impurities segregated to the junctions may reduce the junction mobility, retarding the overall surface motion. The effect should be pronounced if the grain size is very small.

From (2.21), the junction may reach equilibrium only when $\gamma_b < 2\gamma_S$—that is, when the grain boundary is energetically more favored than two surfaces. If $\gamma_b > 2\gamma_S$, equilibrium will not be reached until the grain boundary is completely replaced by two parallel surfaces. In this case, a finite junction mobility prevents the junction from running at an infinite velocity.

Another example involves atomic decohesion along a grain boundary when the body is subject to a tensile stress normal to the grain boundary. The triple junction may be out of equilibrium, and the dihedral angle between the two free surfaces approaches 0°, instead of the equilibrium value of (2.21). The unbalanced force at the triple junction may drive a reaction that leads to the environmentally-assisted cleavage. Section VIII.C discusses a similar situation.

III. Interface Migration Driven by Surface Tension and Phase Difference

This section gives examples of interface migration under surface tension and free energy density differences between the two phases. Finite element schemes have been formulated on the basis of the weak statement (Cocks and Gill, 1995; Du *et al.*, 1996; Sun *et al.*, 1997). It is too early to judge them critically. Instead, this section gives an elementary demonstration of the Galerkin procedure, and describes several analytical solutions.

A. Spherical Particle in a Large Mass of Vapor

When a small solid particle is introduced into a large mass of a vapor, the particle may change both shape and volume, as atoms evaporate to, or condense from, the vapor. We start with the simplest situation where the surface tension is isotropic and the solid particle is spherical. The system has only one degree of freedom, the radius of the sphere.

1. *Free Energy*

The introduction of a spherical particle of radius R into a large mass of vapor changes the free energy by

$$G = 4\pi R^2\gamma + \frac{4}{3}\pi R^3 g. \tag{3.1}$$

Here γ is the surface tension, and g the free-energy density difference between the two phases; γ is always positive, but g can be either positive or negative. If $g > 0$, the volume term reduces the free energy when the particle shrinks. If $g < 0$, the volume term reduces the free energy when the particle grows. We will concentrate on the case $g < 0$. Figure 3(a) sketches the free energy as a function of the particle radius. As R increases, G first increases when the surface term in (3.1) dominates, and then decreases when the volume term dominates.

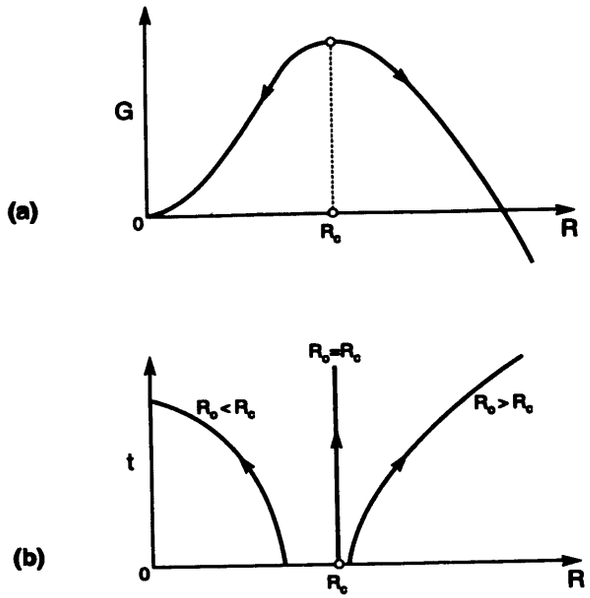

FIG. 3. A small solid particle in contact with a large mass of its vapor ($g < 0$). a) Free energy as a function of the particle radius. b) Particle of different initial radii evolve with the time.

The free energy maximizes at a finite particle radius, R_c. The significance of this maximum is readily understood. Imagine a particle of radius $R \neq R_c$. Thermodynamics requires that the particle change size to reduce G. If $R < R_c$, the particle shrinks to reduce G. If $R > R_c$, the particle grows to reduce G. The critical particle radius is determined by setting $dG/dR = 0$, giving

$$R_c = -2\frac{\gamma}{g}. \tag{3.2}$$

The two energetic parameters, γ and g, have different dimensions; their ratio defines this length.

2. *Kinetics*

Section II.B applies because the surface tension is isotropic. The driving pressure on the surface of the spherical particle of radius R is

$$\mathscr{P} = -\frac{2\gamma}{R} - g. \tag{3.3}$$

The kinetic law (2.3) relates the surface velocity to the driving pressure:

$$\frac{dR}{dt} = -L\left(\frac{2\gamma}{R} + g\right). \tag{3.4}$$

This ordinary differential equation governs the particle radius as a function of the time, $R(t)$. The energetic competition shows up again: the particle growth rate is positive if $R > -2\gamma/g$, and negative if $R < -2\gamma/g$.

Let R_0 be the particle radius at time $t = 0$. The solution to (3.4) is

$$(R - R_0) + R_c \ln\left|\frac{R - R_c}{R_0 - R_c}\right| = -Lgt. \tag{3.5}$$

Figure 3(b) sketches the radius as a function of the time. The behavior depends on the initial radius. A supercritical particle ($R_0 > R_c$) grows with the time without limit. A subcritical particle ($R_0 < R_c$) shrinks and disappears.

B. Anisotropic Surface Tension: Rod- or Plate-Shaped Particles

In the example above, the free energy alone decides whether the particle grows or shrinks, and the kinetics sets the time. This division in roles between energies and kinetics comes about because the system has only one degree of freedom. As discussed in Section II.D, when the system has more than one degree of freedom, the free energy alone does not determine the evolution path or the final equilibrium state. The following example has two degrees of freedom, and is used to illustrate the Galerkin procedure.

Imagine a crystal having anisotropic surface tension such that it grows to a prism with a square cross section. When a small particle of such a crystal is introduced into its vapor, it has two degrees of freedom: the base side B and the height C. The surface tensions on the prism bases and sides are γ_1 and γ_2, and the mobilities are L_1 and L_2. When the crystal grows by unit volume at the expense of the vapor, the phase change alone increases the free energy by g. The total free energy of the system, relative to the vapor without the particle, is

$$G(B,C) = 2\gamma_1 B^2 + 4\gamma_2 BC + gB^2C. \tag{3.6}$$

Associated with the virtual changes δB and δC, the free energy varies by

$$\delta G = (4\gamma_1 B + 4\gamma_2 C + 2gBC)\,\delta B + (4\gamma_2 B + gB^2)\,\delta C. \quad (3.7)$$

The kinetic term on the left-hand side of (2.7) is

$$\int \frac{v_n}{L}\,\delta r_n\,dA = \frac{\dot{B}BC}{L_2}\,\delta B + \frac{\dot{C}B^2}{2L_1}\,\delta C. \quad (3.8)$$

The weak statement requires that the sum of the two equations above vanish. Collect the coefficients of δB and δC, giving

$$\dot{B} = -L_2\left(\frac{4\gamma_1}{C} + \frac{4\gamma_2}{B} + 2g\right), \dot{C} = -L_1\left(\frac{8\gamma_2}{B} + 2g\right). \quad (3.9)$$

These are coupled ordinary differential equations, to be integrated numerically once the initial particle dimensions are given. No numerical results will be presented here.

Brada *et al.* (1996) have used this approach to study coarsening of grains of a crystal with high surface-tension anisotropy. See Carter *et al.* (1995) for a demonstration of the effects of surface-tension anisotropy.

C. Self-Similar Profile: Thermal Grooving

In a polycrystalline particle, a grain boundary intersects with the particle surface, forming a triple junction, Figure 2. When heated, the surface *grooves* at the triple junction. The problem was solved by Mullins (1957). The surface motion reduces the grain-boundary area but increases the surface area, so that the total free energy decreases. Mass relocates by either evaporation or surface diffusion. This section summarizes Mullins' analysis for evaporation; Section VI.C will summarize his analysis for surface diffusion. When the groove depth d is so small that $gd/\gamma \to 0$, the effect of g on grooving is negligible. Mullins assumed that $g = 0$, namely, the vapor is in equilibrium with the flat solid surface. The groove depth is taken to be much smaller than the grain size, so that the two grains in Figure 2 are infinitely large. This is a two-dimensional problem in the plane normal to the triple junction.

In Figure 2, the x-axis coincides with the surface remote from the groove, and the y-axis with the grain boundary. Describe the surface shape at time t by function $y(x,t)$. The curvature of the surface is

$$K = -\frac{\partial^2 y/\partial x^2}{\left[1 + (\partial y/\partial x)^2\right]^{3/2}}.$$

The velocity normal to the surface is

$$v_n = \frac{\partial y/\partial t}{\left[1 + (\partial y/\partial x)^2\right]^{1/2}}.$$

The equation of motion (2.6) becomes

$$\frac{\partial y}{\partial t} = L\gamma_s \frac{\partial^2 y/\partial x^2}{1 + (\partial y/\partial x)^2}. \quad (3.10)$$

The initial and boundary conditions are as follows. The surface is initially flat, i.e.

$$y(x,0) = 0. \quad (3.11)$$

The surface remote from the groove is immobile at all times:

$$y(\pm\infty, t) = 0. \quad (3.12)$$

The triple junction is taken to be in equilibrium during grooving, so that the two surfaces meet at the equilibrium dihedral angle, Ψ_e, given by (2.21). This dihedral angle fixes the slope of the surface at the triple junction:

$$\frac{\partial}{\partial x} y(0,t) = m \equiv \frac{\cos(\Psi_e/2)}{\sin(\Psi_e/2)} = \frac{\gamma_b}{(4\gamma_s^2 - \gamma_b^2)^{1/2}}. \quad (3.13)$$

The partial differential equation (3.10), the initial condition (3.11), and the boundary conditions (3.12) and (3.13) determine the evolving surface profile, $y(x,t)$.

The initial geometry has no length scale, but the time and the mobility set a length scale, $\sqrt{L\gamma_s t}$. Consequently, the groove grows with a self-similar profile. Define the dimensionless coordinates:

$$X = \frac{x}{\sqrt{L\gamma_s t}}, Y = \frac{y}{\sqrt{L\gamma_s t}}. \quad (3.14)$$

Describe the groove profile by a function $Y(X)$. The partial differential equation (3.10) becomes an ordinary differential equation

$$2\frac{d^2Y}{dX^2} + \left[1 + \left(\frac{dY}{dX}\right)^2\right]\left(X\frac{dY}{dX} - Y\right) = 0. \quad (3.15)$$

The initial condition (3.11) and the boundary condition (3.12) both become

$$Y(\infty) = 0. \quad (3.16)$$

The boundary condition (3.13) becomes

$$\frac{d}{dX} Y(0) = m. \tag{3.17}$$

The boundary-value problem (3.15)–(3.17) is integrated numerically (Sun *et al.*, 1997). Figure 4 shows the groove profile for various dihedral angles. For a system with a larger ratio γ_b/γ_s, the dihedral angle Ψ_e is smaller, and the groove is deeper.

When the ratio γ_b/γ_s is small, the slope of the surface, dY/dX, is small. Dropping the high-order term $(dY/dX)^2$ in (3.15), the ordinary differential equation is linear, so that the groove depth must be linear in m. Mullins' (1957) calculation showed that, under the small-slope approximation, the groove depth is

$$d \approx 1.13m\sqrt{L\gamma_s t}\,. \tag{3.18}$$

Figure 5 plots the numerical solutions of the groove depth determined by both the exact and the linearized equations, indicating that Mullins' linear approximation is good for most purposes. The exact nonlinear solution has been used as a benchmark to check the accuracy of a finite element code (Sun *et al.*, 1997).

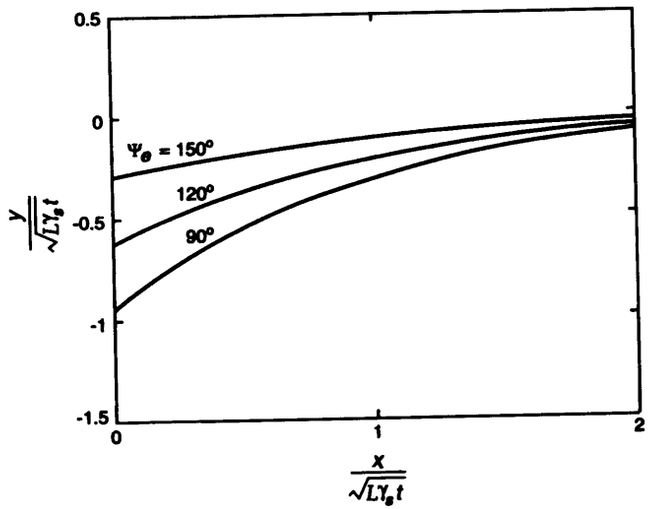

FIG. 4. The profile of the groove over a grain-boundary caused by evaporation.

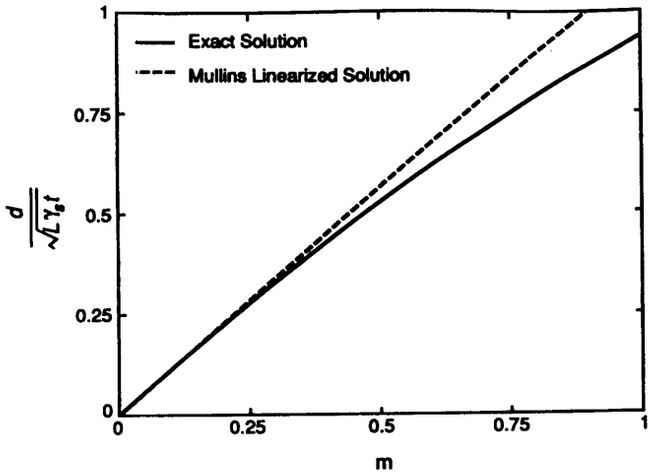

FIG. 5. The groove depth as a function of parameter m, which relates to the ratio γ_b/γ_s by (3.13).

D. Steady-State Profile

1. *General Solution*

Mullins (1956) studied the steady-state surface motion, i.e., the entire surface moves in the same direction at the same velocity. The motion is motivated by surface tension, and the mass transport mechanism is evaporation-condensation. Both the surface tension and the mobility are taken to be isotropic. The governing equation is (2.6), setting $g = 0$. Figure 6 shows a surface moves in the y-direction at velocity v. The coordinates x and y move with the surface. A plane problem is considered where the surface shape is invariant along the axis normal to the x-y plane.

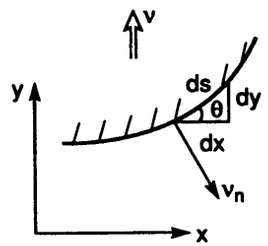

FIG. 6. Geometry of a steadily moving surface.

Let ds be the curve element, θ the angle of the element from the x-axis. Surface tension drives the surface to move toward the center of the curvature. Consequently, the surface must concave in the direction of the velocity, and the slope is restricted between $-\pi/2 \le \theta \le \pi/2$. According to our sign convention, the curvature, $K = d\theta/ds$, is positive on the entire curve, and the normal surface speed is $v_n = -v\cos\theta$. Equation (2.6) becomes

$$v\cos\theta = \frac{L\gamma d\theta}{ds}. \tag{3.19}$$

Observing that $\cos\theta\, ds = dx$, one readily integrates the above equation, giving

$$x = \frac{L\gamma}{v}\theta + x_0, \tag{3.20}$$

where x_0 is a constant to be determined by the boundary conditions. Similarly, with $\sin\theta\, ds = dy$, one integrates (3.19) and obtains

$$y = -\frac{L\gamma}{v}\ln(\cos\theta) + y_0, \tag{3.21}$$

where y_0 is another constant to be determined by the boundary conditions. Equations (3.20) and (3.21) together describe the shape of the steadily moving surface, with θ as a parameter. The following paragraphs illustrate simple applications.

2. *Steady-State Grooving*

When the groove size becomes appreciable relative to the grain size, the grooves of two adjacent grain boundaries interact, and the self-similar solution in Section III.C is no longer valid. The particle surface may recede with a profile and velocity independent of the time. Consider an idealized geometry with periodic grain boundaries of spacing D, Figure 7. The dihedral angle Ψ relates to the ratio γ_b/γ_s by (2.21). The surfaces move down to decrease the area of the grain boundaries, with no further

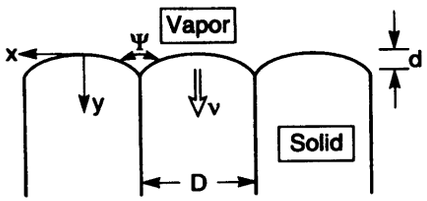

FIG. 7. Steady-state grooving over periodic grain boundaries caused by evaporation.

change in the surface area. The slopes are $\theta = \pm(\pi - \Psi)/2$ at the two adjacent triple junctions $x = \pm D/2$. With these as the boundary conditions, (3.20) determines the velocity:

$$v = (\pi - \Psi)\frac{L\gamma_s}{D}, \tag{3.22}$$

which is inversely proportional to the grain size. Equation (3.21) determines the groove depth:

$$\frac{d}{D} = -\frac{\ln\left(\sin\dfrac{\Psi}{2}\right)}{\pi - \Psi}. \tag{3.23}$$

3. *Velocity of an Abnormally Growing Grain*

Under certain conditions, in a polycrystal one grain grows much larger than the others, at the expense of the neighboring grains (Hillert, 1965). In Figure 7 replace the vapor phase with the large grain, and keep the small grains of size D. For one reason or another, the small grains do not grow, but the boundary between the large grain and the small grains moves with the mobility L_b. All the grain boundaries have the same surface tension γ_b, so that the dihedral angle is $\Psi = 2\pi/3$. Equation (3.22) becomes

$$v = \frac{\pi L_b \gamma_b}{3D}. \tag{3.24}$$

The large grain grows at a velocity inversely proportional to the size of the small grains.

E. Grain-Boundary Migration in a Thin Film; Effect of Surface Evaporation

Consider a polycrystalline film on a single crystal substrate. The grains have a columnar structure. Due to crystalline anisotropy, some grains have lower film-surface tension and film-substrate interface tension than other grains. When the film is heated, the grains with low combined surface and interface tensions grow at the expense of other grains. The survival grains may have (in-plane) diameters much larger than the film thickness.

For example, Thompson *et al.* (1990) studied a thin Au film on a (100) surface of NaCl substrate. When the film is deposited at room tempera-

ture, the Au grains are very small and are of several orientations. After anneal at 325°C for three hours, the grains grow and the survival grains are predominantly of (111)Au || (001)NaCl, with two in-plane orientations, $[1\bar{1}0]$Au || [110]NaCl and $[1\bar{1}0]$Au || $[1\bar{1}0]$NaCl. The two types of grains are crystallographically equivalent, and therefore have the same free energy. When the equivalent grains impinge, they stop growing. The NaCl substrate has a fourfold symmetry, and the (111) Au grains have a threefold symmetry. Minimization of the free energy in this case does not require lattice matching.

Yet another phenomenon may intervene: grooving at the intersections of the grain boundaries and the film surface may break the film. Assuming that the grain boundaries are immobile, Srolovitz and Safran (1986) and Miller *et al.* (1990) showed that the film breaks into islands if the ratio of the grain size to the film thickness exceeds a critical value. Miller *et al.* (1990) demonstrated that the prediction is consistent with the observation of a ZrO_2 film on a single crystal Al_2O_3 substrate.

Clearly the two processes—grain-boundary migration and surface grooving—compete to determine the fate of a polycrystalline film. Grain-boundary migration may lead to a large-grained, continuous film. Surface grooving may break the film into islands. Mullins (1958) analyzed the effect of grooving on grain-boundary motion, where the surface grooves via surface diffusion. He obtained a steady-state solution for a moving triple junction, but left the velocity of the motion undetermined because the grain-boundary motion was not analyzed. In simulating grain growth in thin films, Frost *et al.* (1992) modeled the effect of grooving by setting a threshold curvature in the kinetic law, below which grain boundaries remain stationary.

Brokman *et al.* (1995) analyzed a grain boundary moving in a thin sheet, including both surface diffusion and grain-boundary migration, which allow them to determine the steady-state velocity. In an independent study, Sun *et al.* (1997) analyzed a similar problem with either surface diffusion or surface evaporation. The following discussion draws on these studies, assuming surface evaporation. Surface diffusion will be discussed in Section VI.D.

1. *Grain-Boundary Motion When the Surface Remains Flat*

First imagine that the surface of the film is immobile and remains flat as the grain boundary migrates, Figure 8(a). The in-plane grain size is much larger than the film thickness, so that we focus on one grain boundary and

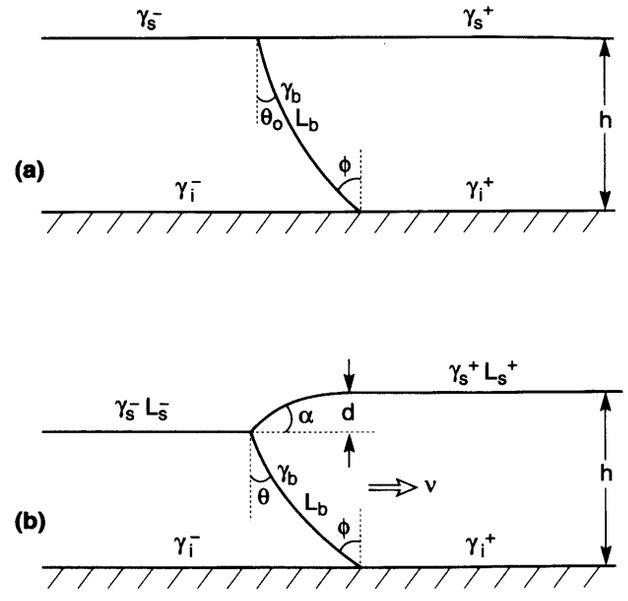

FIG. 8. A grain boundary migrates in a thin film. a) The free surface is immobile and remains flat. b) The free surface grooves due to evaporation.

ignore all the others. The two grains, labeled as + and −, have different surface tensions γ_s^+ and γ_s^-, and interface tensions γ_i^+ and γ_i^-. Denote the grain-boundary tension by γ_b, and the grain-boundary mobility by L_b. The grain boundary is taken to migrate to the right.

Because the film surface and the film-substrate interface are immobile, at the triple junctions the surface tensions do not balance in the vertical direction. Junction equilibrium in the horizontal direction determines the two angles in Figure 8(a):

$$\sin\phi = \frac{\gamma_i^+ - \gamma_i^-}{\gamma_b}, \sin\theta_0 = \frac{\gamma_s^- - \gamma_s^+}{\gamma_b}. \tag{3.25}$$

In the steady-state motion, the grain boundary is concave to the right, so that the two angles must satisfy $\phi > \theta_0$. Using (3.25), this condition becomes

$$\gamma_s^- + \gamma_i^- < \gamma_s^+ + \gamma_i^+. \tag{3.26}$$

Thus, grain − must have smaller free energy than grain + for the grain boundary to migrate to the right.

The general solution (3.20) determines the grain-boundary velocity:

$$v = \frac{L_b \gamma_b (\phi - \theta_0)}{h}. \tag{3.27}$$

In the limiting case when both ϕ and θ_0 are small, (3.25) and (3.27) give

$$v = \frac{L_b[(\gamma_i^+ + \gamma_s^+) - (\gamma_i^- + \gamma_s^-)]}{h}$$

This limiting result reproduces that of Thompson *et al.* (1990).

2. *Simultaneous Grain-Boundary Migration and Surface Evaporation*

Now two kinetic processes occur simultaneously: the grain boundary migrates at mobility L_b, and the surface evaporates at mobility L_s, Figure 8(b). Assume that the vapor is in equilibrium with a flat-film surface, but atoms at the triple junction can evaporate. The entire configuration moves at a uniform speed v to the right. All the moving surfaces must concave in the direction of the velocity. The surface of the new grain must be straight, because a curved surface would concave to the wrong direction. Evaporation causes the new grain to be thinner than the parent grain by d.

Equilibrium at the top triple junctions in both horizontal and vertical directions requires that

$$\sin\theta = \frac{(\gamma_b)^2 + (\gamma_s^-)^2 - (\gamma_s^+)^2}{2\gamma_b\gamma_s^-}, \quad \gamma_s^+ \sin\alpha = \gamma_b \cos\theta. \tag{3.28}$$

The film-substrate interface is immobile, so that the angle ϕ is the same as in (3.25). The steadily moving grain boundary must concave in the direction of the velocity. Consequently, the two angles must satisfy $\phi > \theta$, namely

$$\gamma_i^+ - \gamma_i^- > \frac{(\gamma_b)^2 + (\gamma_s^-)^2 - (\gamma_s^+)^2}{2\gamma_s^-}. \tag{3.29}$$

An application of (3.20) to the grain boundary and to the surface of grain + gives

$$v(h - d) = L_b\gamma_b(\phi - \theta), \; vd = L_s^+\gamma_s^+\alpha.$$

Solving the equations, we have the velocity

$$v = \frac{1}{h}[L_b\gamma_b(\phi - \theta) + L_s^+\gamma_s^+\alpha] \tag{3.30}$$

and the groove depth

$$\frac{d}{h} = \frac{1}{1 + \dfrac{L_b\gamma_b(\phi - \theta)}{L_s^+\gamma_s^+\alpha}}. \tag{3.31}$$

The thickness of the new grain depends, among other things, on the mobility ratio.

The effect of surface evaporation on the grain-boundary motion may be appreciated as follows. In the limiting case $L_S \ll L_b$, the groove depth is negligible compared to the film thickness (3.31). Even in this case, a tiny amount of evaporation significantly affects the grain-boundary motion by rotating the surfaces at the triple junction. Take, for example, $\gamma_s^+ = \gamma_s^- = \gamma_b$. Without evaporation (Figure 8(a)), $\theta_0 = 0°$; the grain boundary can move steadily to the right if $\phi > 0°$, i.e., if the two grains have infinitesimal differences in the film-substrate interface tensions. With evaporation (Figure 8(b)), $\theta = 30°$; the grain boundary can move steadily to the right if $\phi > 30°$, i.e., if the two grains have a finite difference in the film-substrate interface tensions.

On the basis of the weak statement (2.7), Sun *et al.* (1997) used finite elements to simulate the non-steady motion. When $\phi > \theta$, an initial configuration quite different from the steady-state quickly settles down to the steady-state. When $\phi < \theta$, the grain boundary drags the triple junction toward the substrate, and finally breaks the film.

F. Steady-Moving Interface Driven by Surface Tension and Phase Difference

Under the small slope assumption, Brokman *et al.* (1995) gave an approximate steady-state solution for an interface driven by both surface tension and phase difference. The exact steady-state solution to the full nonlinear equation (2.6) follows. The problem has a length scale,

$$l = \gamma/g. \tag{3.32}$$

With the reference to Figure 6, $v_n = -v\cos\theta$ and $K = d\theta/ds$, (2.6) becomes

$$\frac{ds}{l} = \frac{d\theta}{c\cos\theta - 1}, \tag{3.33}$$

with the dimensionless constant being

$$c = \frac{v}{Lg}.$$

Noting that $dx = \cos ds$ and $dy = \sin\theta\, ds$, one can integrate (3.33) to give

$$\frac{x}{l} = \begin{cases} \dfrac{\theta}{c} + \dfrac{1}{c\sqrt{1-c^2}} \tan^{-1}\left(\dfrac{\sqrt{1-c^2}\sin\theta}{c-\cos\theta}\right) + \dfrac{x_0}{l}, & c^2 < 1 \\ \dfrac{\theta}{c} + \dfrac{1}{c\sqrt{c^2-1}} \tanh^{-1}\left(\dfrac{\sqrt{c^2-1}\sin\theta}{c-\cos\theta}\right) + \dfrac{x_0}{l}, & c^2 > 1 \end{cases} \tag{3.34}$$

$$\frac{y}{l} = -\frac{1}{c}\ln|c\cos\theta - 1| + \frac{y_0}{l}. \tag{3.35}$$

Here x_0 and y_0 are integration constants to be determined by boundary conditions.

IV. Interface Migration in the Presence of Stress and Electric Fields

In many material processes, elastic and electrostatic fields allow additional means of free-energy variation. For example, during a phase transition, the difference in the crystalline structures of the two phases induces a stress field (e.g., Eshelby, 1970; Abeyartne and Knowles, 1990; Lusk, 1994; Rosakis and Tsai, 1994). In a polycrystalline film, grains of different orientations have different elastic energy densities due to elastic or plastic anisotropy (e.g., Sanchez and Arzt, 1992; Floro *et al.*, 1994). In a ferroelectric crystal, domains of different polar directions have different elastic and electrostatic fields (e.g., Pompe *et al.*, 1993; Roytburd 1993; Jiang, 1994).

The main concepts in Section II.A still apply, with the modification that the free energy G includes the elastic energy and electrostatic energy. This, in turn, requires that the stress and electric fields be solved as boundary-value problems. After the fields are solved and the free energy

G computed, (2.2) defines the driving pressure on an interface, $\mathscr{P}$. The kinetic law (2.3) then updates the position of the interface.

The weak statement (2.7) still applies. A two-step finite element method would proceed as follows. At a given time, the first step solves the boundary-value problem of the stress and electric fields by using a conventional finite element code. The second step updates the interface position according to (2.13), where the driving forces on interface nodes can be calculated with a procedure described by Socrate and Parks (1993), and the viscosity matrix calculated according to (2.12). The whole procedure repeats for the next time increment. The approach would allow a relatively crude mesh to determine the elastic and electric field.

Often, the mismatch strain is too large to be accommodated elastically, and dislocations appear to partially relieve the stress. Similarly, electric charge carriers diffuse to partially accommodate the polarization mismatch. Finite element approach could also treat relaxation due to combined plastic deformation, electric conduction, and interface migration. These important effects are beyond the scope of this article and will be ignored. This section collects basic equations and gives elementary demonstrations.

A. Free Energy

1. *Field Equations*

Subject a solid insulator to a field of displacement $\mathbf{u}$ and electric potential ϕ. The strain tensor $\mathbf{e}$ and the electric field vector $\mathbf{E}$ are the gradients:

$$e_{ij} = \frac{1}{2}(u_{i,j} + u_{j,i}), \quad E_i = -\phi_{,i}. \tag{4.1}$$

The conventional index notation is adopted. The insulator is separated into domains by interfaces (or domain walls). Consider an interface between two domains labeled as $+$ and $-$, with the unit vector normal to the interface, $\mathbf{n}$, pointing to domain $+$. Force $\mathbf{t}$ and charge ω are externally supplied on per unit area of the interface. The body force and the space charge inside the domains are taken to be negligible. In a domain both stress tensor σ and electric displacement vector $\mathbf{D}$ are divergence free:

$$\sigma_{ij,i} = 0, \quad D_{i,i} = 0. \tag{4.2}$$

Across the interface, they jump by

$$n_i[\sigma_{ij}^- - \sigma_{ij}^+] = t_j, \quad n_i[D_i^- - D_i^+] = -\omega. \tag{4.3}$$

Applying the divergence theorem, one obtains

$$\int t_i u_i \, dA = \int \sigma_{ij} e_{ij} \, dV, \quad \int \omega\phi \, dA = \int D_i E_i \, dV. \tag{4.4}$$

The integrals extend over the interface area A and the volume V. The equations above hold for any constitutive law.

2. *Free-Energy Density Function*

We will make the standard local equilibrium assumption: a free-energy function exists for every phase in the crystal, even though the crystal as a whole is not in equilibrium. At a fixed temperature, the Helmholtz free energy per unit volume of a phase, W, is a function of the strain and the electric displacement, $W(\mathbf{e}, \mathbf{D})$. When the state of the crystal varies, the energy density varies by

$$dW = \sigma_{ij} de_{ji} + E_i \, dD_i. \tag{4.5}$$

Once the energy density function is prescribed, the field equations and the boundary conditions define the boundary-value problem.

The crystal also stores energy in interfaces. Denote the surface energy per unit area of an interface by γ. An interface is assumed to be a sharp transition within a few atomic layers, so that electro-mechanical field is unaffected by the interface tension, and the interface tension unaffected by the electro-mechanical field.

3. *Free Energy of a Polydomain Crystal*

Prescribe a distribution of traction $\mathbf{t}$ and electric potential ϕ on the external surface of the crystal. On the part of the surface where the electric potential is not prescribed, e.g., the interface between the crystal and the air, we assume that negligible electric field lines escape from the crystal. This is a good approximation for a crystal having a large permittivity, where the prescribed electric potential does work on the crystal, not on the air.

The combination of the energy function and the field equations defines an electro-mechanical boundary-value problem. Once the field is solved, the Gibbs free energy of the entire crystal is calculated from

$$G = \int \gamma \, dA + \int W dV - \int \phi\omega \, dA - \int t_i u_i \, dA. \tag{4.6}$$

The first integral extends over the interfaces, the second over the volume of the body, the third over the potential-prescribed surface, and the fourth over the traction-prescribed surface.

4. *Deep-Well Approximation*

So far, the free-energy density W can be an arbitrary function of the electric displacements and strains. A useful approximation has often been adopted. Figure 9(a) illustrates the free-energy density for a one-dimensional model of a ferroelectric crystal at a fixed temperature. When the temperature is far below the Curie point, the free-energy density has two *deep wells* at D_s and $-D_s$, corresponding to the spontaneous polar states. Due to crystal symmetry, the spontaneous states have the same free energy, g. Figure 9(b) shows the D-E curve derived from the free energy function, $E = dW/dD$. The peak, E_c, is the field needed to switch polarization uniformly over the entire crystal, which is often much larger than the field needed to cause domain wall motion. Consequently, the state in each domain is near one of the spontaneous states, with approximately a linear D-E relation.

Consider in general a spontaneous state with the strain $\mathbf{e}^{(s)}$, the electric displacement $\mathbf{D}^{(s)}$, and the Helmholtz free energy per unit volume $g^{(s)}$. Expand the free energy density function by the Taylor series around this spontaneous state, retaining up to the quadratic terms:

$$\begin{aligned} W^{(s)} = g^{(s)} &+ \frac{1}{2} C_{ijkl}^{(s)} \left(e_{ij} - e_{ij}^{(s)}\right)(e_{kl} - e_{kl}^{(s)}) \\ &+ \frac{1}{2} \beta_{ik}^{(s)} (D_i - D_i^{(s)})(D_k - D_k^{(s)}) \\ &+ h_{ikl}^{(s)} (D_i - D_i^{(s)})(e_{kl} - e_{kl}^{(s)}) \end{aligned} \tag{4.7}$$

The first-order terms vanish because the stress and the electric field vanish at the spontaneous state. The coefficients C, β, and h characterize the elastic, dielectric, and piezoelectric responses near the spontaneous state.

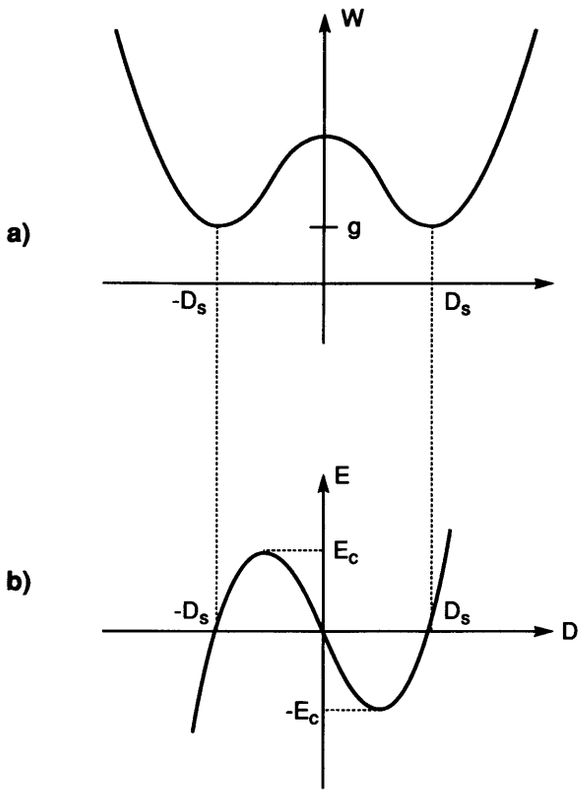

FIG. 9. a) The free-energy density as a function of the electric displacement. The free energy has deep wells when the crystal is in the ferroelastic state, far below the Curie temperature. b) The elastic field vs electric displacement curve. Only the linear parts of the curve near the spontaneous states are realized in a crystal.

The stress and the electric field are differential coefficients, (4.5), so that

$$\sigma_{ij} = C^{(s)}_{ijkl}(e_{kl} - e^{(s)}_{kl}) + h^{(s)}_{kij}(D_k - D^{(s)}_k), \tag{4.8}$$

$$E_i = \beta^{(s)}_{ik}(D_k - D^{(s)}_k) + h^{(s)}_{ikl}(e_{kl} - e^{(s)}_{kl}). \tag{4.9}$$

These linear relations are valid inside each domain. Together with the field equations, they define a linear, coupled, electro-mechanical boundary-value problem.

B. Ellipsoidal Transformation Particle in Infinite Matrix under Remote Loading

Numerical analysis is usually required to solve the boundary-value problem above. Fortunately, many analytic solutions exist for an ellipsoid inclusion in an infinite matrix subject to remote loads; see Osborn (1945) for dielectric, Eshelby (1957) for elastic, and Dunn and Wienecke (1996) for piezoelectric inclusions. The shape of ellipsoids is versatile enough to model many phenomena. A nice feature common to this class of problems is that all fields inside the ellipsoid are uniform. Here we will not list these solutions, but will discuss the calculation of the free energy. The discussion parallels that of Eshelby (1957) for an elastic inclusion.

Consider a transition from one solid phase to another. Without the constraint of the parent phase, the new phase would have a spontaneous strain $\mathbf{e}^s$, a spontaneous electric displacement $\mathbf{D}^s$, and a free energy change per volume g. All the three quantities are relative to the parent phase. When a small particle of the new phase grows inside the parent phase, both phases have stress and electric field. No dislocations, free charges, or other defects are present to relieve the field. Model the new phase particle by an ellipsoid, and denote its surface area by A and volume by V. Model the matrix as an infinite medium, and load it such that a uniform stress σ^A_{ij} and a uniform electric field E^A_i prevail far away from the particle. The free energy of the matrix in the absence of the particle, remotely loaded as described above, is the reference state. The free energy G defined by (4.6) is the sum of five contributions.

a) *Surface energy*

The phase boundary increases the free energy by

$$G_S = \int \gamma \, dA. \tag{4.10}$$

The integral extends over the ellipsoid surface. When the surface tension is isotropic, $G_S = \gamma A$. The surface energy resists particle growth.

b) *Energy due to phase difference*

When both phases are free from the stress and electric fields, the free-energy change due to the phase difference is

$$G_P = gV. \tag{4.11}$$

In our sign convention, the phase difference resists particle growth if $g > 0$.

The following three terms arise from various fields. Owing to the linearity of the problem, the free energy must be a bilinear form of the spontaneous quantities e_{ij}^s and D_i^s and the applied loads σ_{ij}^A and E_i^A. They may be grouped according to their physical significance.

c) *Work done by the applied load through spontaneous strain and electric displacement*

The work done by the applied load on the spontaneous strain and electric displacement changes the free energy by

$$G_W = -\left(\sigma_{ij}^A e_{ij}^s + E_i^A D_i^s\right)V. \tag{4.12}$$

A positive work reduces the free energy, and thereby motivates particle growth.

d) *Energy due to strain and polarization misfit*

In the absence of the applied loads, the spontaneous strain and electric displacement cause fields in the matrix and the inclusion. Let σ_{ij}^I and E_i^I be the fields in the inclusion; they are linear in e_{ij}^s and D_i^s, and various coefficients may be found in the above cited papers. The free-energy change due to the misfit is

$$G_M = -\frac{1}{2}\left(\sigma_{ij}^I e_{ij}^s + E_i^I D_i^s\right)V. \tag{4.13}$$

This contribution is a positive-definite quadratic form of e_{ij}^s and D_i^s, and resists particle growth.

e) *Energy due to heterogeneity (i.e., modulus difference)*

Imagine two infinite bodies, each subject to σ_{ij}^A and E_i^A at the infinity. One body is an infinite matrix without inclusion, and the other body is an infinite matrix containing an ellipsoidal inclusion. The constitutive laws are given by (4.8) and (4.9) with the spontaneous strain and electric displacement removed; C, β, and h are moduli for the matrix, and C^*, β^*, and h^* for the inclusion. The first body has uniform strain $\mathbf{e}$ and electric displacement $\mathbf{D}$ everywhere, and the second body has strain $\mathbf{e}^*$ and electric displacement $\mathbf{D}^*$ in the inclusion. The free-energy difference between the two bodies is

$$G_H = -\frac{1}{2}\left[(C_{ijpq} - C_{ijpq}^*)e_{ij}e_{pq}^* + (\beta_{ij} - \beta_{ij}^*)D_i D_j^* + (h_{ikl} - h_{ikl}^*)(e_{kl}D_i^* + e_{kl}^* D_i)\right]V. \tag{4.14}$$

This contribution is quadratic in σ_{ij}^A and E_i^A, and either motivates or resists particle growth, depending on the relative moduli of the two phases.

C. Growth of a Spherical Particle of Dilation

As an illustration, consider two phases of an identical chemical composition but with different crystalline structures. Without the constraint of the parent phase, the new phase would have a pure volume expansion with linear strain e_s, and a free-energy change per volume g, both being relative to the parent phase. The parent phase is loaded remotely by a hydrostatic stress σ. The electric effect is absent. We will assume that the new phase grows like a spherical particle in an infinite matrix. The system has one degree of freedom, the radius of the particle, R. Such an assumption excludes shape change, which may be important in some phenomena; for example, Johnson and Cahn (1984) showed that the spherical particle is unstable against shape change under certain conditions.

The elastic stress field for a spherical inclusion in an infinite matrix can be readily solved. For simplicity, we first assume that the two phases have similar elastic constants, with Y being Young's modulus, and ν Poisson's ratio. The free energy change due to the introduction of the particle into the matrix is

$$G(R) = 4\pi R^2\gamma + \frac{4}{3}\pi R^3\left(g - 3\sigma e_s + \frac{Ye_s^2}{1-\nu}\right). \tag{4.15}$$

The physical significance of each item is evident from the previous discussion.

The free energy has the same dependence on the radius as in the problem studied in Section III.A, so that the previous discussion applies. The driving pressure is given by

$$\mathscr{P} = -\frac{dG}{4\pi R^2\, dR} = -\frac{2\gamma}{R} - g + 3\sigma e_s - \frac{Ye_s^2}{1-\nu}. \tag{4.16}$$

The radius changes at rate

$$\frac{dR}{dt} = L\left(-\frac{2\gamma}{R} - g + 3\sigma e_s - \frac{Ye_s^2}{1-\nu}\right). \tag{4.17}$$

The solution to this ordinary differential equation is similar to (3.5).

Consider the case that the elastic constants for the two phases are different. Denote the bulk modulus and shear modulus of the parent phase by $B = Y/3(1-2\nu)$ and $\mu = Y/2(1+\nu)$, and B^* and μ^* for the corresponding quantities for the particle. The fourth term in (4.15) should be modified to

$$\frac{3e_s^2}{2}\left(\frac{1}{3B^*} + \frac{1}{4\mu}\right)^{-1}. \tag{4.18}$$

A fifth term should be added to (4.15),

$$\frac{\sigma^2}{2}\left(\frac{1}{B} - \frac{1}{B^*}\right)\left(\frac{1}{3B} + \frac{1}{4\mu}\right)\left(\frac{1}{3B^*} + \frac{1}{4\mu}\right)^{-1}. \tag{4.19}$$

This term motivates particle growth if the new phase has a lower bulk modulus than the parent phase.

D. Growth of a 180° Domain in Barium Titanate

Barium titanate ($BaTiO_3$) undergoes a phase transition at 130°C. Figure 10 shows the unit cells of the two phases. Above 130°C, the crystal is cubic, and the ions lie symmetrically in the unit cell. Between 0 and 130°C, the crystal is tetragonal, and the ions lie asymmetrically in the unit cell. We next concentrate on the changes at a fixed temperature between 0 and 130°C.

Depending on the position of the titanium ion relative to the center of the unit cell, the crystal may have polar direction of any one of the six *variants*. A load may shift the position of the titanium ion, and thereby rotate the polar axis from one direction to another. An electric field may rotate the polar direction by either 180° or 90°, but a stress may only rotate it by 90°. A 180° polar rotation does not result in any strain; a 90° polar rotation results in a strain.

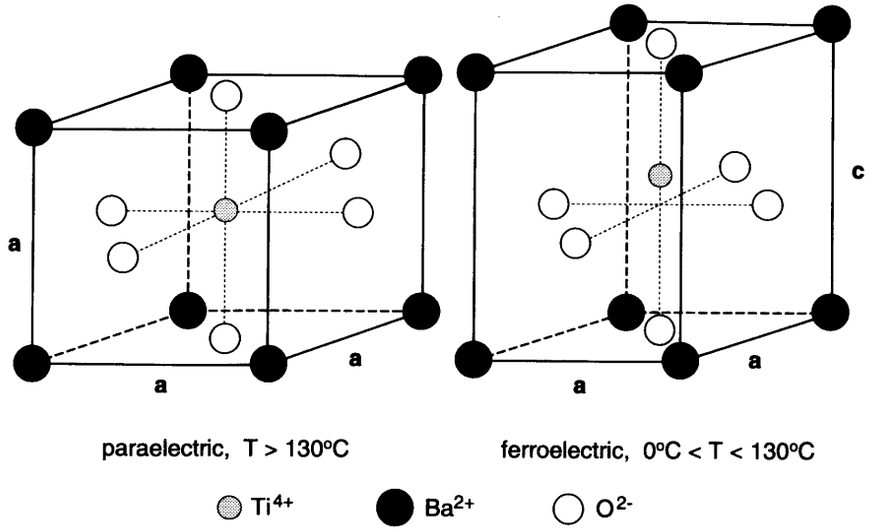

FIG. 10. The crystal structures of barium titanate ($BaTiO_3$). The high-temperature phase is nonpolar. The low-temperature phase is polar and the Ti ion is off the cell center.

The crystal changes its state by domain-wall migration. The loads needed to move the domain walls are much lower than the loads theoretically predicted to uniformly switch the crystal. In fact, the latter has never been observed. Miller and Savage (1959) observed that the domain walls in $BaTiO_3$ move at a wide range of velocities (10^{-9}–10^{-1} m/s). The new domains tend to start as spikes. In the following we review a model study of the growth of a small 180° domain, assuming that the growing domain is elliptic (Landauer, 1957; Loge and Suo, 1996). Rosakis and Jiang (1995) showed that sharp tips can emerge from the growing domain; their analysis will not be reviewed here.

Figure 11 illustrates the cross section of a cylindrical domain in a large parent domain having the opposite polarization. Because both domains have the identical spontaneous strain, the elastic and the piezoelectric effects may be ignored compared to the dielectric effects. The problem is further simplified by assuming isotropic domain wall energy, permittivity, and mobility. To avoid solving an electrostatic problem for complex-shaped inclusions, we approximate the cross section of the domain by a sequence of ellipses, evolving the domain with two generalized coordinates, the semi-axes α_1 and α_2.

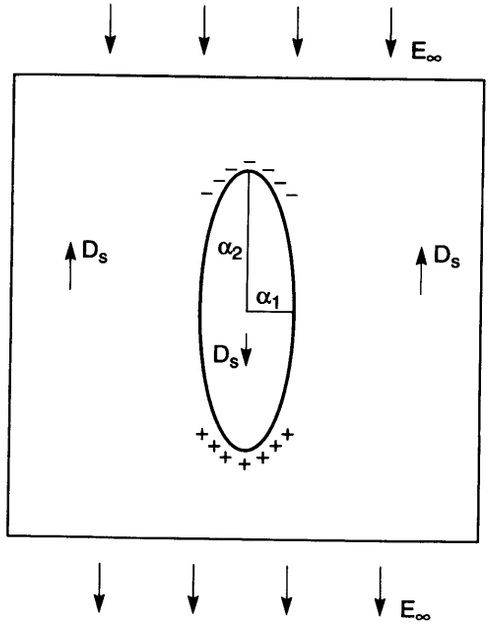

FIG. 11. A 180° domain grows in a parent phase driven by an electric field.

The free energy due to the introduction of the nucleus into the parent crystal is

$$G(\alpha_1, \alpha_2) = \gamma_S - 2D_s E_\infty \pi \alpha_1 \alpha_2 + \frac{2\pi \alpha_1^2 \alpha_2 D_s^2}{\varepsilon(\alpha_1 + \alpha_2)}. \qquad (4.20)$$

Here, s is the perimeter of the ellipse, and ε is the permittivity. The first term is the domain wall energy, which resists the growth and tends to make the domain circular. The second term is the work term associated with polarization reversal, which drives the nucleus to grow and tends to make the nucleus circular. The third term is the depolarization energy induced by the discontinuity of the spontaneous polarization, which strongly resists the growth in the α_1 direction, but weakly resists the growth in the α_2 direction.

The problem has a characteristic length, $l_0 = \gamma\varepsilon/D_s^2$, which we will use to normalize the semi-axes of the ellipse. Figure 12 shows the contours of constant levels of free energy, normalized as $G/(2\pi l_0 \gamma)$. The loading level for the simulation is $\varepsilon E_\infty / D_s = 0.05$. The free-energy surface has a saddle

point at $\alpha_1 = 13l_0$ and $\alpha_2 = 500l_0$, indicated by SP in Figure 12. The physical origin of this saddle point is evident. Along either the axis $\alpha_1 = 0$ or $\alpha_2 = 0$, when the needle-shaped domain elongates, both the work term and the depolarization energy vanish, and the domain-wall energy increases the total free energy. Along a path with a large aspect ratio α_2/α_1, the total free energy is low for both a very small and a very large nucleus, and reaches a peak for an intermediate one. The fate of a nucleus depends on its initial position on the thermodynamic surface. To decrease the free energy, a very small nucleus shrinks, and a very large nucleus grows. For a nucleus near the saddle point, its fate is determined by both the energetics and the kinetics. In all cases, the free-energy landscape alone does not determine the evolution path.

We next calculate the evolution path and rate. The differential equations (2.13) become

$$\begin{bmatrix} H_{11} & H_{12} \\ H_{21} & H_{22} \end{bmatrix} \begin{bmatrix} \dot{\alpha}_1 \\ \dot{\alpha}_2 \end{bmatrix} = \begin{bmatrix} f_1 \\ f_2 \end{bmatrix}. \qquad (4.21)$$

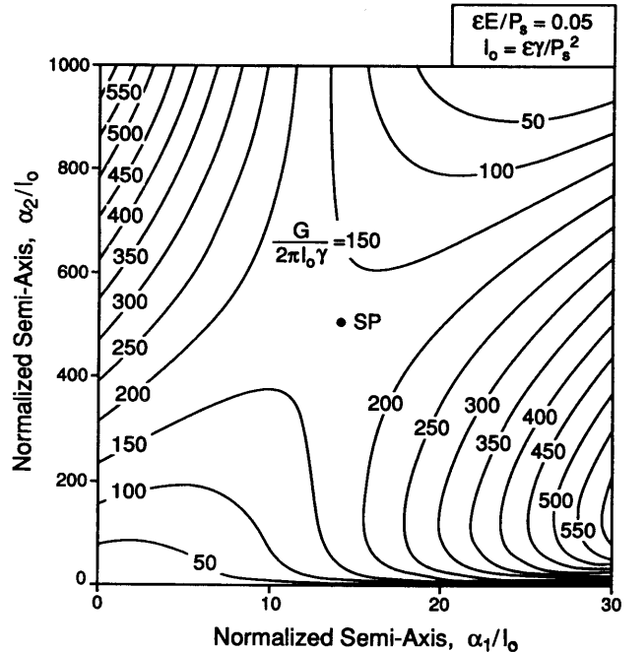

FIG. 12. Free energy contours for a 180° domain nucleus.

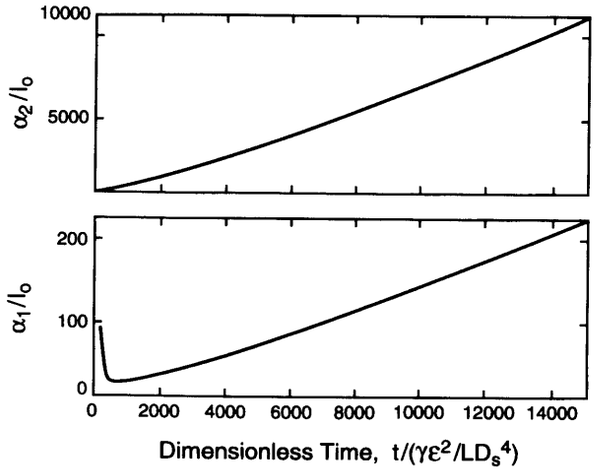

FIG. 13. The semi-axes of a 180° domain nucleus as functions of the time.

The expressions for the generalized forces and viscosities are given in Loge and Suo (1996). Given initial semi-axes of a nucleus, we trace its evolution by numerically integrating (4.31). The problem has a characteristic time, $t_0 = l_0^2/(L\gamma)$, which is used to normalize the time. Figure 13 shows the evolution of a nucleus of initial axes $\alpha_2 = 500l_0$ and $\alpha_1 = 200l_0$. The α_2-axis increases almost linearly with the time after some initial adjustment. The α_1-axis decreases first, and then increases slowly relative to the α_2-axes. The domain grows to a long needle in the direction of spontaneous polarization, because of the large effect of the depolarization energy.

E. Explicit Formula for the Driving Pressure

Eshelby (1956, 1970) called the following quantity the energy momentum tensor

$$P_{ij} = W\delta_{ij} - \sigma_{ik}e_{kj} - E_iD_j. \tag{4.22}$$

An interface separates domain + and domain −, with the unit normal vector **n** pointing toward domain +. Denote the sum of the principal curvatures of the interface by K. Assume that no external force or charge

lie on the domain wall. Eshelby showed that, when the interface moves in the direction **n** by distance δr_n, the free energy of the crystal changes by

$$\delta G = \int \left[\gamma K - n_i(P_{ij}^+ - P_{ij}^-)n_j\right] \delta r_n \, dA. \tag{4.23}$$

The interface tension γ is taken to be isotropic. A comparison of (4.23) with (2.2) gives the driving pressure on the interface

$$\mathscr{P} = -\gamma K + n_i(P_{ij}^+ - P_{ij}^-)n_j. \tag{4.24}$$

If medium − is taken to be a traction-free but strained solid, and medium + the vacuum, (4.24) becomes

$$\mathscr{P} = -\gamma K - W. \tag{4.25}$$

Asaro and Tiller (1972) obtained this formula in analyzing surface motion. The equation of motion (2.3) becomes

$$v_n = -L(\gamma K + W). \tag{4.26}$$

V. Diffusion on Interface: Formulation

This section formulates mass diffusion on an interface. The interface may be either a free surface, or a grain boundary. The diffusion species are taken to be electrically neutral, so that only mass conservation need be enforced. The free energy has the same contributions as before, e.g., surface tension, external work, and elastic energy.

A. General Considerations

1. *Virtual Motion, Mass Conservation, and Interface Motion*

Figure 14 illustrates in three dimensions a surface that represents either a free surface or a grain boundary. Denote the unit vector normal to a surface element by **n**. An arbitrary contour lies on the surface, with the curve element dl, and the unit vector in the surface and normal to the curve element **m**. At a point on the contour, **m** and **n** are perpendicular to each other, and both are perpendicular to the tangent vector of the curve at the point.

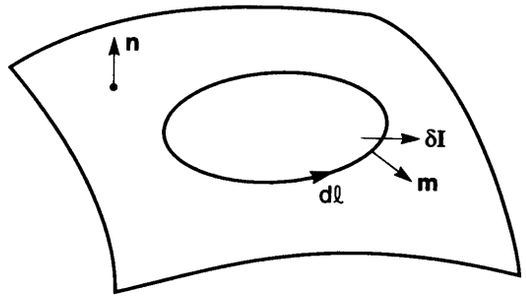

FIG. 14. An interface in the third dimension. Also drawn is an arbitrary contour lying on the interface.

Let $\delta\mathbf{I}$ be a vector field on the interface, such that $\delta\mathbf{I}\cdot\mathbf{m}$ is the number of atoms crossing unit length of the curve. As before, δ indicates a virtual motion, namely, the number of atoms is small and need not obey any kinetic law. Following Biot (1970), we refer to $\delta\mathbf{I}$ as the virtual mass displacement, to distinguish it from the atomic flux used below. Let $\delta\xi$ be the number of atoms added to the interface per unit area. Consider the interface area enclosed by the contour in Figure 14. Atoms move only on the interface, so that the number of atoms added to the area equals the number of atoms flowing in across the contour. Thus,

$$\int \delta\xi\, dA + \oint \delta\mathbf{I}\cdot\mathbf{m}\, dl = 0. \tag{5.1}$$

The first integral extends over the area of the interface enclosed by the contour, and the second over the contour. Equation (5.1) holds for any contour on the interface. Recall the surface divergence theroem, $\oint \delta\mathbf{I}\cdot\mathbf{m}\, dl = \int \nabla\cdot(\delta\mathbf{I})\, dA$, where the operator ∇ is carried on the surface. (Some writers signify the surface operator with ∇_s.) Mass conservation requirements can also be expressed in terms of the surface divergence:

$$\delta\xi + \nabla\cdot(\delta\mathbf{I}) = 0. \tag{5.2}$$

The atomic flux, $\mathbf{J}$, is a vector field on the interface, such that $\mathbf{J}\cdot\mathbf{m}$ is the number of atoms across per length per time. Let $\dot{\xi}$ be the number of atoms added to unit area of the interface in unit time. Mass conservation requires an expression similar to (5.1),

$$\int \dot{\xi}\, dA + \oint \mathbf{J}\cdot\mathbf{m}\, dl = 0, \tag{5.3}$$

and an expression similar to (5.2),

$$\dot{\xi} + \nabla\cdot\mathbf{J} = 0. \tag{5.4}$$

We next connect $\dot{\xi}$ to the motion of the free surface and the grain boundary. The expressions are similar between $\delta\xi$ and the virtual motion of the interfaces. On a *free surface*, atoms of the solid diffuse from one part of the surface to another. Atoms added to a surface element cause the element to move in the direction toward the vacuum at the velocity $v_n = \Omega\dot{\xi}$. Here Ω is the volume per atom.

A *grain boundary* is taken to be in local equilibrium. The atoms inserted to the grain boundary instantaneously crystallize, rendering the atomic structure of the grain boundary invariant. Yet the inserted atoms may add to either one of the two grains. Evidently, $\dot{\xi}$ only determines the relative motion of one grain with respect to the other, but *not* the migration of the grain boundary itself. Denote the velocity of one grain relative to another by Δv_n, being positive when the two grains recede from each other. The atoms added to a grain-boundary element cause the two grains to drift apart at velocity $\Delta v_n = \Omega\dot{\xi}$.

The migration of the grain boundary is a degree of freedom independent of the relative motion of the two grains, and should be treated by the interface migration kinetics in the previous sections. Relative sliding of the two grains are often taken to be fast; see Section VII.B. Cocks (1992) considered a locally nonequilibrium grain boundary, which will not be reviewed here.

2. *Defining Diffusion Driving Force*

Associated with the virtual motion, $\delta\mathbf{I}$ and $\delta\xi$, the free energy of the system varies by δG. Define the driving force for diffusion, $\mathbf{F}$, as the reduction of the free energy associated with one atom moving unit distance on the interface. That is,

$$\int \mathbf{F}\cdot\delta\mathbf{I}\, dA = -\delta G. \tag{5.5}$$

The integral extends over the interface. Equation (5.5) holds for arbitrary virtual motion. The force $\mathbf{F}$ is a vector on the interface, and has a unit of force/atom.

3. *Kinetic Law*

Following Herring (1951), we adopt a linear kinetic law:

$$\mathbf{J} = M\mathbf{F}. \tag{5.6}$$

This equation defines the atomic mobility on the interface, M, which is a second-order tensor at any one point on the interface, and may also vary from point to point. In this article we will assume that the mobility is independent of the crystalline direction. The mobility is determined in practice either by observing a phenomenon such as surface grooving, or by an atomistic simulation.

The mobility relates to the self-diffusivity by the Einstein relation, $M = D\delta/\Omega kT$, where D is the self-diffusivity on the interface, δ the effective thickness of atoms that participate in mass transport, Ω the volume per atom, k Boltzmann's constant, and T the absolute temperature. The self-diffusivity is approximately $D = \nu b^2 \exp(-q/kT)$, where ν is the frequency of atomic vibration, b the atomic spacing, and q the activation energy.

Atomic mobility on an interface is sensitive to impurities. When the impurity atoms segregate to the interface, the interface has a much higher impurity concentration than the bulk crystal. For example, adding a few percents of copper to aluminum substantially slows down aluminum diffusion on grain boundaries (Ames *et al.*, 1970). This empirical fact has been used to make electromigration-resistant interconnects in integrated circuits.

B. Differential Equations

The considerations above specify the surface diffusion problem. At a given time, the free-energy variation determines the driving force, the kinetic law relates the driving force to the flux, and the flux then updates the surface shape according to mass conservation. The procedure repeats for the next time increment.

These general considerations lead to two approaches for computation. One approach, due to Herring (1951), defines the chemical potential on the surface, leading to partial differential equations. This subsection lists these equations. The following subsection formulates an alternative approach on the basis of a weak statement. The two subsections can be read independently, in any order.

1. *Chemical Potential*

First consider an interface which is a closed surface in the third dimension. Herring (1951) defined the chemical potential of an interface element, μ, as the increase of the free energy associated with the addition of one atom to the element. Thus,

$$\delta G = \int \mu \, \delta\xi \, dA. \tag{5.7}$$

The integral extends over the surface. The chemical potential has a unit of energy/atom.

Using (5.6) and the divergence theorem, one obtains that

$$\begin{aligned} \delta G &= -\int \mu \nabla \cdot (\delta \mathbf{I}) \, dA \\ &= -\int [\nabla \cdot (\mu \, \delta \mathbf{I}) - (\nabla \mu) \cdot \delta \mathbf{I}] \, dA \\ &= -\oint \mu \, \delta \mathbf{I} \cdot \mathbf{m} \, dl + \int (\nabla \mu) \cdot \delta \mathbf{I} \, dA \end{aligned} \tag{5.8}$$

A closed interface does not have a boundary curve, so that the line integral vanishes.

A comparison of (5.5) and (5.8) equates the two area integrals for arbitrary distribution of $\delta\mathbf{I}$, so that the two integrands must be identical:

$$\mathbf{F} = -\nabla \mu. \tag{5.9}$$

The driving force is the negative gradient of the chemical potential. As expected, atoms diffuse from an interfacial element with high chemical potential to an interfacial element with low chemical potential.

Next consider the continuity conditions at a triple junction. As discussed in Section II.F, the local equilibrium assumption requires that the free-energy variation associated with the translation of the junction vanish. Consequently, the three interfaces meet at angles determined by the surface tensions. These considerations apply here. In addition, the local equilibrium assumption requires that the chemical potentials on the three interfaces be equal at the triple junction.

To see the last statement, consider three interfaces that meet at a straight line of length l. On the three interfaces I_1, I_2, and I_3 are the components of the $\mathbf{I}$ vector pointing to the junction. The junction is

neither a mass sink nor a mass source, so that the net mass coming to the junction vanishes, $\delta I_1 + \delta I_2 + \delta I_3 = 0$. Recall that the chemical potential is the free-energy change associated with adding one atom. The free-energy change due to the atoms moving to the triple junction is $\delta G = -l(\mu_1 \delta I_1 + \mu_2 \delta I_2 + \mu_3 \delta I_3)$. A combination of the above two equations give $\delta G = -l(\mu_1 - \mu_3)\delta I_1 - l(\mu_2 - \mu_3)\delta I_2$. The local equilibrium assumption requires that $\delta G = 0$ for any virtual mass displacements δI_1 and δI_2. Consequently, the chemical potential is continuous across the triple point, $\mu_1 = \mu_2 = \mu_3$.

2. *Free Surface*

Mass conservation relates the velocity normal to the free surface to the flux divergence:

$$v_n + \Omega \nabla \cdot \mathbf{J} = 0. \tag{5.10}$$

As stated in Section IV.E, associated with adding atoms on the interface, the free energy varies by

$$\delta G = \int (\gamma K + W)\Omega \, \delta\xi \, dA. \tag{5.11}$$

The surface tension γ is isotropic, the sum of the two-principle curvature K is positive when the surface is convex, and W includes energy density due both to stress and electric field. A comparison between (5.7) and (5.11) gives the chemical potential on the surface,

$$\mu = \Omega(\gamma K + W). \tag{5.12}$$

The diffusion driving force is

$$\mathbf{F} = -\nabla(\Omega\gamma K + \Omega W). \tag{5.13}$$

A combination of (5.6), (5.10), and (5.13) gives

$$v_n = M\Omega^2 \nabla^2(\gamma K + W). \tag{5.14}$$

This partial differential equation governs the motion of a free surface when the surface tension is isotropic.

3. *Grain Boundary*

Mass conservation relates the relative velocity of the two grains to the flux divergence:

$$\Delta v_n + \Omega \nabla \cdot \mathbf{J} = 0. \tag{5.15}$$

Let σ_n be the normal stress component on the grain boundary. To insert one atom to the grain boundary, the normal stress does work, varying the free energy by

$$\delta G = -\int \sigma_n \Omega \, \delta\xi \, dA. \tag{5.16}$$

Consequently, the chemical potential is

$$\mu = -\Omega \sigma_n. \tag{5.17}$$

The driving force for diffusion on the grain boundary is

$$\mathbf{F} = \Omega \nabla \sigma_n. \tag{5.18}$$

Atoms diffuse on the grain boundary from an element of low-normal stress to an element of high-normal stress. A combination of (5.6), (5.15), and (5.18) gives

$$\Delta v_n = -M\Omega^2 \nabla^2 \sigma_n. \tag{5.19}$$

This partial differential equation governs the normal-stress distribution in the grain boundary.

C. Weak Statements

1. *Weak Statement When Interface Diffusion Is the Sole Rate Process*

Ignore Section V.B and start from Section V.A again. Consider a polycrystal particle with grain boundaries and free surfaces. We first assume that the grain boundaries do not migrate and grains are rigid, so that diffusion on interfaces is the only kinetic process. Replace the force in (5.5) with the flux using the kinetic law (5.6), giving

$$\int \frac{\mathbf{J} \cdot \delta \mathbf{I}}{M} dA = -\delta G. \tag{5.20}$$

The integral extends over all the interfaces in the system. Different interfaces, of course, may have different mobilities. The actual flux J satisfies (5.20) for all virtual motions that conserve mass, dictated by (5.1)–(5.4) on each interface and by flux continuity at every triple junction.

This formulation circumvents the differential equations in Section V.B, and the local quantities such as the chemical potential, the curvature of a free surface, and the normal stress in a grain boundary. The statement also

enforces local equilibrium at the triple junctions, namely, (a) the interfaces meet at a junction with angles determined by the surface tensions, and (b) the chemical potentials of all the interfaces are equal at the junction. Should for any reason the two types of junction mobilities be finite, one could add them to the weak statement in the manner described in Section II.F.

2. *Variational Principle*

Needleman and Rice (1980) formulated a variational principle that includes grain-boundary diffusion, and devised a finite-element method on the basis of the variational principle. Extensions have been made to analyze several phenomena involving interface diffusion (e.g., Bower and Freund, 1993, 1995; Cocks, 1994; McMeeking and Kuhn, 1992; Sofronis and McMeeking, 1994; Suo and Wang, 1994; Svoboda and Riedel, 1995). Following the steps in Section II.E, one can prove the following variational principle. Of all virtual flux $\tilde{\mathbf{J}}$ that conserves mass, the actual flux minimizes the functional

$$\Pi = \dot{G} + \int \frac{\tilde{\mathbf{J}} \cdot \tilde{\mathbf{J}}}{2M} \, dA. \tag{5.21}$$

The weak statement and the variational principle lead to identical ordinary differential equations that evolve the generalized coordinates.

3. *Galerkin Procedure*

Interface diffusion differs from interface migration in one significant way. For interface diffusion, mass conservation is expressed by partial differential equations, (5.2) and (5.4). When the shape of the surface is axisymmetric or invariant in one direction, the surface divergence involves one-dimensional differentiation, which can be integrated readily. The Galerkin method proceeds as follows. Model the surface with n degrees of freedom, writing $q_1, \ldots, q_n$ for the generalized coordinates, and $\dot{q}_1, \ldots, \dot{q}_n$ for the generalized velocities. Following the same procedure as in Section II.C to compute the generalized forces f_i, the virtual displacement of the interfaces δr_n, and the velocity of the interfaces v_n. Integrate (5.2) and (5.4), and one obtains

$$\delta I = \sum Q_i \, \delta q_i, \quad J = \sum Q_i \dot{q}_i,$$

where Q_i plays the similar role as the shape functions. The weak statement (5.20) then leads to the same equation as (2.13), with the viscosity matrix being

$$H_{ij} = \int \frac{Q_i Q_j}{M} \, dA.$$

The shape of the surface is updated as before. We will demonstrate this method in later sections.

4. *Include Mass Conservation in Weak Statement*

The procedure above, however, fails for a general surface in three dimensions, because the surface divergence in (5.2) now consists of differentiation of two surface coordinates. Consequently, one cannot integrate (5.2) to relate $\delta \mathbf{I}$ to $\delta q_2, \ldots, \delta q_n$. What happens physically is clear. When the virtual motion of the surface is prescribed, mass conservation does not fully determine the virtual mass displacement. That is, a general surface requires degrees of freedom for $\delta \mathbf{I}$, in addition to the degrees of freedom for the surface shape. The following notes may be useful in this connection.

Mass conservation is a constraint, much like incompressibility in deformation analysis. One may use one of several methods in finite element methodology to include mass conservation in the weak statement. Here we use a penalty method as an illustration. Consider a closed surface for simplicity. Allow $\delta\xi$ and $\delta \mathbf{I}$ to vary independently, and associate a driving force λ with the new degree of freedom $\delta\xi + \nabla \cdot (\delta \mathbf{I})$, writing

$$\int \mathbf{F} \cdot \delta \mathbf{I} \, dA + \int \lambda [\delta\xi + \nabla \cdot (\delta \mathbf{I})] \, dA = -\delta G. \tag{5.22}$$

The integrals extend over the closed surface. Prescribe an independent kinetic law for this new degree of freedom:

$$\dot{\xi} + \nabla \cdot \mathbf{J} = M_0 \lambda. \tag{5.23}$$

The mobility M_0 is an adjustable parameter in the finite element analysis; when M_0 is very small, mass conservation (5.4) is recovered approximately. The weak statement becomes

$$\int \frac{\mathbf{J} \cdot \delta \mathbf{I}}{M} \, dA + \int \frac{1}{M_0} \left[\dot{\xi} + \nabla \cdot \mathbf{J} \right] [\delta\xi + \nabla \cdot (\delta \mathbf{I})] \, dA = -\delta G. \tag{5.24}$$

Incidentally, one can confirm that the parameter λ has a simple physical interpretation, $\lambda = -\mu$.

D. *Multiple Kinetic Processes*

Consider a grain boundary which both migrates and acts as a diffusion path. Let δr_n be the virtual migration of the grain boundary, $\delta \mathbf{I}$ be the virtual mass displacement on the grain boundary, and δG be the free-energy variation associated with the combined virtual motion. Define the migration driving pressure $\mathscr{P}$ and the diffusion driving force $\mathbf{F}$ simultaneously by

$$\int \mathscr{P}\, \delta r_n \, dA + \int \mathbf{F} \cdot \delta \mathbf{I} \, dA = -\delta G. \tag{5.25}$$

The integrals extend over the grain-boundary area. Equation (5.25) holds for any mass-conserving virtual motion. Replacing the driving forces by the kinetic laws of the two processes, (2.3) and (5.6), we have

$$\int \frac{v_n \, \delta r_n}{L} \, dA + \int \frac{\mathbf{J} \cdot \delta \mathbf{I}}{M} \, dA = -\delta G. \tag{5.26}$$

The actual migration velocity v_n and flux J satisfy this weak statement for arbitrary mass-conserving virtual motion.

Other kinetic processes can be similarly added to the weak statement. Take, for example, a system of interfaces that move by diffusion on the interfaces, and creep in the grains. The free energy consists of the external work and various interface tensions. The problem was first treated by Needleman and Rice (1980). Denote the virtual displacement field in the grains by δu_i, and the actual velocity field in the grains by v_i. We will assume that the solid is incompressible, i.e.,

$$v_{i,i} = 0. \tag{5.27}$$

Define the stress tensor, σ_{ij}, and the diffusion driving force F_i on the same basis, namely, as the energy-conjugates of their respective kinematic quantities. Thus,

$$\int \sigma_{ij} \, \delta u_{i,j} \, dA + \int F_i \, \delta I_i \, dA = -\delta G. \tag{5.28}$$

Interface diffusion obeys the kinetic law (5.6). For this demonstration, the grains deform according to a linear creep law:

$$\sigma_{ij} = \sigma_m \, \delta_{ij} + \eta(v_{i,j} + v_{j,i}). \tag{5.29}$$

Here, σ_m is the mean stress; η is the viscosity of the material; and $\delta_{ij} = 1$ when $i = j$, $\delta_{ij} = 0$ when $i \neq j$.

Replacing the diffusion driving force with the flux by (5.6), and the stress with the velocity gradient by (5.29), we obtain

$$\int 2\eta v_{i,j} \delta u_{i,j} \, dA + \int \frac{J_i \, \delta I_i}{M} \, dA = -\delta G. \tag{5.30}$$

The actual velocity and flux satisfy this weak statement for arbitrary virtual motion.

VI. Shape Change due to Surface Diffusion under Surface Tension

This section gives examples of shape changes motivated by surface tension. Most examples invoke surface diffusion as the only mass-transport mechanism. One example involves simultaneous grain-boundary migration and surface diffusion.

A. Rayleigh Instability

Over a century ago, John William Strutt Rayleigh noted that a jet of water is unstable and breaks to droplets under the action of surface tension. Similar phenomena occur in a solid state; see Rodel and Glaeser (1990) for an experimental demonstration and literature survey. For example, at a high temperature, a crack-like pore in a solid undergoes a sequence of morphological changes until the crack breaks into many small cavities. The crack first blunts its edge, from which finger-like channels emerge, and the channels then break into small cavities. The morphological changes shorten the distance over which mass transports, and therefore accelerate the crack healing.

Assume that the surface tension is isotropic, and the free energy of the system is the surface area times the surface tension. Of all figures of the same volume, the sphere has the lowest surface area, and therefore the lowest free energy. Why, then, does a cylinder evolve into many small spheres, rather than one, single large sphere?

Consider a long cylinder of radius R. Perturb the surface along the longitudinal direction of the cylinder. It can be shown that the perturbation reduces the surface area if its wavelength exceeds $2\pi R$. Further, Srolovitz and Safran (1986) compared a row of identical spheres with the long cylinder having the same total volume, and noted that the spheres have a smaller total surface area than the cylinder if the sphere radius exceeds $3R/2$. This sphere radius corresponds to an initial perturbation wavelength of $9R/2$. From these geometric (energetic) considerations, one expects that a sequence of configurations exists, from a cylinder to a row of spheres of large enough radii, with decreasing surface areas.

But these energetic considerations do not answer the question raised above. The answer has to do with kinetics. It takes a short time for a cylinder to evolve into a row of spheres. The spheres break the mass-transport path, preventing the system from reaching the minimal energy configuration, a single, large sphere. Here we have assumed a certain kind of mass-transport mechanism, such as fluid flow or solid diffusion. If, instead, the cylinder is sealed in a small bag, it will evolve to a single, large sphere via vapor transport.

Nichols and Mullins (1965a, b) carried out a linear stability analysis of a cylinder using several mass-transport mechanisms. For surface diffusion, they showed that a perturbation of wavelength, $\lambda_m = 2\sqrt{2}\,\pi R$, amplifies most rapidly. If the initial imperfections of all wavelengths have a similar amplitude, it is reasonable to expect that the finite sphere size corresponds to wavelength λ_m.

In what follows, the Rayleigh instability is used to illustrate the application of the weak statement. Surface-tension anisotropy is also included in the end of the analysis.

1. *Free Energy*

Figure 15 illustrates a long cylinder of initial radius R with isotropic surface tension γ. Perturb the cylinder to a wavy surface of revolution

$$r(z,t) = R\left[\rho(t) + \varepsilon(t)\cos\frac{2\pi z}{\lambda}\right], \tag{6.1}$$

where r is the radius of the perturbed surface, z the axis of revolution, t the time, ρR the average radius, εR the amplitude, and λ the wavelength. If the family of the assumed virtual motion contains the exact solution, the Galerkin procedure leads to the exact solution; otherwise the

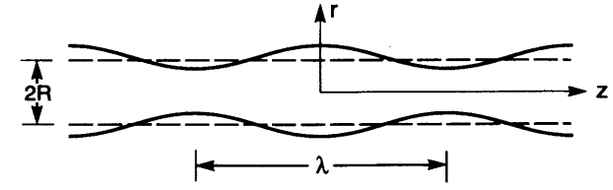

FIG. 15. Perturb a cylindrical surface to a surface of revolution with an undulation along the axial direction.

Galerkin procedure leads to an approximate solution. In this case, the family (6.1) happens to contain the exact solution of Nichols and Mullins (1965a, b).

Mass conservation requires that the volume be constant. Thus,

$$\int_0^\lambda \pi r^2\,dz = \pi R^2\lambda, \tag{6.2}$$

which, to the leading term in ε, gives $\rho = 1 - \varepsilon^2/4$. Thus, the surface profile is

$$r = R\left[1 - \frac{\varepsilon^2}{4} + \varepsilon\cos\frac{2\pi z}{\lambda}\right]. \tag{6.3}$$

The wavelength λ is fixed in the linear stability analysis, so that this model has only one generalized coordinate: the perturbation amplitude ε.

The free energy of the column is the surface tension integrated over the column surface. In one wavelength the free energy is

$$G = \int_0^\lambda 2\pi r\gamma\left[1 + (\partial r/\partial z)^2\right]^{1/2} dz, \tag{6.4}$$

and to the leading term in ε,

$$G = 2\pi R\lambda\gamma + \frac{\pi}{2}R\lambda\gamma\left[\left(\frac{2\pi R}{\lambda}\right)^2 - 1\right]\varepsilon^2. \tag{6.5}$$

If the quantity in the bracket is negative, the free energy decreases as ε increases. Consequently, the amplitude of a perturbation grows if its wavelength exceeds a critical value

$$\lambda_c = 2\pi R. \tag{6.6}$$

This reproduces the condition established by Rayleigh.

2. *Kinetics*

Because of symmetry, $J = 0$ at $z = 0$. Mass conservation relates the flux $J(z)$ to the rate of the change of the volume between 0 and z. Thus,

$$2\pi r\Omega J = -\frac{\partial}{\partial t}\int_0^z \pi r^2\, dz. \tag{6.7}$$

To the first order in the perturbation, the above is

$$J = -\frac{R\lambda}{2\pi\Omega}\sin\left(\frac{2\pi z}{\lambda}\right)\dot{\varepsilon}. \tag{6.8}$$

The weak statement (5.20) becomes

$$\dot{\varepsilon} = \frac{\varepsilon}{\tau}, \tag{6.9}$$

with the characteristic time τ being

$$\tau = \frac{R^4}{\lambda\Omega^2 M}\left[1 - \left(\frac{2\pi R}{\lambda}\right)^2\right]^{-1}\left(\frac{2\pi R}{\lambda}\right)^{-2}. \tag{6.10}$$

For the initial condition $\varepsilon = \varepsilon(0)$ at $t = 0$, the solution to (6.9) is

$$\varepsilon(t) = \varepsilon(0)\exp\left(\frac{t}{\tau}\right). \tag{6.11}$$

Figure 16 shows the trend of the characteristic time (6.10). When $\lambda < 2\pi R$, the perturbation increases the free energy, $\tau < 0$, and the perturbation

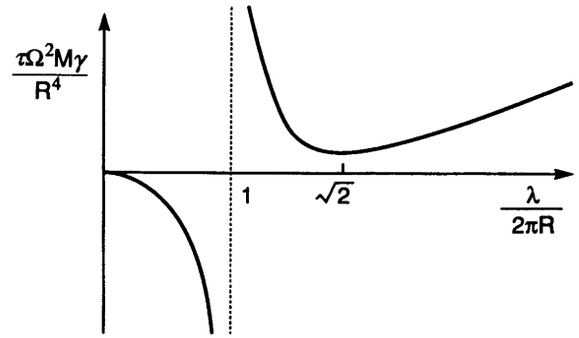

FIG. 16. The characteristic time as a function of the wavelength.

diminishes with the time. When $\lambda > 2\pi R$, the perturbation decreases the free energy, $\tau > 0$, and the perturbation amplifies with the time; τ minimizes at $\lambda_m = 2\sqrt{2}\,\pi R$, agreeing with the analysis of Nichols and Mullins (1965a, b).

The conclusion above is made on the basis of the linear stability analysis, where high-order terms of ε have been ignored. A complete simulation of the surface evolution is necessary to take into account the actual initial imperfection and large shape change (Nichols, 1976).

3. *Surface-Tension Anisotropy*

Imagine a crystal having transversely isotropic surface tension. The long cylinder of circular cross section has constant surface tension γ_0. When the cylinder becomes a surface of revolution, the surface tension is nonuniform along the longitudinal direction. Denote θ as the angle of the normal vector of an arbitary crystal plane, measured from the normal vector of the perfect cylinder. For small θ, the surface energy γ can be expanded in the powers of θ, assuming γ is a smooth function of θ. The crystal is assumed to have such a symmetry that the crystal plane at θ and the crystal plane at $-\theta$ have the identical surface energy. Consequently, the expansion only contains the even powers of θ. Take only the first two terms:

$$\gamma(\theta) = \gamma_0(1 - \alpha\theta^2). \tag{6.12}$$

Here the dimensionless number α indicates the anisotropy. When $\alpha > 0$, the crystal plane of the perfect cylinder has the largest surface tension of all the neighboring crystal planes.

Perturb the cylinder to a surface of revolution with profile (6.3). To the first order of ε,

$$\theta = -\frac{\partial r}{\partial z} = \frac{2\pi R}{\lambda}\,\varepsilon\sin\left(\frac{2\pi z}{\lambda}\right). \tag{6.13}$$

The free energy (6.4), to the leading order in ε, is

$$G = 2\pi R\lambda\gamma_0 + \frac{\pi}{2}R\lambda\gamma_0\left[(1 - 2\alpha)\left(\frac{2\pi R}{\lambda}\right)^2 - 1\right]\varepsilon^2. \tag{6.14}$$

The cylinder is unstable when the perturbation wavelength exceeds a critical value λ_c, given by

$$\left(\frac{\lambda_c}{2\pi R}\right)^2 = 1 - 2\alpha. \tag{6.15}$$

If the surface tension is very anisotropic, i.e., $\alpha > 1/2$, the cylinder is unstable for perturbations of any wavelength.

B. A Row of Grains—A Model with Two Degrees of Freedom

An important distinction exists between a system of one degree of freedom and a system of multiple degrees of freedom. For a system of one degree of freedom (e.g., the spherical particle studied in Section III.A), the free energy is a function of the generalized coordinate (i.e., the particle radius), represented by a curve in a plane with the free energy as the vertical axis and the generalized coordinate as the horizontal axis. A point on the curve represents a nonequilibrium state; a minimum point on the curve represents an equilibrium state. Energetics requires that the state descend on the curve. Consequently, energetics alone determines the final state. Kinetics is restricted to the role of determining the time needed to approach the equilibrium state.

For a system of two degrees of freedom, the free energy is a function of two generalized coordinates. This function is a surface in a three-dimensional space, with the free energy as the vertical axis, and the two generalized coordinates as horizontal axes. A point on the surface represents a nonequilibrium state in general; the bottom of a valley represents an equilibrium state. Energetics requires that an evolution path be a descending curve on the surface. There are, however, countless descending curves on a surface from any point other than a bottom of a valley. Consequently, when a system has two or more degrees of freedom, energetics by itself does not determine the evolution path. Kinetics plays a more significant role than just timekeeping.

In the analysis above of the Rayleigh instability, the system is modeled with only one degree of freedom, the amplitude of the perturbation, ε. It gives the sensible predictions when the perturbation amplitude is small, but cannot predict the spacing of the final spheres. In fact, the system has

infinitely many final equilibrium configurations, and simply cannot be modeled with one degree of freedom.

We next illustrate these general points in some detail with a row of grains (Sun *et al.*, 1996). Similar problems arise in an electrical interconnect (Srolovitz and Thompson, 1986), powder sintering (Cannon and Carter, 1989), and a fiber constrained on a substrate (Miller and Lange, 1989). Figure 17(a) illustrates a fiber of bamboo-like grain structure. The fiber consists of a row of identical grains, initially cylindrical in shape and connected at their ends, each grain being of length L_0 and diameter D_0. The grains change shape by mass diffusion on the surfaces and grain boundaries, under the action of surface and grain-boundary tensions, γ_s and γ_b. The fiber is unconstrained in the longitudinal direction. The grains are assumed to remain identical to one another (Figure 17(b)). They will evolve to either one of two equilibrium configurations: the isolated spheres (Figure 17(c)), or connected disks of truncated spheres (Figure 17(d)).

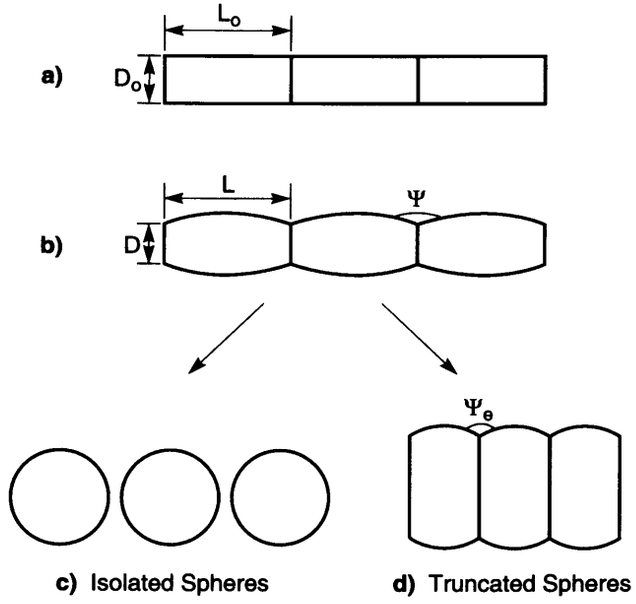

FIG. 17. (a) The initial cylinder-shaped grains. (b) Barrel-shaped grains approximate an intermediate, nonequilibrium state. (c) Grains pinch off and spheroidize, approaching an equilibrium state, a row of isolated spheres. (d) The array contracts as atoms diffuse out from the grain-boundaries and plate onto the free surfaces, approaching another equilibrium state, a touching array of truncated spheres.

The final equilibrium state is selected by an interplay between the free energy and the kinetic process. For most materials, $\gamma_b < 2\gamma_s$, and the isolated spheres in Figure 17(c) have higher free energy than the truncated spheres in Figure 17(d). For the fiber to groove along the triple junction, pinch off, and spheroidize, atoms need only diffuse on the surfaces of the grains. For the fiber to become truncated spheres, atoms must diffuse out of the grain boundaries to allow the grain length to shrink. If the atomic mobility on the grain boundary is much lower than that on the surface, $M_b \ll M_s$, which is true for many materials, the grains do not have the time to shorten significantly before they pinch off.

1. *Energy Landscape*

Approximate the shape of a nonequilibrium grain by a barrel formed by rotating a circular arc about a prescribed axis. The geometry is fully specified by three lengths: the arc radius R, the grain length L, and the grain-boundary diameter D. The volume of each grain is constant during evolution, which places a constraint. Consequently, within the approximation, the structure has only two degrees of freedom, which we chose to be the grain length L, and the dihedral angle, Ψ. Note that this approximation violates local equilibrium assumption at the triple junction.

Denote the area of the surface of a grain by A_s, and the area of a grain boundary by A_b. Consequently, the free energy per grain is

$$G = \gamma_s A_s + \gamma_b A_b . \tag{6.16}$$

When the triple junction reaches equilibrium, the dihedral angle, Ψ, reaches Ψ_e determined by (2.21). We will use Ψ_e to indicate the ratio γ_b/γ_s. The free-energy function, $G(L, \Psi)$, is computed in Miller and Lange (1989) and Sun *et al.* (1996).

Figure 18 shows the energy landscape for $L_0/D_0 = 2.5$ and $\Psi_e = 150°$. The upper-left corner terminates when the grains pinch off. Indicated on the landscape are the three special states: the initial cylinders, the isolated spheres, and the truncated spheres. From the initial state of the cylinders, the landscape descends steeply towards the minimum energy state of the truncated spheres. The landscape, however, does contain descending paths from the state of cylinders to the state of isolated spheres. Energy landscape, by itself, does not determine the evolution path.

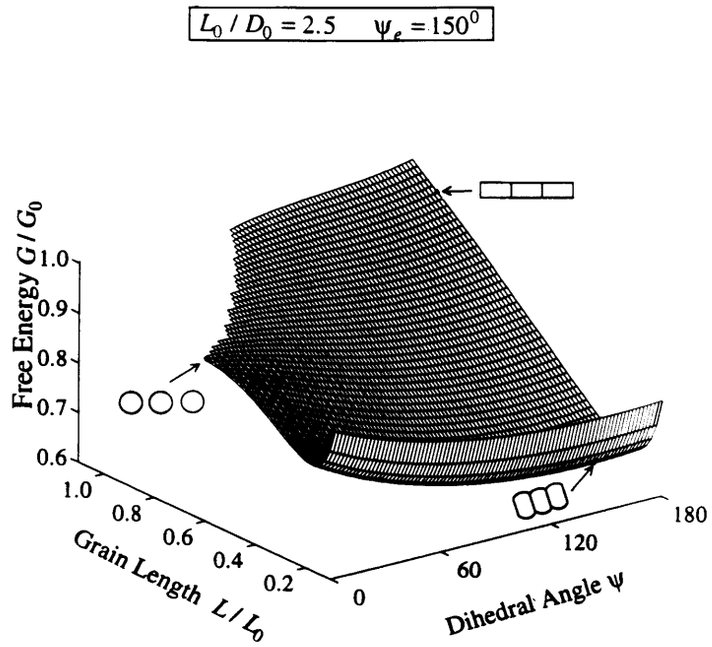

FIG. 18. Energy landscape: the free energy is a function of the generalized coordinates, the grain length and (nonequilibrium) dihedral angle. Three special states are indicated: the initial cylinders, the isolated spheres, and the truncated spheres.

2. *Evolution Path*

Denote the mobility on the grain boundary by M_b, and the mobility on the surface by M_s. The weak statement of the problem is

$$\int \frac{J_s}{M_s}\,\delta I_s dA_s + \int \frac{J_b}{M_b}\,\delta I_b dA_b = -\delta G. \tag{6.17}$$

The two integrals are over the surface and the grain boundary, respectively. Mass conservation relates the fluxes to the generalized velocities $\dot{L}$ and $\dot{\Psi}$. The Galerkin procedure leads to two ordinary differential equations that evolve the generalized coordinates, L and Ψ (Sun *et al.*, 1996).

The numerical solutions are plotted in Figure 19. The solid lines are the energy contours. After the grains pinch off, they spheroidize with only one degree of freedom, Ψ, as represented by the dashed line at the upper-left corner. The dotted lines are the evolution paths for various mobility ratios,

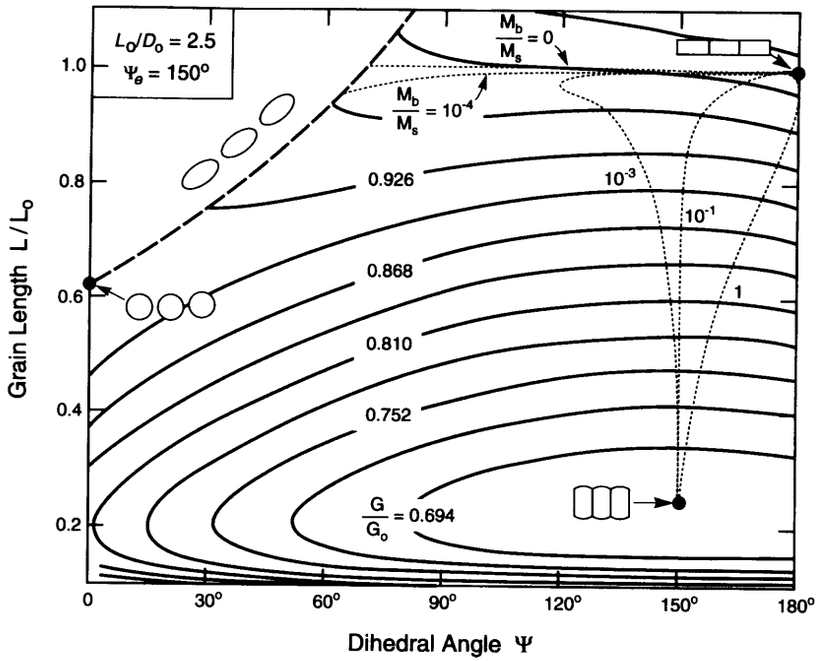

FIG. 19. The solid lines are the energy contours. The dotted lines are the evolution path when the grains are connected. The dashed line is the evolution path after the grains pinch off.

M_b/M_s. When the grain-boundary mobility is vanishingly small, $M_b/M_s = 0$, the grain length remains constant while the surface grooves; the grains pinch off and spheroidize, approaching a row of isolated spheres. Increasing the mobility ratio to $M_b/M_s = 10^{-3}$ allows the grains to contract to the state of truncated spheres. Consequently, everything else being fixed, a critical grain-boundary mobility exists, above which the grains contract to the lowest energy state, the truncated spheres. The evolution path depends on both energetics and kinetics.

Figure 20 draws a *morphological diversity map*. A point on the map represents a pair of parameters, L_0/D_0 and M_b/M_s. A boundary divides the plane into two regions. A parameter pair in one region makes the grains evolve to isolated spheres, and a parameter pair in the other region makes the grains evolve to truncated spheres.

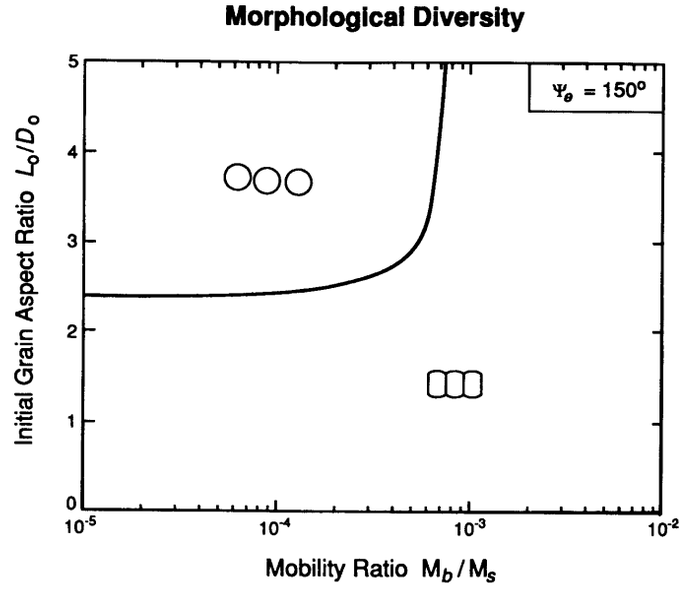

FIG. 20. A diversity map. The coordinates are the control parameters that do not change when the structure evolves. A boundary separates the plane into two regions. A fiber with the parameter group falling above the boundary evolves to isolated spheres. A fiber with the parameter group falling below the boundary evolves to truncated spheres.

C. GROOVING AND PITTING

Figure 21(a), page 256, illustrates a triple junction formed by a grain boundary and the free surface. The free surface is initially flat. When heated, atoms diffuse on the surface, leaving an indent along the triple junction, and two bumps over the grains. The size of the groove increases with the time. The forces that cause grooving are the surface and grain-boundary tensions. When the groove grows, the surface area increases somewhat, but the grain-boundary area decreases, so that the total free energy of the system reduces. Mullins (1957) analyzed this phenomenon, assuming that the surface and grain-boundary tensions, γ_s and γ_b, are isotropic, the grain boundary remains stationary, and no mass flows out from, or into, the grain boundary.

The equation for surface motion (5.14) becomes

$$v_n = B\nabla^2 K; \quad B \equiv M\Omega^2\gamma_s. \tag{6.18}$$

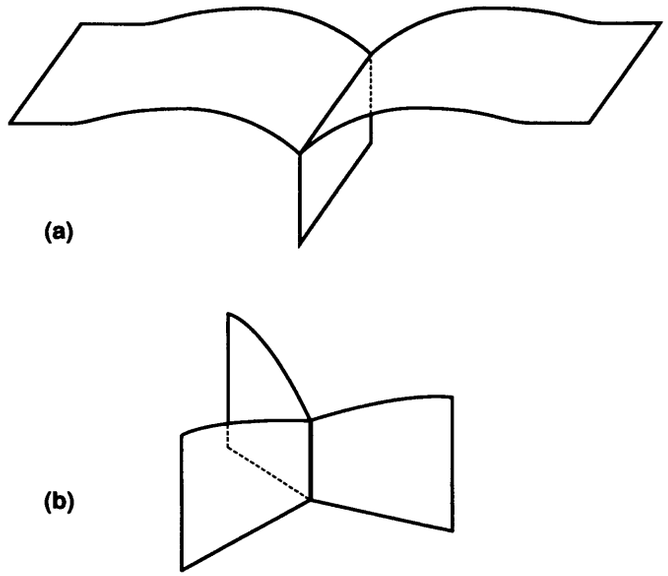

FIG. 21. (a) A surface groove over a grain boundary. (b) A surface pit over a three-grain junction.

Because the initial geometry has no length scale, the surface evolves with a self-similar profile: all lengths in the subsequent geometry scale with the time as $(Bt)^{1/4}$. For example, the groove depth (i.e., the distance from the groove root to the plane of the initial flat surface) scales as

$$d = k(Bt)^{1/4}. \tag{6.19}$$

The dimensionless coefficient k depends on the ratio γ_b/γ_s only. Mullins further simplified the problem by noting that the slope of the profile is typically small and the equation can be linearized. Under this simplification, k must be linear in the slope of the surface at the triple junction, m, defined by (3.13). Mullins' analysis gave $k = 0.78m$. The spacing between the peaks of the two bumps, w, has the same time scaling, but is independent of m under the small slope simplification. Mullins's analysis gave

$$w = 4.6(Bt)^{1/4}. \tag{6.20}$$

The groove width and depth may be measured experimentally. One can therefore deduce the surface tension and the surface diffusivity if γ_b has been determined by some other experiments. See Tsoga and Nikolopoulos (1994) for an experimental demonstration.

Figure 21(b) illustrates an intersection between the free surface and a three-grain junction. The surface grooves along the grain boundaries, and pits at the point of emergence of the three-grain junction. The surface profile is still self-similar, all lengths following the same time scaling as above. The pit depth obeys (6.19), the coefficient k depending on the ratios of various surface tensions involved. Genin *et al.* (1992) analyzed the problem, and found that k is greater than 0.78m, but within a factor of 3 for all the configurations considered by them.

Grain-boundary grooving and pitting may break a polycrysalline thin film on a substrate. If the grain size is much larger than the film thickness, (6.19) estimates the time needed for a three-grain junction to pit through the film thickness. However, if the grain size is comparable to the film thickness, mass transported from the grooves piles up on the grains, stopping the grooving process. Srolovitz and Safran (1986) and Miller *et al.* (1990) demonstrated that a critical ratio of grain size and film thickness exists, below which the grains reach an equilibrium configuration without breaking the film. Such an equilibrium state, however, may be unstable against grain growth. The coupled process of grain growth and surface grooving-pitting has not been analyzed.

D. Grain-Boundary Migration in Thin Film; Effect of Surface Diffusion

Mullins (1958) investigated the effect of surface diffusion on the migration of a grain boundary. Figure 22 illustrates a triple junction of a grain boundary and two free surfaces. Two rate processes are involved: migration of the grain boundary and diffusion on the free surfaces. Dragged by the grain boundary, the groove moves to the right. Mullins solved the problem of the groove moving in a steady state, with constant velocity v

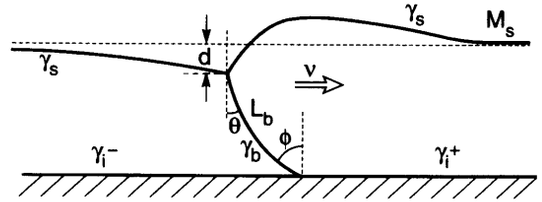

FIG. 22. A grain boundary moving in a thin film. Surface diffusion causes grooving at the triple junction.

and depth d. The significant features of his solution may be summarized as follows.

The steady velocity v and the material constant B in (6.18) define a length:

$$l = (B/v)^{1/3}. \tag{6.21}$$

This length sets the *scale* of the steady-state profile of the free surfaces. In particular, the groove depth, d, is linear in l. The *shape* of the translating groove depends on the ratio of the mobilities of the two surfaces, and the ratios of various surface tensions. Mullins assumed that the two surfaces have the identical mobility and surface tension. Consequently, only the ratio of the grain boundary and surface, γ_b/γ_s, enters the problem. Under the assumption that the surface slope is small, Mullins found that the steady-state groove depth is

$$d = \frac{\gamma_b}{3\gamma_s}\left(\frac{B}{v}\right)^{1/3}. \tag{6.22}$$

Everything else being equal, the larger the velocity, the smaller the groove depth.

Like surface evaporation, surface diffusion rotates the surfaces at the triple junction. The rotation angle θ in Figure 22 only depends on γ_b/γ_s. Mullins' solution gives

$$\theta = \frac{\gamma_b}{6\gamma_s}. \tag{6.23}$$

The rotation angle is independent of the steady velocity.

In his original analysis, Mullins (1958) did not specify the force that drives the grain-boundary migration, leaving the steady velocity undetermined. Following the works cited in Section III.E, we consider a grain boundary migrating in a thin film, driven by the difference in the interface tensions, γ_i^+ and γ_i^- (Figure 22). The slope ϕ is determined by the equilibrium of the triple junction in the horizontal direction (3.25). For the grain boundary to move to the right, it must concave toward the right, $\phi > \theta$, namely,

$$\frac{\gamma_i^+ - \gamma_i^-}{\gamma_b} > \frac{\gamma_b}{6\gamma_s}. \tag{6.24}$$

The effect of surface diffusion on grain-boundary migration is similar to surface evaporation discussed in Section III.E.

When $\phi > \theta$, from (3.20), the velocity of the grain boundary is given by

$$v = L_b\gamma_b\frac{(\phi - \theta)}{(h - d)}. \tag{6.25}$$

Simultaneously solving (6.22) and (6.25) gives v and d. The nonlinear equations have a unique real-valued solution. The solution depends on ϕ, θ, and the dimensionless ratio

$$\frac{\Omega^2 M_s}{h^2 L_b}, \tag{6.26}$$

involving the surface diffusion mobility M_s, the grain-boundary migration mobility L_b, the film thickness h, and the atomic volume Ω. Everything else being fixed, d/h increases with the parameter (6.26). Consequently, a thin film is more likely to break than a thick film.

E. Steady Surface Motion

1. *Surface Invariant in One Direction*

The profile of such a surface is described by the curve in a cross section. Assume, as a boundary condition or a symmetry condition, that the flux at a point on the surface vanishes. Let the origin of the coordinate (x, y) coincide with this point, Figure 23. Focus on a segment of the curve

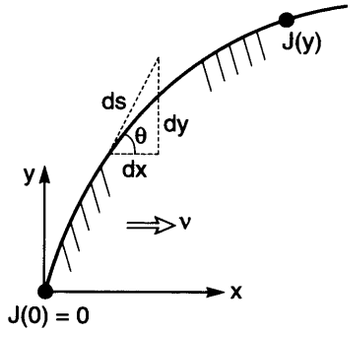

FIG. 23. Geometry of a steady-state surface profile.

between the origin and the point at y. Mass conservation relates the flux out of the segment, $J(y)$, to the steady velocity v:

$$J = \frac{vy}{\Omega}. \tag{6.27}$$

Assume isotropic surface tension γ and diffusion mobility M. The curvature K is positive for a convex surface. The flux relates to the curvature gradient along the surface:

$$J = -\frac{M\gamma\Omega\, dK}{ds}. \tag{6.28}$$

A combination of the two equations above gives that

$$\frac{dK}{ds} = -\frac{y}{l^3}. \tag{6.29}$$

The length l is defined by (6.21). Recall geometric relations,

$$\frac{d\theta}{ds} = -K, \frac{dy}{ds} = \sin\theta, \frac{dx}{ds} = \cos\theta. \tag{6.30}$$

Equations (6.29) and (6.30) give the complete set of ordinary differential equations. Note that only the last two equations are nonlinear, which may be linearized when the slope is small, as Mullins (1958) did. The equation set can be integrated with suitable boundary conditions. For a closed curve, the size of the problem is set by giving the area enclosed by the curve.

Chuang and Rice (1973) showed that a slit-like cavity may extend on a grain boundary if mass diffuses rapidly into the boundary ahead of the tip. Thouless (1993) and Klinger *et al.* (1995) studied slit formation on parallel grain boundaries. The co-evolution of pores and grains during sintering sets the microstructure of a final product. Spears and Evans (1982) examined the steady motion of a pore on a three-grain junction, and its relation with coarsening of pores and grains. The stability of the steady-state solutions has not been studied in general, but the available transient solutions show the validity of some steady-state solutions. Pharr and Nix (1979) and Thouless (1993) demonstrated that, under certain conditions, a

rounded void on a grain boundary stressed in tension evolves to the steady-state slit solution of Chuang and Rice (1973).

2. *Surface of Revolution*

Now Figure 23 represents a surface of revolution around the x-axis. Assume that the flux at the apex vanishes, $J = 0$ at $y = 0$. Mass conservation relates the flux $J(y)$ to the steady velocity v:

$$J = \frac{vy}{2\Omega}. \tag{6.31}$$

The flux relates to the curvature gradient still by (6.28). For the surface of revolution, the sum of the principal curvatures is

$$K = -\frac{d\theta}{ds} + \frac{\cos\theta}{y}. \tag{6.32}$$

The set of ordinary equations are

$$\frac{dK}{ds} = -\frac{y}{2l^3}, \quad \frac{d\theta}{ds} = -K + \frac{\cos\theta}{y}, \quad \frac{dy}{ds} = \sin\theta, \frac{dx}{ds} = \cos\theta. \tag{6.33}$$

They may be solved under analogous conditions as above.

Hsueh *et al.* (1982) examined the steady motion of a pore attached on a grain boundary, and the conditions under which the pore detaches from the grain boundary.

VII. Diffusion on an Interface between Two Materials

An interface between two materials is a rapid diffusion path for impurity atoms and atoms of the two materials. This section concerns with the latter. Both materials are taken to be rigid. (Sofronis and McMeeking, 1994 considered the combined interface diffusion and matrix creep in composite materials, which will not be considered here.) On an Al-Al_2O_3 interface, for example, one expects that aluminum diffuses much faster than oxygen, the latter being tied by the stronger atomic bonds. The situation is unclear on an Al-Al_2Cu interface: either aluminum or copper may be the dominant diffusion species on the interface. If aluminum diffusion dominates, the situation is similar to the aluminum-alumina interface. If copper diffusion dominates, in order for one copper atom to

leave an interface element, one Al_2Cu unit dissolves and donates two aluminum atoms to the aluminum crystal. Similarly, for one copper atom to add to an interface element, one Al_2Cu unit forms and accepts two aluminum atoms from the aluminum crystal. See Ma and Suo (1993) for a discussion on such an interface. This section focuses on the situation exemplified by the aluminum-alumina interface, where no mass exchanges across the interface.

A. Rigid Inclusion Moving in a Matrix

Refer to the material that diffuses on the interface as *matrix*, and the material that does not diffuse as *inclusion*. Subject to a force, atoms of the matrix diffuse from one part of the interface to another. To accommodate the space, the inclusion moves like a rigid body—translating and rotating—relative to the matrix. The shape of the interface remains invariant. The mobility of the atoms on the interface determines both the translation and rotation velocities, which may change with time. This situation arises in several important phenomena in materials. For example, when an inclusion attaches to a grain boundary, the speed of the combined entity depends on the mobilities of both the inclusion and the grain boundary. Consequently, the inclusion may retard the grain-boundary migration.

As a demonstration, we will only consider inclusion translation. Let $\mathbf{v}$ be the translation velocity of the inclusion relative to the matrix, $\mathbf{J}$ the flux of the matrix atoms, Ω the volume per matrix atom, and $\mathbf{n}$ the unit vector normal to the interface pointing to the matrix. Assume that neither the inclusion nor the matrix deforms, so that the volume added to an interface element must be accommodated by the inclusion motion:

$$\mathbf{n} \cdot \mathbf{v} = \Omega \nabla \cdot \mathbf{J}. \tag{7.1}$$

Similarly, let $\delta\mathbf{r}$ be the virtual translation of the inclusion, and $\delta\mathbf{I}$ the virtual mass displacement. Mass conservation requires that

$$\mathbf{n} \cdot \delta\mathbf{r} = \Omega \nabla \cdot (\delta\mathbf{I}). \tag{7.2}$$

The driving force for the inclusion translation, $\mathbf{f}$, is the free-energy reduction associated with the inclusion translating unit distance, namely,

$$\delta G = -\mathbf{f} \cdot \delta\mathbf{r}. \tag{7.3}$$

This force can be calculated once the free energy is known as a function of the inclusion position. Equation (5.5) defines the diffusion driving force, and (5.6) prescribes the kinetic law. The weak statement (5.20) still applies.

Analytical solution can be readily found for an inclusion having a shape invariant in one direction subject to a force perpendicular to that direction, or for an axisymmetric inclusion subject to a force in the direction of the symmetry axis.

1. *Axisymmetric Inclusion*

With reference to Figure 23, the interface is a surface of revolution. The force f, defined by (7.3), is in the direction of the axis of revolution, the x-axis; y is the radius of the surface of revolution. The inclusion translates at velocity v in the x-direction. Mass conservation relates the flux J to the velocity v, and the virtual mass displacement δI to the virtual translation δr:

$$J = \frac{y}{2\Omega} v, \quad \delta I = \frac{y}{2\Omega} \delta r. \tag{7.4}$$

The weak statement (5.20) becomes

$$\int \left(\frac{y}{2\Omega}\right)^2 \frac{v\,\delta r}{M} dA = f \delta r,$$

giving

$$v = \frac{4M\Omega^2 f}{\int y^2 dA}. \tag{7.5}$$

The integral extends over the area of the interface. For a spherical inclusion of radius R, $\int y^2 dA = 8\pi R^4/3$, so that

$$v = \frac{3M\Omega^2 f}{2\pi R^4}. \tag{7.6}$$

The approximate solution given by Shewmon (1964) has the same form as (7.6), but a different coefficient.

2. *Two-Dimensional Problem*

Figure 23 now represents an inclusion having a shape invariant along the axis normal to the plane of the paper, subject to a force in the x-axis. Energy is on a per thickness basis, so that f is the force on a per unit

thickness of the inclusion. We will assume that the particle translates in the x-axis; the method, however, is general. Let J_0 be the flux on the interface at $y = 0$, and J the flux at a general point y on the interface. Mass conservation requires that

$$J = J_0 + \frac{y}{\Omega} v, \quad \delta I = \delta I_0 + \frac{y}{\Omega} \delta r. \tag{7.7}$$

The weak statement (5.20) becomes

$$\int \frac{1}{M}\left(J_0 + \frac{y}{\Omega} v\right)\left(\delta I_0 + \frac{y}{\Omega} \delta r\right) ds = f\delta r.$$

The integral extends over the cross-section curve of the interface. Because the two virtual variations, δr and δI_0, are independent, the equation splits above to two equations

$$\Omega J_0 \int ds + v \int y ds = 0. \tag{7.8}$$

$$\Omega J_0 \int y ds + v \int y^2 ds = \Omega^2 M f. \tag{7.9}$$

They solve J_0 and v.

When a problem has a symmetry, and the origin of the y-axis is so placed that $\int y ds = 0$, the solution is $J_0 = 0$ and

$$v = \frac{M\Omega^2 f}{\int y^2 ds}. \tag{7.10}$$

For example, a cylindrical inclusion of radius R translates at velocity

$$v = \frac{M\Omega^2 f}{\pi R^3}. \tag{7.11}$$

B. Diffusion-Controlled Interfacial Sliding

Two-bonded materials under a shear stress may slide relative to each other. If the interface is flat, they slide by a viscous shear process on the interface. If the interface deviates from a perfect plane, the shear process alone does not accommodate the sliding. The asperity on the interface may be accommodated by plastic flow or fracture. Raj and Ashby (1971) proposed an alternative process, which operates at low stresses and high temperatures, when the bulk of the materials is rigid. Figure 24 illustrates two materials bonded by an interface with steps. Under the applied shear stress, τ, the interface is under tension at locations like A, and compression at locations like B. The gradient of the normal stress causes atoms of at least one material to diffuse on the interface, and thereby accommodates sliding. In this picture, sliding consists of two rate processes: viscous shear and interfacial diffusion. The two processes are in series; the slower one limits the sliding rate. Raj and Ashby gave experimental evidence indicating that it is often mass diffusion, rather than viscous shear, that limits the sliding rate. Similar considerations suggest that inclusion particles on a grain boundary may retard grain-boundary sliding (Raj and Ashby, 1972).

Following Raj and Ashby (1971), we consider an interface with periodic steps (Figure 24). The ratio of the step height to the period, h/λ, is typically small and is exaggerated in the figure. Due to symmetry, the flux vanishes at the middle of the step height, where the origin of the y-axis is placed. We next apply (7.10) to one period of the bi-material. The force on one period is

$$f = \tau\lambda.$$

The integral over the interface within one period is

$$\int y^2 ds = \frac{1}{4}\lambda h^2 + \frac{1}{6} h^3. \tag{7.12}$$

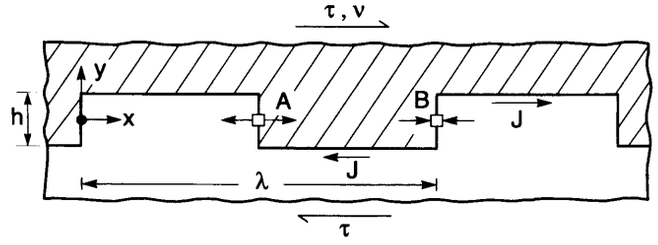

FIG. 24. A bi-material interface with periodic steps. The rate of sliding is limited by diffusion on the interface to accommodate the asperity.

Consequently, the two materials slide at a relative velocity

$$v = \frac{4M\Omega^2\tau}{h^2\left(1 + \dfrac{2h}{3\lambda}\right)}. \tag{7.13}$$

This reproduces the approximate result of Raj and Ashby (1971) in the limit $h/\lambda \to 0$.

C. Grain-Boundary Migration in Thin Film; Effect of Inclusion

Figure 25 illustrates a grain boundary migrating in a thin film of thickness h, motivated by the difference in the film-substrate interface tensions of the two grains, γ_i^+ and γ_i^-. The grain boundary also drags a semi-circular inclusion of radius R on the film surface. The surface tensions of the two grains at the free surfaces, γ_s, are taken to be the same. The inclusion retards the grain-boundary motion if the inclusion itself has low mobility. We will only consider a two-dimensional problem where the inclusion is a cylinder. The film-substrate interface is taken to be immobile, so that the angle at the triple junction, ϕ, is given by (3.25).

The grain-boundary migration can be modeled by the steady-state solution in Section III.D. The grain boundary moves at a velocity

$$v = \frac{L\gamma_b(\phi - \theta)}{h - R}. \tag{7.14}$$

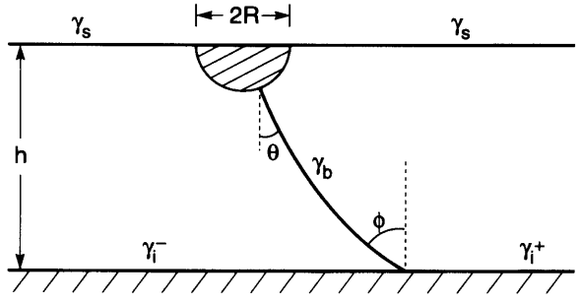

Fig. 25. A grain boundary in a thin film, pinned by an inclusion.

The grain-boundary tension exerts a force on the inclusion, $f = \gamma_b \sin\theta$. Equation (7.11) gives the velocity of the inclusion

$$v = \frac{2M\Omega^2\gamma_b \sin\theta}{\pi R^3}. \tag{7.15}$$

The angle θ falls between 0 and ϕ, and is determined by equating the velocities above. Consequently, the angle θ is solved from

$$\frac{\sin\theta}{\phi - \theta}\left(1 - \frac{R}{h}\cos\theta\right) = \frac{\pi LR^3}{2M\Omega^2 h}. \tag{7.16}$$

The inclusion retards the grain-boundary migration substantially if $\theta \to \phi$, or

$$\frac{LR^3}{M\Omega^2 h} \gg 1. \tag{7.17}$$

This condition involves the film thickness and particle radius, the migration mobility of the grain-boundary L, and the diffusion mobility of the inclusion-film interface M.

VIII. Surface Diffusion Driven by Surface- and Elastic-Energy Variation

A small crystal can sustain a high stress without fracture or plastic deformation. At an elevated temperature, the elastic energy can motivate mass diffusion. For example, when a film is deposited on a substrate with similar crystal structure having a few percent difference in lattice constant, the film strains to match the substrate lattice constant. The stress in the film would exceed 1 GPa were all relaxation processes suppressed. When the film is thick, the stress is relieved by dislocations or cracks. When the film is thin and the temperature is high, the stress is relieved by mass diffusion, breaking the film into islands. See Leonard *et al.* (1994) for a demonstration with InAs on GaAs.

Surface diffusion driven by strain-energy variation is difficult to analyze. The stress field has to be solved as a boundary-value problem for every surface shape during evolution, which is analytically intractable for most technically interesting problems. The high-order differential equation (5.14) requires great care in the numerical analysis. In many situations, the stress

is partially relieved by misfit dislocations; linear elasticity is inadequate. Due to these difficulties, only a few idealized problems have been solved.

This section discusses two such problems to give an impression of this class of phenomena. Each problem deals with an elastic body subject to a constant load. The free energy of the crystal, G, has three contributions: the surface energy U_S, the elastic energy U_E, and the applied load times the displacement, i.e., $G = U_S + U_E -$ load $\times$ displacement. Linear elasticity dictates that $2U_E =$ load $\times$ displacement. Consequently, the free energy of an elastic solid under constant load is

$$G = U_S - U_E. \tag{8.1}$$

A. Instability of a Flat Surface

First consider a large piece of crystal under no external stress. A surface of the crystal is flat and has isotropic surface tension. If scratched, the surface heals as the surface tension motivates mass to flow to restore the minimum energy configuration, the flat surface. Mullins (1959) analyzed the flattening process via several mass-transport mechanisms, including surface diffusion.

Next, subject the crystal to a uniaxial stress parallel to the flat surface. The crystal is taken to deform elastically. The flat surface is unstable: a small-amplitude perturbation amplifies if its wavelength exceeds a critical value. The phenomenon was independently analyzed by Asaro and Tiller (1972), Grinfeld (1986), Srolovitz (1989), and Gao (1991). The perturbation grows to a surface crack running into the bulk of the crystal, transverse to the applied stress direction (Chiu and Gao, 1993; Yang and Srolovitz, 1993; Yakobson, 1993). Suo and Yu (1997) extended the analysis to an elastic polycrystal surface. Gao (1994) and Freund (1995) surveyed the related problems.

Spencer *et al.* (1991) and Freund and Jonsdottir (1993) analyzed the similar instability in a film strained by a substrate. The undulation may break the film into islands, if atoms of the substrate do not diffuse at the temperature. Wong and Thouless (1995) studied the ratio of the island height and radius as a function of the misfit strain and various surface tensions. Seifert *et al.* (1996) demonstrated that the surface energy anisotropy is important in island formation.

1. *Energetics*

What follows describes the essential findings of the initial surface instability. To focus on main ideas, we treat the plane stress problem of a semi-infinite elastic crystal subject to a uniform stress, σ, parallel to the free surface of the crystal. The surface tension of the crystal, γ, is isotropic.

Consider the energy variation when the flat surface is perturbed. The perturbed surface has a larger area than the flat surface, so that U_S increases with the perturbation. Under a constant load, a body with a perturbed surface has a larger displacement at the loading point than a body with the flat surface (i.e., the undulation makes a body more compliant), so that U_E also increases with the perturbation. According to (8.1), the surface tension favors the flat surface, but the stress favors the perturbed surface: the two forces compete to determine whether the perturbation diminishes or amplifies.

To be specific, perturb the flat surface by a wave of amplitude q and period λ:

$$y(x,t) = q(t)\cos\frac{2\pi x}{\lambda}. \tag{8.2}$$

Here, y is the height of the perturbed free surface from the initial flat surface, the x-axis coincides with the flat surface, and t is the time. The amplitude q is the generalized coordinate in this problem. Following the previous authors, we will carry out a linear stability analysis, with $q/\lambda \ll 1$. The energies will be calculated to the leading order in q/λ, per period per unit thickness, relative to the energies of the stressed crystal with the flat surface.

The undulation increases the surface energy by

$$U_S = \frac{\pi^2\gamma}{\lambda} q^2. \tag{8.3}$$

This is readily obtained by calculating the length of the curve (8.2). Because a change in the sign of q leaves the curve length unchanged, U_S is proportional to q^2 to the leading order in q.

For a similar reason, the elastic energy variation U_E is proportional to q^2 to the leading order in q. In addition, linear elasticity dictates that U_E

be proportional to σ^2/Y, where Y is Young's modulus. A dimensional analysis shows that

$$U_E = \beta \frac{\sigma^2}{Y} q^2, \tag{8.4}$$

where β is a dimensionless number of order unity. An elasticity problem of the wavy surface can be solved analytically to the leading order in q/λ, giving $\beta = \pi$; see the papers cited previously.

A combination of (8.3) and (8.4) gives the free-energy difference between the solid with a wavy surface and the solid with a flat surface:

$$G = \left(\frac{\pi^2 \gamma}{\lambda} - \frac{\pi \sigma^2}{Y} \right) q^2. \tag{8.5}$$

The free energy decreases when the quantity in the bracket is negative. Consequently, the perturbation amplifies when the wavelength λ exceeds a critical value, given by

$$\lambda_c = \pi Y \gamma / \sigma^2. \tag{8.6}$$

Because the elastic energy is quadratic in the applied stress σ, the flat surface undulates under both tension and compression.

2. *Kinetics*

The profile (8.2) with $q/\lambda \ll 1$ has velocity normal to the surface $v_n = \dot{q} \cos(2\pi x/\lambda)$. Mass conservation relates the atomic flux to the normal velocity by $\partial J/\partial s = -v_n/\Omega$. For a small-amplitude perturbation, the curve length s can be replaced by x. An integration gives

$$J = -\left[\frac{\lambda}{2\pi\Omega} \sin \frac{2\pi x}{\lambda} \right] \dot{q}. \tag{8.7}$$

A similar relation connects the virtual mass displacement δI and virtual amplitude δq. The weak statement (5.20) leads to

$$\dot{q} = \frac{q}{\tau}, \tag{8.8}$$

with the characteristic time being

$$\tau = \frac{\lambda^4}{32\pi^4 M \Omega^2 \gamma} \left(\frac{\lambda}{\lambda_c} - 1 \right)^{-1}. \tag{8.9}$$

The solution to (8.8) is $q(t) = q(0)\exp(t/\tau)$, where $q(0)$ is the wave amplitude at $t = 0$. When $\lambda < \lambda_c$, $\tau < 0$ and the perturbation diminishes with the time. When $\lambda > \lambda_c$, $\tau > 0$ and the perturbation grows with the time; τ minimizes at the wavelength $\lambda_m = 4\lambda_c/3$. If perturbations of all wavelengths have an identical initial amplitude, the perturbation of wavelength λ_m grows most rapidly at $t = 0$.

The solution above is derived on the basis of the weak statement, and agrees with the exact solution of the previous authors obtained from the differential equations. This agreement is due to the choice of the perturbation (8.2), which is the form of the exact solution. If the form of the perturbation is inexact, the weak statement would yield an approximate solution.

One may also use the same procedure to estimate the effect of surface-tension anisotropy. For example, assume that the initial flat surface has surface tension γ_0, which is higher than the surface tensions of neighboring crystal orientations. Take the surface anisotropy to be of form (6.12), and the same procedure as above gives the critical wavelength

$$\lambda_c = \pi Y \gamma_0 \frac{(1 - 2\alpha)}{\sigma^2}. \tag{8.10}$$

As expected, such anisotropy decreases the critical wavelength.

B. Pore-Shape Change

1. *Qualitative Considerations*

Consider the high temperature rupture of sapphire fibers. Pores (diameter about 1 μm) are left inside the fibers (diameter about 150 μm) after fabrication. Newcomb and Tressler (1993) demonstrated that, when a sapphire fiber is pulled at an elevated temperature, a crack emerges from an internal pore, grows slowly at first and, upon attaining a critical size, causes the fiber to fracture.

When a crystal is under uniaxial tension at a high temperature, a pore in the crystal may change volume and shape for several reasons. Elastic

distortion changes the pore volume and shape by a small amount; large changes require creep or mass transport. If the crystal creeps rapidly and surface diffusion is slow, the pore increases volume and becomes needle-shaped in the pulling direction (e.g., Budiansky *et al.*, 1982; Needleman and Rice, 1980).

This subsection is concerned with the situation where surface diffusion is so rapid that the crystal creeps negligibly during the time of interest. On the basis of several theoretical studies (Stevens and Dutton, 1971; McCartney, 1976; Gao, 1992, 1995; Suo and Wang, 1994; Sun *et al.*, 1994; Wang and Suo, 1997), we suggest the following sequence of events in the Newcomb and Tressler experiments. When the fiber is under no stress, the pore has a rounded shape maintained by the surface tension. When the fiber is under a tensile stress, the pore changes shape via surface diffusion. Two outcomes are expected. If the applied stress is small, the pore reaches an equilibrium shape close to an ellipsoid, as a compromise between the stress and the surface tension (Figure 26(a)). If the applied stress is large, the pore keeps changing shape and develops a sharp crack tip which grows in the direction transverse to the applied tensile stress (Figure 26(b)).

On forming the sharp tip, further crack elongation is no longer limited by self-diffusing on the pore surface. Atomic bonds break at the crack tip by the intense stress, possibly assisted by the environmental species inside

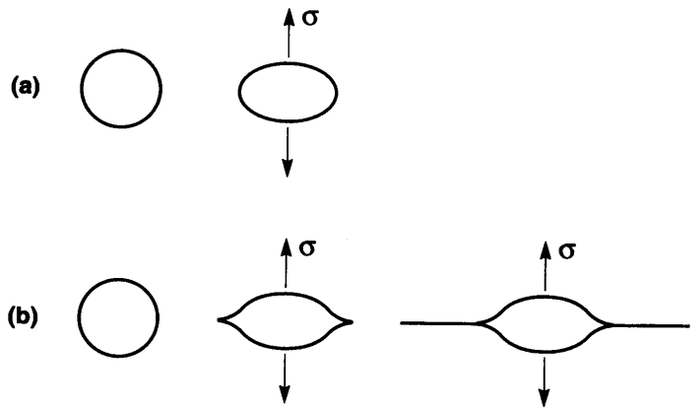

FIG. 26. a) A pore under a small stress reaches an equilibrium configuration, which is approximately an ellipse. b) A pore under a large stress develops sharp noses, followed by subcritical cracking.

the pore. The rate of crack growth may be limited by transport of the environmental species to, or reaction at, the crack tip (Lawn, 1993). Once the crack grows large enough, fast fracture breaks the entire crystal. The fiber spends its lifetime mainly in two stages: self-diffusion to grow the sharp tip, and the subcritical cracking after the sharp tip has formed. Which stage takes the longer time depends on the material, chemical environment, and temperature.

2. *Energetics of Crack Emergence*

Compare two crystals, one with a spherical pore, and the other a nonspherical pore. Both crystals are subject to the same tensile load remote from the pores. The pores have the same volume. Because the sphere has the minimal surface area among pores of the same volume, the nonspherical pore increases the surface energy U_S. Because a body with a flattening pore transverse to the loading axis is more compliant than a body with a spherical pore, the nonspherical pore increases the elastic energy U_E. Consequently, according to (8.1), the two forces compete to determine the pore shape: the surface tension favors a spherical pore, and the applied stress favors a crack.

Let a_0 be the initial pore radius, σ the stress, γ the surface tension, and Y Young's modulus. Express the relative importance of the elastic energy and the surface-energy variations with a dimensionless number

$$\Lambda = \frac{\sigma^2 a_0}{Y\gamma}. \tag{8.11}$$

When Λ is small, the surface energy variation dominates, and the pore reaches an equilibrium state of approximately ellipsoidal shape. When Λ is large, the elastic-energy variation dominates, and a crack emerges from the pore.

The following reviews the calculation of Suo and Wang (1994). The surface tension is taken to be isotropic. Consider a plane-stress problem of a cylindrical pore in an infinite crystal, subject to stresses σ_1 and σ_2 in the x- and y-directions. Initially, the pore is a circle of radius a_0. Under the action of the surface tension and stresses, atoms diffuse on the pore surface, causing the pore to evolve to a sequence of noncircular shapes.

We will first approximate the evolving shapes by a family of ellipses. Mass conservation requires that the area of the ellipses be the same as the

area of the initial circle, πa_0^2. Consequently, the system has only one degree of freedom, the ratio of the two semi-axes of the ellipses, written as

$$\frac{(1+m)}{(1-m)}. \tag{8.12}$$

The circle corresponds to $m = 0$, the slit in the x-direction to $m \to 1$, and the slit in the y-direction is $m \to -1$.

Energies are calculated on the unit thickness basis, and the initial state is taken to be the ground state. The surface energy equals the surface tension times the perimeter of the ellipse. Relative to the circular pore, an elliptic pore has surface energy

$$U_S = \frac{a_0\gamma}{\sqrt{1-m^2}} \int_0^{2\pi} (1 + m^2 - 2m\cos 2\theta)^{1/2}\, d\theta - 2\pi a_0\gamma. \tag{8.13}$$

The integral is evaluated numerically.

The stress field can be found in elasticity textbooks. The elastic-energy difference between a body with an elliptic pore and a body with a circular pore is computed from (4.14), giving

$$U_E = \frac{2\pi a_0^2}{Y}\left(\frac{m}{1-m}\sigma_2^2 - \frac{m}{1+m}\sigma_1^2\right). \tag{8.14}$$

The total free energy G is given by (8.1).

Figure 27(a) displays the free energy at several constant levels of Λ for a pore in a body under $\sigma_1 = \sigma_2$. Here, G is the free energy of the crystal with an elliptic pore, and the G_0 is the free energy of the crystal with a circular pore. Each minimum and maximum represents a stable and unstable equilibrium state, respectively. Three types of behaviors emerge depending on the value of Λ, i.e., the relative importance of elastic and surface energy, as follows.

(1) When $\Lambda = 0$, the surface tension dominates; G reaches a minimum at $m = 0$, and maxima at $m = \pm 1$. The circular void is stable and the two slits are unstable: any ellipse will relax to the circle.

(2) When $\lambda > \frac{3}{8}$, the stress dominates; G reaches the maximum at $m = 0$, and minima at $m = \pm 1$. The circle is unstable but the slits are stable: any elliptic void will collapse to the slits.

(3) For an intermediate level, $0 < \Lambda < \frac{3}{8}$, G reaches a local minimum at $m = 0$, two maxima at some $\pm m_c$, and two minima at $m = \pm 1$. The

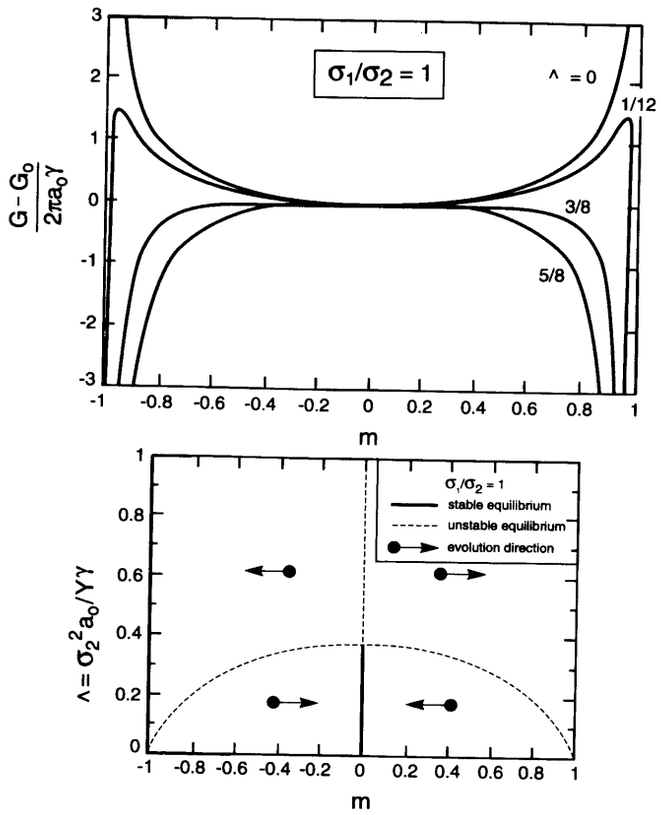

FIG. 27. Biaxial stress state $\sigma_1 = \sigma_2 = \sigma$. a) The free energy as a function of the void shape m at several levels of Λ. b) The bifurcation diagram is a combination of a subcritical pitchfork and two Griffith cracks.

maxima act as energy barriers: an ellipse of $|m| < m_c$ will relax to the circle, but an ellipse of $|m| > m_c$ will collapse to the slits.

The information above is projected onto the (Λ, m) plane, Figure 27(b). The heavy solid and dotted lines correspond to the stable and unstable equilibrium states, respectively. The two slits are stable for any $\Lambda > 0$, but unstable for $\Lambda = 0$. The circle $m = 0$ is metastable when $\Lambda < \frac{3}{8}$, but unstable when $\Lambda > \frac{3}{8}$. The dotted curve is the unstable equilibrium states, referred to as m_c in the preceding paragraph. These lines divide the (Λ, m) plane into four regions. A point in each region corresponds to an ellipse under a constant level of Λ, evolving toward a stable equilibrium

state, either the circle or the slits. The evolution direction in each region is indicated by an arrow. An ellipse below the dotted curve relaxes to the circle, and an ellipse above the dotted curve collapses to a slit. An initially circular void will collapse if Λ exceeds the critical value $\Lambda_c = \frac{3}{8}$.

Figure 28(a) and 28(b) are for $\sigma_1/\sigma_2 = 0.8$, representative of any stress ratios in the interval $0 < \sigma_1/\sigma_2 < 1$. Several asymmetries are noted. For small Λ, the local minimum no longer occurs at $m = 0$, nor do the two maxima at the same value of $|m|$. At a critical value, still denoted as Λ_c, the minimum and the maximum on the right-hand side annihilate, but the maximum on the left-hand side persists. In Figure 28(b), the values of m minimizing G are the heavy-solid lines, and the values of m maximizing G

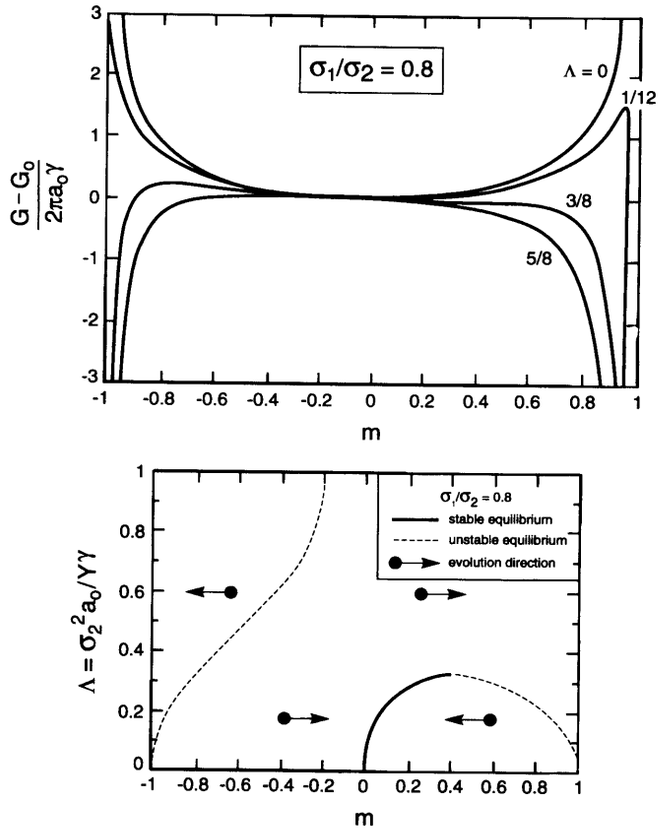

FIG. 28. Biased biaxial stress state $\sigma_1/\sigma_2 = 0.8$. a) The free energy as a function of the void shape m at several levels of Λ. b) Stability conditions projected on the (m, Λ) plane.

are the dotted lines. As expected, under the biased stress, the equilibrium shape is noncircular even for a small value of Λ. The heavy-solid curve ends at Λ_c, and is continued by the dotted curve.

Figure 29 gives the calculation Λ_c as a function of the stress ratio. The critical number does not vary significantly for the entire range of the stress ratio. Sun *et al.* (1994) gave the corresponding results for a three-dimensional pore.

3. *Kinetics*

Next, examine the kinetics of the pore-shape change using the weak statement. Normalize all the geometric lengths by the radius of the initial circular pore, a_0. From the weak statement we find that the problem has a characteristic time scale

$$t_0 = \frac{a_0^4}{M\Omega^2\gamma}, \tag{8.15}$$

which is used to normalize the time. Figure 30 plots the semi-axis of the ellipse, a, as a function of the time, for several levels of the loading parameter Λ. The body is remotely under stress state $\sigma_1 = \sigma_2$. The initial value is arbitrarily assigned to be $a/a_0 = 1.01$ at $t = 0$. The pore spends

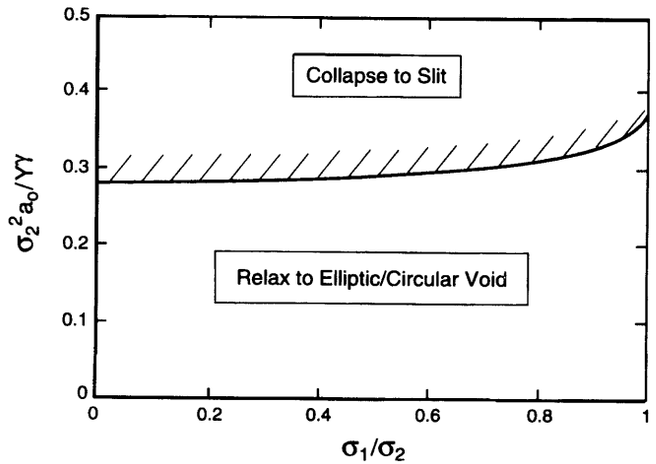

FIG. 29. The critical number Λ_c as a function of the stress ratio.

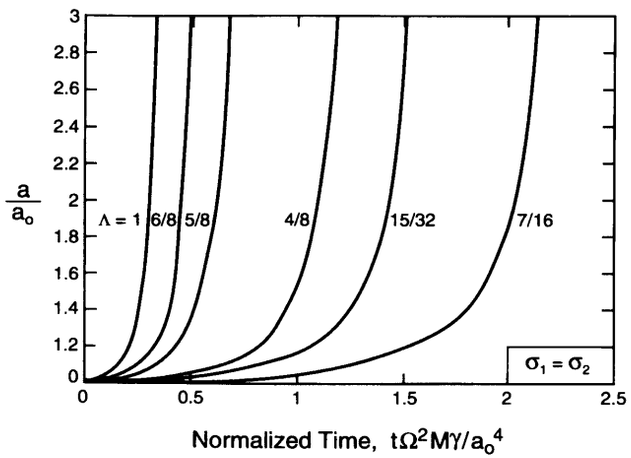

FIG. 30. The time for one ellipse to evolve to another.

most of its time deviating from the circle. After it became somewhat elliptic, the shape change is rapid.

C. Nosing, Cusping, and Subcritical Cracking

Chiu and Gao (1993) and Yang and Srolovitz (1993) went beyond the linear stability analysis of Section VIII.A, and studied large deviation from the flat surface. They found that surface cracks emerge and grow into the bulk of the crystal. In Section VIII.B, we have approximated the evolving pore as ellipses. The pore shape, however, may significantly deviate from an ellipse during evolution. Wang and Suo (1997) allowed more degrees of freedom for the pore shape, determined the elastic field around the pore with a conformal mapping, and traced the evolution of the pore shape.

We next summarize the findings of these studies in the context of the shape change of a pore. The critical loading level, Λ_c, is still given approximately by the curve in Figure 29. When the loading level is below Λ_c, the circular pore evolves to a rounded shape, approximately elliptical if $\sigma_1 \neq \sigma_2$.

When the loading level exceeds Λ_c, the circular pore evolves with nearly elliptical shapes in the beginning, then develops noses, and sharpens to become cusps, as schematically illustrated in Figure 28(b). The noses shorten diffusion length and further concentrate stress: this is a self-

amplifying process. The time needed from a circular shape to develop cusps takes the form

$$t_{\text{cusp}} = t_0 g(\Lambda). \tag{8.20}$$

When Λ just exceeds Λ_c, t_{cusp} is on the same order of the characteristic time t_0. When $\Lambda \gg \Lambda_c$, t_{cusp} is only a small fraction of the characteristic time t_0.

When the curvature at the nose tips increases and the noses become cusps, the stress becomes singular at the cusp tip. The stress field around a cusp tip has the same structure as that around a crack tip. The chemical potential at the cusp tip is ill-defined, because the cusp tip is no longer in local equilibrium. The situation is analogous to a triple junction with very low surface tension compared to the grain-boundary energy, Section II.E. Physically, another kinetic process takes over to limit the crack-extension velocity. If dislocations are unavailable or immobile, atomic bonds may cleave on the plane directly ahead of the cusp. The rate of crack extension may be limited by the transport of the environmental species or reaction at the crack tip (Lawn, 1993).

A common phenomenological description gives the crack velocity $\dot{a}$ depending on the driving force at the cusp, f, such as

$$\dot{a} = Cf^n, \tag{8.21}$$

where C is a rate coefficient, and typically $n > 1$; both parameters are used to fit the data of subcritical cracking experiments. The driving force here is defined as the free-energy reduction associated with the crack-advancing unit distance, namely

$$\delta G = -f\delta a. \tag{8.22}$$

The driving force is related to Irwin's elastic-energy rate, $\mathscr{G}$, and surface tension γ as

$$f = \mathscr{G} - 2\gamma. \tag{8.23}$$

IX. Electromigration on Surface

Interconnects in integrated circuits are made of aluminum alloys. They have small cross sections (less than 1 μm wide and about 0.5 μm thick), carry electric current up to 10^{10} A/m^2, and operate near half of aluminum's

melting temperature (933° K). The flowing electrons exert a force on aluminum atoms (i.e., the electron wind force), motivating aluminum atoms to diffuse. The phenomenon—mass diffusion directed by electric current, known as electromigration—causes reliability problems in integrated circuits; see Thompson and Lloyd (1993) for a survey. This section reviews phenomena related to electromigration on surfaces.

A. Surface Diffusion Driven by the Electron Wind

1. *Electron Wind Force*

To outline essential behaviors, we examine a plane problem of a cylindrical pore in a conductor, Figure 31. Assume that atomic diffusion on the pore surface is the only mass-transport process. The electric field vector $\mathbf{E}_i$ is the gradient of the potential ϕ:

$$\mathbf{E}_i = -\phi_{,i}. \tag{9.1}$$

Electric charge conservation requires that the electric current density vector, $\mathbf{j}_i$, be divergence-free:

$$\mathbf{j}_{i,i} = 0. \tag{9.2}$$

The electric field relates to the current density by Ohm's law

$$\mathbf{E}_i = \rho \mathbf{j}_i, \tag{9.3}$$

where ρ is the resistivity. Aluminum crystal has a cubic symmetry, so that the resistivity is the same in all directions.

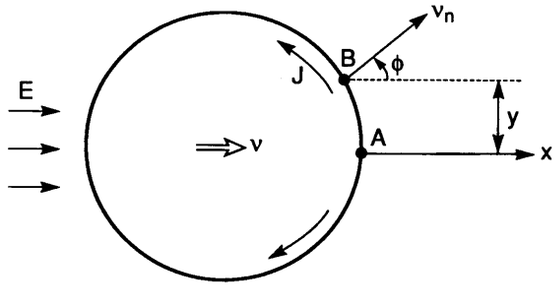

Fig. 31. A pore in an interconnect subjected to an electric field.

An aluminum interconnect is typically subject to an electric field below 1000 V/m. This electric field is amplified at the pore. For a pore without sharp edges, the amplification factor is about 2. Consequently, the electric field inside the pore is much lower than the electrical breakdown field of vacuum or dry air (around 1 MV/m). The pore can be modeled as an insulator, namely, $j_i n_i = 0$ at the pore surface.

The component of the electric field tangential to the pore surface is $E_t = -\partial\phi/\partial s$, where s is the curve length along the pore surface. The electron wind exerts a force on atoms on the pore surface. The force per atoms is proportional to the electric field E_t:

$$F_E = -Z^* e E_t, \tag{9.4}$$

where $Z^*(>0)$ is the effective valence, and $e(>0)$ the magnitude of the electron charge. The negative sign means that the force is in the direction of the electron flow. The effective valence may depend on crystal orientation.

2. *Weak Statements*

Let G be the free energy of the system, consisting of surface energy and electrostatic energy. They both vary when the pore changes shape. The relative magnitude of the two energies is described by a dimensionless number $\varepsilon E^2 R_0/\gamma$, where R_0 is the length representative of the pore size, γ the surface tension, and ε the permittivity of the medium inside the pore. For typical values, this number is much smaller than unity. Consequently, we will ignore the electrostatic energy, and take the free energy to be the surface energy:

$$G = \int \gamma ds. \tag{9.5}$$

The integral extends over the pore surface. The surface tension γ may depend on crystal orientation.

As before, we define the driving force for mass diffusion using virtual motion. Let δI be the mass displacement (i.e., the number of atoms across unit length on the surface). Associated with this virtual motion, the free energy changes by δG, and the electron wind force does work $\int F_E \delta I ds$. Define the diffusion driving force, F, by

$$\int F \delta I ds = -\delta G + \int F_E \delta I ds. \tag{9.6}$$

In other words, F is the reduction in the free energy plus the work done by the electron wind, associated with one atom moving unit distance on the surface. Evidently, (9.6) is an extension of (5.5).

Mass conservation takes the same form as in Section V, but a different sign convention is adopted here: the normal vector on the pore surface $\mathbf{n}$ now points to the solid. Mass conservation relates the virtual migration of the surface δr_n to the virtual mass displacement δI:

$$\delta r_n = \frac{\Omega \partial(\delta I)}{\partial s}. \tag{9.7}$$

Here Ω is the volume per atom. The surface velocity, v_n, relates to the atomic flux, J, by a similar relation:

$$v_n = \frac{\Omega \partial J}{\partial s}. \tag{9.8}$$

The linear kinetic law connects the flux with the total diffusion driving force:

$$J = MF. \tag{9.9}$$

Inserting (9.9) into (9.6), we obtain the weak statement of the problem:

$$\int \frac{J}{M}\,\delta I ds = -\delta G + \int F_E\,\delta I ds. \tag{9.10}$$

The actual flux J satisfies (9.10) for arbitrary virtual motion of the surface.

Of all virtual flux $\tilde{J}$, the actual flux minimizes the functional

$$\Pi = \dot{G} - \int F_E \tilde{J} ds + \int \frac{\tilde{J}^2}{2M} ds. \tag{9.11}$$

3. *Equations for Isotropic Conductor*

Next, consider a conductor having isotropic surface tension and effective charge. The total driving force for atomic diffusion on the pore surface is

$$F = -Z^* e E_t + \frac{\Omega \gamma \partial K}{\partial s}. \tag{9.12}$$

The first term is the electron wind force, and the second the capillary force. The curvature K is positive for a rounded pore.

A combination of equations (9.8), (9.9), and (9.12) gives

$$\mathbf{n} \cdot \frac{\partial \mathbf{x}}{\partial t} = M \frac{\partial^2}{\partial s^2}(Z^* e\phi + \Omega \gamma K). \tag{9.13}$$

The left-hand side is the velocity normal to the pore surface. This equation governs the motion of the pore surface.

B. Pore Drifting in the Electron Wind

Small pores often appear in aluminum interconnects to relieve stresses caused by thermal-expansion mismatch or electromigration. The pores may move in the electron wind (Shingubara and Nakasaki, 1991; Besser *et al.*, 1992; Arzt *et al.*, 1994; Marieb *et al.*, 1995). Since electrons flow in the direction opposite to the electric field direction, atoms diffuse on the pore surface as indicated in Figure 31. Consequently, the pore migrates in the direction of the applied electric field.

Ho (1970) showed that, in an infinite isotropic conductor under a remote electric field, a circular pore can migrate without changing its shape. His solution is summarized as follows. Figure 31 illustrates a circular pore, radius R_0, in an infinite conductor subject to a remote electric field E. The electric field is nonuniform in the conductor, but is uniform inside the pore and equals $2E$. Because the electric potential is continuous across the pore surface, E_t is also continuous across the surface. Consequently, the electric field component tangential to the pore surface is

$$E_t = -\frac{2Ey}{R_0}. \tag{9.14}$$

The electron wind force is

$$F_E = \frac{2eZ^*Ey}{R_0}. \tag{9.15}$$

The isotropic surface tension does not cause diffusion on the surface of a circular pore, so that (9.15) is also the total diffusion-driving force.

On the pore surface in Figure 31, A is a symmetry point where the flux vanishes, and B is a point at height y. Let the circular pore translate at a uniform velocity v in the x-direction. In unit time, atoms of volume yv (per interconnect thickness) are removed from the segment AB, and flow

out of the segment at point B. Mass conservation requires that the flux at point B be

$$J = \frac{yv}{\Omega}. \tag{9.16}$$

Connecting (9.15) and (9.16) with the kinetic law $J = MF$, one obtains the velocity of the pore

$$v = 2\frac{\Omega MZ^*eE}{R_0}. \tag{9.17}$$

The pore drifts in the direction of the applied electric field, at a velocity proportional to the applied electric field, and inversely proportional to the pore radius.

For a spherical pore in an infinite conductor subject to a remote electric field E, the electric field in the pore is uniform and equals $3E/2$. The velocity of the pore takes the same form as (9.17), with the coefficient 2 replaced with 3. Ho (1970) also studied drifting of a rigid inclusion. Ma and Suo (1993) showed how an Al_2Cu particle drifts in an aluminum matrix, as both copper and aluminum atoms diffuse on the particle-matrix interface. Suo (1994) studied the migration of edge-dislocation loops when atoms diffuse along the dislocation cores in the electron wind, and proposed the process as a mass transport mechanism in aluminum interconnects when other mechanisms are slow or absent.

The phenomena of defect migration provide means to determine atomic mobility experimentally. For example, by measuring the velocity and radius of a pore migrating in aluminum under a given electric field, one determines the parameter Z^*M from (9.17). An aluminum interconnect is usually covered by a thin film of aluminum oxide. The oxide film usually covers a pore near the surface, which should insulate the pore surface from contamination.

C. Pore Breaking Away from Trap

Grain boundaries and triple junctions may trap pores. Figure 32 shows a pore attached on a grain boundary. In the absence of the electric field, the pore eliminates part of the grain-boundary area, and therefore is in a low-energy state. Subject to an electric field, the pore moves by surface diffusion, and may break away from the grain boundary. Li *et al.* (1992)

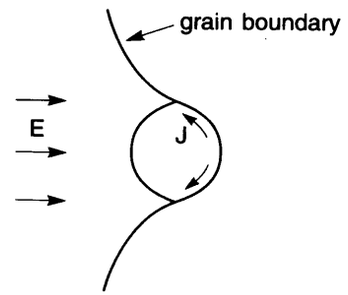

FIG. 32. A pore trapped by the grain boundary and driven by the electron wind.

and Wang *et al.* (1996) estimated the electric field needed for the pore to break away from a grain boundary.

Denote f_T as the force acting on the pore by the trap. For example, when the pore tries to break away from a grain boundary of tension γ_b, the grain boundary exerts a force (per interconnect thickness) on the pore, $f_T = 2\gamma_b$, in the direction opposing the breakaway. In equilibrium this force balances the electron wind force, and surface diffusion stops. Let the pore undergo a virtual translation in the x-direction by a displacement δa. Mass conservation requires that $\delta I = y\delta a/\Omega$. In equilibrium, the total virtual work vanishes:

$$\int F_E \delta I ds - f_T \delta a = 0. \tag{9.18}$$

Approximating the pore by a circle in integration, we obtain that

$$\frac{Z^*eER_0^2}{\Omega f_T} = \frac{1}{2\pi}. \tag{9.19}$$

With material properties fixed, there exists a critical value of ER_0^2, above which the pore breaks away from the grain boundary. The numerical value on the right-hand side of (9.19) will change if the pore surface is allowed to change shape in the electron wind. The problem has not been solved exactly.

Pore attachment and breaking away are evident in many experimental studies (e.g., Besser *et al.*, 1992; Kraft *et al.*, 1993; Marieb *et al.*, 1995). Careful observations would lead to an estimate of the effective valence Z^*.

D. Transgranular Slits

Experimental evidence accumulated in the last few years has shown that an aluminum interconnect with a bamboo-like grain structure often fails by a transgranular slit. Micrographs of such slits were first published by Sanchez *et al.* (1992) and Rose (1992). The slits are about 100 nm thick, and nearly perpendicular to the current direction. The faces of a slit and its running direction favor special crystalline orientations. Joo and Thompson (1993) observed slits in single crystal aluminum interconnects.

It was, however, uncertain how the slits form by looking at the micrographs taken after the aluminum interconnects had failed. In a sequence of micrographs taken in interrupted electromigration tests, Kraft *et al.* (1993) and Arzt *et al.* (1994) discovered that pores not only drift, but also change shape. A rounded pore forms somewhere in the aluminum interconnect, travels for some distance, enlarges, and collapses to a slit. These authors also suggested a mechanism by which a pore changes shape. Figure 33 illustrates two asymmetric pore shapes. The shape in Figure 33(a) is critical because the electromigration flux from b to c is larger than that from a to b, so that mass depletes from b, and the pore elongates in the direction normal to the interconnect. By contrast, the shape in Figure 33(b) is uncritical because the electromigration flux from c to b is larger than that from b to a, so that mass accumulates at b, and the pore elongates in the direction along the interconnect.

Two forces compete to determine the pore shape: the electron wind favors a slit, but the surface tension favors a rounded pore. On examining the expression for the driving force (9.11), Suo *et al.* (1994) pointed-out

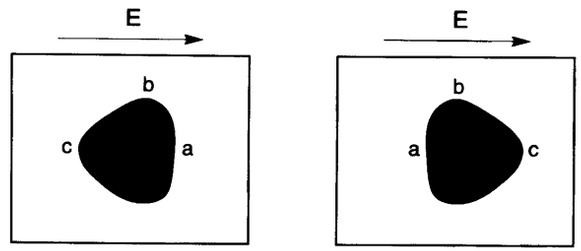

FIG. 33. a) A pore with the critical asymmetric shape. b) A pore with the uncritical asymmetric shape.

that the relative importance of the electron-wind force and the capillary force is measured by a dimensionless number

$$\chi = \frac{Z^* e E R_0^2}{\Omega \gamma} \tag{9.20}$$

where R_0 is the radius of the rounded pore, and E the applied electric field. When χ is small, the surface energy dominates, and the pore remains rounded. When χ is large, the electron wind dominates, and the pore collapses to a slit. Note that the number has the same form as that for a pore to break away from a trap (9.19). Suo *et al.* (1994) also estimated the velocity and width of a well-formed slit.

Yang *et al.* (1994) and Maroudus (1995) attempted to estimate the critical number for the shape instability, χ_c. To circumvent the difficulty of solving the electric field around the pore, Yang *et al.* considered a model problem where the medium inside the pore is conducting and has the same resistivity as that of aluminum, and showed that such a pore becomes unstable above $\chi_c = 10.65$.

Marder (1994) carried out a rigorous linear-stability analysis. He confirmed the result above of the conducting pore. However, for the more realistic model, i.e., a circular insulating pore in an infinite conductor, he found that the pore is *stable* against infinitesimal shape perturbation for arbitrarily high χ. Mahadevan and Bradley (1996) independently carried out the same analysis.

Linear stability analysis has its limitation. A pore that is stable against infinitesimal perturbation need not be stable against finite perturbation. In practice, the initial pore is never a perfect circle; deviation may result from surface-tension anisotropy, finite-interconnect width, thermal stress, etc. To determine the pore stability under practical conditions, one must study finite initial imperfection and large shape change.

Kraft and Arzt (1995) and Bower and Freund (1995) studied numerically the stability of an insulating pore in an interconnect of a finite width. They determined the electric field in the conductor by using finite-element methods, and updated the pore shape according to the electron wind and capillary forces. A rounded pore is unstable above a critical level, χ_c, whose value depends on the initial pore radius to the linewidth ratio, R_0/w. Marder's linear-stability analysis shows that $\chi_c \to \infty$ as $R_0/w \to 0$. The complete $\chi_c(R_0/w)$ function is unavailable at this time.

Wang *et al.* (1996) considered an unsulating pore in an infinite conductor, and introduced finite imperfection to the initial pore shape. They used a conformal mapping to determine the electric field, and the weak statement to update the pore shape. They showed that the pore becomes unstable above χ_c, the magnitude of which depends on the type and magnitude of the initial imperfection. For example, the initial pore is taken to be an ellipse with the two semi-axis

$$\left(\sqrt{1+\varepsilon^2}-\varepsilon\right)R_0, \left(\sqrt{1+\varepsilon^2}+\varepsilon\right)R_0 .$$

The form is chosen so that the area of the ellipse is πR_0^2. The imperfection ε takes finite values. As before, we use the characteristic time

$$t_0 = \frac{R_0^4}{\Omega^2 M\gamma} \tag{9.21}$$

to normalize the time. Figure 34 shows the snapshots at time interval $0.06t_0$ of a pore with initial imperfection $\varepsilon = 0.1$. When χ is small, the pore migrates and changes its shape, but finally reaches a steady state. When χ is large, the pore collapses to a slit. Figure 35 plots χ_c as a function of the imperfection ε. The critical value drops sharply when moderate initial imperfection is introduced, and decreases somewhat thereafter.

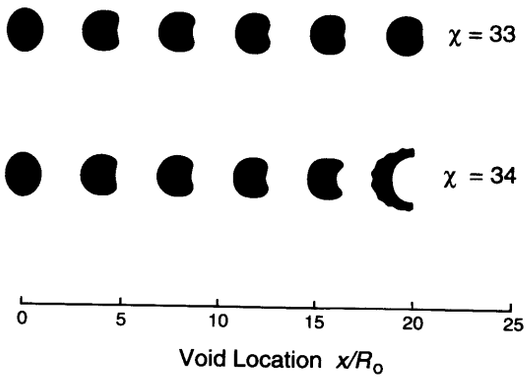

FIG. 34. Each row is a sequence of snapshots of a pore migrating in an interconnect, in the direction of the applied electric field, from the left to the right. The void is a perfect insulator. The initial perturbation is $\varepsilon = 0.1$.

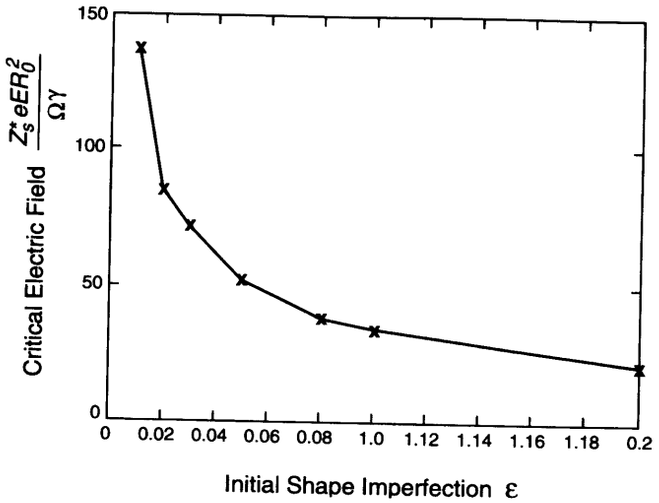

FIG. 35. The critical electric field as a function of the magnitude of the initial pore shape imperfection ε.

Acknowledgments

The writer is grateful to the National Science Foundation for a Young Investigator Award, to the Humboldt Foundation and the Max Planck Society for financing a sabbatical leave at the Max Planck Institute in Stuttgart hosted by Directors M. Ruhle and E. Arzt, and to Advanced Micro Devices for a grant under the supervision of Dr. J. E. Sanchez. Part of the work reviewed here was supported by ARPA through a URI contract N-0014-92-J-1808, by ONR through contract N00014-93-1-0110, and by NSF through grant MSS-9202165.

References

Abeyaratne, R., and Knowles, J. K. (1990). On the driving traction acting on a surface of strain discontinuity in a continuum, *J. Mech. Phys. Solids* **38**, 345–360.

Ames, I., d'Heurle, F. M., and Horstmann, R. (1970). Reduction of electromigration in aluminum films by copper doing. *IBM J. Res. Dev.* **14**, 461–463.

Arzt, E., Kraft, O., Nix, W. D., and Sanchez, J. E. Jr., (1994). Electromigration failure by shape change of voids in bamboo lines. *J. Appl. Phys.* **76**, 1563–1571.

Asaro, R. J., and Tiller, W. A. (1972). Interface morphology development during stress corrosion cracking: Part I. Via surface diffusion. *Metall. Trans.* **3**, 1789–1796.

Besser, P. R., Madden, M. C., and Flinn, P. A. (1992). *In situ* scanning electron microscopy observation of the dynamic behavior of electromigration voids in passivated aluminum lines. *J. Appl. Phys.* **72**, 3792–3797.

Biot, M. A. (1970). "Variational Principles in Heat Transfer." Oxford Univ. Press, Oxford.

Bower, A. F., and Freund, L. B. (1993). Analysis of stress-induced void growth mechanisms in passivated interconnect lines. *J. Appl. Phys.* **74**, 3855–3868.

Bower, A. F., and Freund, L. B. (1995). Finite element analysis of electromigration and stress induced diffusion in deformable solids. *Mater. Res. Soc. Symp Proc.* **391**, 177–188.

Brada, M., Clarke, D. M., and Suo, Z. (1996). Unpublished work.

Brokman, A., Kris, R., Mullins, W. W., and Vilenkin, A. J. (1995). Analysis of boundary motion in thin films. *Scr. Metall. Mater.* **32**, 1341–1346.

Budiansky, B., Hutchinson, J. W., and Slutsky, S. (1982). Void growth and collapse in viscous solids. "Mechanics of Solids, The Rodney Hill 60th Anniversaty Volume," (H. G. Hopkins and J. Sewell, eds.), pp. 13–45, Pergamon, Oxford.

Cannon, R. M., and Carter, W. C. (1989). Interplay of sintering microstructures, driving forces, and mass transport mechanisms. *J. Am. Ceram. Soc.* **72**, 1550–1555.

Carter, W. C., Roosen, A. R., Cahn, J. W., and Taylor, J. E. (1995). Shape evolution by surface diffusion and surface attachment limited kinetics on completely faceted surfaces. *Acta Metall. Mater.* **43**, 4309–4323.

Chiu, C. H., and Gao, H. (1993). Stress singularities along a cycloid rough surface. *Int. J. Solids Struct.* **30**, 2981–3012.

Chuang, T.-J., and Rice, J. R. (1973). The shape of intergranular creep cracks growing by surface diffusion. *Acta Metall.* **21**, 1625–1628.

Cocks, A. C. F. (1992). Interface reaction controlled creep. *Mech. Mater.* **13**, 165–174.

Cocks, A. C. F. (1994). The structure of constitutive laws for the sintering of fine grained materials. *Acta Metall. Mater.* **42**, 2197–2210.

Cocks, A. C. F., and Gill, S. P. A. (1995). A variational approach to two dimensional grain growth. Submitted in publication.

Du, Z.-Z., McMeeking, R. M., and Cocks, A. C. F. (1996). Manuscript in preparation.

Dunn, M. L., and Wienecke, H. A. (1996). Inclusions and inhomogeneities in transversely isotropic piezoelectric solids. *J. Mech. Phys. Solids*. Submitted for publication.

Eshelby, J. D. (1956). The continuum theory of lattice defects. *Solid State Phys.*, **3**, 79–144.

Eshelby, J. D. (1957). The determination of the elastic field of an ellipsoidal inclusion, and related problems. *Proc. R. Soc. London* **A421**, 376–396.

Eshelby, J. D. (1970). Energy relations and the energy-momentum tensor in continuum mechanics. *In* "Inelastic Behavior of Solids" (M. F. Kanninen *et al.*, eds.), pp. 77–115. McGraw-Hill, New York.

Floro, J. A., Thompson, C. V., Carel, R., and Bristowe, P. D. (1994). Competition between strain and interface energy during epitaxial grain growth in Ag films on Ni (001). *J. Mater. Res.* **9**, 2411–2424.

Freund, L. B. (1995). Evolution of waviness on the surface of a strained elastic solid due to stress-driven diffusion. *Int. J. Solids Struct.* **32**, 911–923.

Freund, L. B., and Jonsdottir, F. (1993). Instability of a biaxially stressed thin film on a substrate due to material diffusion over its free surface. *J. Mech. Phys. Solids* **41**, 1245–1264.

Frost, H. J., Thompson, C. V., and Walton, D. T. (1992). Simulation of thin film grain structures—II. Abnormal grain growth. *Acta Metall. Mater.* **40**, 779–793.

Gao, H. (1991). A boundary perturbation analysis for elastic inclusions and interfaces. *Int. J. Solids Struct.* **28**, 703–725.

Gao, H. (1992). Stress analysis of holes in anisotropic elastic solids: Conformal mapping and boundary perturbation. *Q. J. Mech. Appl. Math.* **45**, 149–168.

Gao, H. (1994). Some general properties of stress-driven surface evolution in a heteroepitaxial thin film structre. *J. Mech. Phys. Solids* **42**, 741–772.

Gao, H. (1995). The hypocycloid cavity: A path from a Griffith slit crack to a cusped cycloid surface. *Proc. R. Soc. London* **448**, 465–483.

Genin, F. Y., Mullins, W. W., and Wynblatt, P. (1992). Capillary instabilities in thin films: A model of thermal pitting at grain boundary vertices. *Acta. Metall.* **40**, 3239–3248.

Grinfeld, M. A. (1986). Instability of the separation boundary between non-hydrostatically stressed elastic body and a melt. *Sov. Phys. Dokl*, **31**, 831–834.

Herring, C. (1951). Surface tension as a motivation for sintering. "The Physics of Powder Metallurgy." (W. E. Kingston, ed.), pp. 143–179. McGraw-Hill, New York.

Hillert, M. (1965). On the theory of normal and abnormal grain growth. *Acta Metall.* **13**, 227–238.

Hsueh, C. H., Evans, A. G., and Coble, R. L. (1982). Microstructure development during final/intermediate stage sintering—I. Pore/grain boundary separation. *Acta Metall.* **30**, 1269–1279.

Ho, P. S. (1970). Motion of inclusion induced by a direct current and a temperature gradient. *J. Appl. Phys.* **41**, 64–68.

Isenberg, C. (1978). "The Science of Soap Films and Soap Bubbles." Reprinted in 1992 by Dover, New York.

Jiang, Q. (1994). On the driving traction acting on a surface of discontinuity within a continuum in the presence of electromagnetic fields. *Journal of Elasticity* **34**, 1–21.

Johnson, W. C., and Cahn, J. W. (1984). Elastically induced shape bifurcations of inclusions. *Acta Metall.* **32**, 1925–1933.

Joo, Y.-C., and Thompson, C. V. (1993). Evolution of electromigration-induced voids in single crystalline aluminum lines with different crystallographic orientations. *Mater. Res. Soc. Symp. Proc.* **309**, 351–357.

Klinger, L. M., Glickman, E. E., Fradkov, V. E., Mullins, W. W., and Bauer, C. L. (1995). Extensions of thermal grooving for arbitrary grain-boundary flux. *J. Appl. Phys.* **78**, 3833–3838.

Kraft, O., and Arzt, E. (1995). Numerical simulation of electromigration-induced shape changes of voids in bamboo lines. *Appl. Phys. Lett.* **66**, 2063–2065.

Kraft, O., Bader, S., Sanchez, J. E., and Arzt, E. (1993). Observation and modeling of electromigration-induced void growth in Al-based interconnects. *Mater. Res. Symp. Proc.* **309**, 199–204.

Landauer, R. (1957). Electrostatic considerations in $BaTiO_3$ domain formation during polarization reversal. *J. Appl. Phys.* **28**, 227–234.

Lawn, B. (1993). "Fracture of Brittle Solids." Cambridge Univ. Press, London.

Leonard, D., Pond, K., and Petroff, P. M. (1994). Critical layer thickness for self-assembled InAs islands on GaAs. *Phys. Rev. B* **50**, 11687–11692.

Li. C.-Y., Borgesen, P., and Korhonen, M. A. (1992). Electromigration-induced failure in passivated aluminum-based metallizations—the dependence on temperature and current density. *Appl. Phys. Lett.* **61**, 411–413.

Loge, R. E., and Suo, Z. (1996). Nonequilibrium thermodynamics of ferroelectric domain evolution. *Acta Metall. Mater.* **44**, 3429–3438.

Lusk, M. (1994). On martensitic phase nucleation with surface effects. *J. Mech. Phys. Solids* **42**, 241–282.

Ma, Q., and Suo, Z. (1993). Precipitate drifting and coarsening caused by electromigration. *J. Appl. Phys.* **74**, 5457–5462.
McCartney, L. N. (1977). Cavities under stress at high temperatures. *Acta Metall.* **25**, 221–230.
McMeeking, R. M., and Kuhn, L. T. (1992). A diffusional creep law for powder compacts. *Acta Metall. Mater.* **40**, 961–969.
Mahadevan, M., and Bradley, M. R. (1996). Stability of a circular void in a passivated, current-carrying metal film. *J. Appl. Phys.* in press.
Marder, M. (1994). Unpublished work.
Marieb, T., Flinn, P., Bravman, J. C., Gardner, D., and Madden, M. (1995). Observations of electromigration induced void nucleation and growth in polycrystalline and near-bamboo passivated Al lines. *J. Appl. Phys.* **78**, 1026–1032.
Maroudus, D. (1995). Dynamics of transgranular voids in metallic thin films under electromigration conditions. *Appl. Phys. Lett.* **67**, 798–800.
Miller, K. T., and Lange, F. F. (1989). The morphological stability of polycrystalline fibers. *Acta Metall.* **37**, 1343–1347.
Miller, K. T., Lange, F. F., and Marshall, D. B. (1990). The instability of polycrystalline thin films: Experiment and theory. *J. Mater. Res.* **5**, 151–160.
Miller, R. C., and Savage, A. (1959). Further experiments on the sidewise motion of 180° domain walls in $BaTiO_3$. *Phys. Rev.* **115**, 1176–1180.
Mullins, W. W. (1956). Two-dimensional motion of idealized grain boundaries, *J. Appl. Phys.*, **27**, 900–904.
Mullins, W. W. (1957). Theory of thermal grooving. *J. Appl. Phys.* **28**, 333–339.
Mullins, W. W. (1958). The effect of thermal grooving on grain boundary motion. *Acta Metall.* **6**, 414–427.
Mullins, W. W. (1959). Flattening of a nearly plane solid surface due to capillarity. *J. Appl. Phys.* **30**, 77–83.
Needleman, A., and Rice, J. R. (1980). Plastic creep flow effects in the diffusive cavitation of grain boundaries. *Acta Metall.* **28**, 1315–1332.
Newcomb, S. A., and Tressler, R. E. (1993). Slow crack growth in sapphire fibers at 800° to 1500°C. *J. Am. Ceram. Soc.* **76**, 2505–2512.
Nichols, F. A. (1976). On the spheroidization of rod-shaped particles of finite length. *J. Mater. Sci.* **11**, 1077–1082.
Nichols, F. A., and Mullins, W. W. (1965a). Morphological changes of a surface of revolution due to capillary-induced surface diffusion. *J. Appl. Phys.* **36**, 1826–1835.
Nichols, F. A., and Mullins, W. W. (1965b). Surface- (interface-) and volume-diffusion contribution to morphological changes driven by capillarity. *Trans. Metall. Soc.* **233**, 1840–1848.
Osborn, J. A. (1945). Demagnetizing factors of the general ellipsoid. *Phys. Rev.* **67**, 351–357.
Pharr, G. M., and Nix, W. D. (1979). A numerical study of cavity growth controlled by surface diffusion. *Acta Metall.* **27**, 1615–1631.
Pompe, W., Gong, X., Suo, Z., and Speck, J. S. (1993). Elastic energy release due to domain formation in the strained epitaxy of ferroelectric and ferroelastic films. *J. Appl. Phys.* **74**, 6012–6019.
Raj, R., and Ashby, M. F. (1971). On grain boundary sliding and diffusional creep. *Metall. Trans.* **2**, 1113–1127.
Raj, R., and Ashby, M. F. (1972). Grain boundary sliding, and the effects of particle on its rate. *Metall. Trans.* **3**, 1937–1942.
Rodel, J., and Glaeser, M. (1990). High-temperature healing of lithographically introduced cracks in sapphire. *J. Am. Ceram. Soc.* **73**, 592–601.

Rosakis, P., and Jiang, Q. (1995). On the morphology of ferroelectric domains. *Int. J. Eng. Sci.* **33**, 1–12.
Rosakis, P., and Tsai, H. (1994). On the role of shear instability in the modeling of crystal twinning. *Mech. Mater.* **17**, 245–259.
Rose, J. H. (1992). Fatal electromigration voids in narrow aluminum-copper interconnect. *Appl. Phys. Lett.* **61**, 2170–2172.
Roytburd, A. L. (1993). Elastic domains and polydomain phases in solids. *Phase Transitions* **45**, 1–33.
Sanchez, J. E., and Arzt, E. (1992). Effects of grain orientation on hillock formation and grain growth in aluminum films on silicon substrates. *Scr. Metall. Mater.* **27**, 285–290.
Sanchez, J. E., McKnelly, L. T., and Morris, J. W. (1992). Slit morphology of electromigration induced open circuit failures in finite line conductors. *J. Appl. Phys.* **72**, 3201–3203.
Seifert, A., Vojta, A., Speck, J. S., and Lange, F. F. (1996). Microstructural instability in single crystal thin films. Submitted for publication.
Shewmon, P. G. (1964). The movement of small inclusions in solids by a temperature gradient. *Trans. Am. Inst. Min. Eng.* **230**, 1134–1137.
Shingubara, S., and Nakasaki, Y. (1991). Electromigration in a single crystalline submicron width aluminum interconnection. *Appl. Phys. Lett.* **58**, 42–44.
Socrate, S., and Parks, D. M. (1993). Numerical determination of the elastic driving force for directional coarsening in Ni-superalloys. *Acta Metall. Mater.* **41**, 2185–2209.
Sofronis, P., and McMeeking, R. M. (1994). The effect of interface diffusion and slip on creep resistance of particulate composite materials. *Mech. Mater.* **18**, 55–68.
Spears, M. A., and Evans, A. G. (1982). Microstructure development during final/intermediate stage sintering—II. Grain and pore coarsening. *Acta Metall.* **30**, 1281–1289.
Spencer, B. J., Voorhees, P. W., and Davis, S. H. (1991). Morphological instability in epitaxially strained dislocation-free solid films. *Phys. Rev. Lett.* **67**, 3696–3699.
Srolovitz, D. J. (1989). On the stability of surfaces of stressed solids. *Acta Metall.* **37**, 621–625.
Srolovitz, D. J., and Safran, S. A. (1986). Capillary instabilities in thin films. *J. Appl. Phys.* **60**, 247–260.
Srolovitz, D. J., and Thompson, C. V. (1986). Beading instabilities in thin film lines with bamboo microstructures. *Thin Solid Films* **139**, 133–141.
Stevens, R. N., and Dutton, R. (1971). The propagation of Griffith cracks at high temperatures by mass transport processes. *Mater. Sci. Eng.* **8**, 220–234.
Sun, B., Suo, Z., and Evans, A. G. (1994). Emergence of crack by mass transport in elastic crystals stressed at high temperatures. *J. Mech. Phys. Solids* **42**, 1653–1677.
Sun, B., Suo, Z., and Cocks, A. C. F. (1996). A global analysis of structural evolution in a row of grains, *J. Mech. Phys. Solids* **44**, 559–581.
Sun, B., Suo, Z., and Yang. W. (1997). A finite element method for simulating interface motion, part 1: migration of phase and grain boundaries. *Acta Mater.* in press.
Suo, Z. (1994). Electromigration-induced dislocation climb and multiplication in conducting lines. *Acta Metall. Mater.* **42**, 3581–3588.
Suo, Z., and Wang, W. (1994). Diffusive void bifurcation in stressed solid. *J. Appl. Phys.* **76**, 3410–3421.
Suo, Z., Wang, W., and Yang, M. (1994). Electromigration instability: transgranular slits in interconnects. *Appl. Phys. Lett.* **64**, 1944–1946.
Suo, Z., Yu, H. (1997). Crack nucleation on elastic polycrystal surface in corrosive environment: low dimensional dynamic models. *Acta. Mater.* in press.
Svoboda, J., and Riedel, H. (1995). New solutions describing the formulation of interparticle necks in solid-state sintering. *Acta Metall. Mater.* **43**, 1–10.

Taylor, J. E., Cahn, J. W., and Handwerker, C. A. (1992). Geometric models of crystal growth. *Acta Metall. Mater.* **40**, 1443–1474.

Thompson, C. V., and Lloyd, J. R. (1993). Electromigration and IC interconnects. *MRS Bull.* **December 1993**, 19–25.

Thompson, C. V., Floro, J., and Smith, H. I. (1990). Epitaxial grain growth in thin metal films. *J. Appl. Phys.* **67**, 4099–4104.

Thouless, M. D. (1993). Effect of surface diffusion on the creep of thin films and sintered arrays of particles. *Acta Metall. Mater.* **41**, 1057–1064.

Tsoga, A., and Nikolopoulos, P. (1994). Groove angles and surface mass transport in polycrystalline alumina. *J. Am. Ceram. Soc.* **77**, 954–960.

Turnbull, D. (1956). Phase changes, *Solid State Phys.* **3**, 225–306.

Wang, W. Q., and Suo, Z. (1997). Shape change of a pore in a stressed solid via surface diffusion motivated by surface and elastic energy variation. *J. Mech. Phys. Solids.* in press.

Wang. W. Q., Suo, Z., and Hao, T.-H. (1996). A simulation of electromigration-induced transgranular slits. *J. Appl. Phys.* **79**, 2394–2403.

Wong, D., and Thouless, M. D. (1995). Effect of elastic relaxation on aspect ratios during island growth of isotropic films. Submitted for publication.

Yakobson, B. I. (1993). Stress-promoted interface diffusion as a precursor of fracture. *J. Chem. Phys.* **99**, 6923–6934.

Yang, W. H., and Srolovitz, D. J. (1993). Cracklike surface instabilities in stressed solids. *Phys. Rev. Lett.* **71**, 1593–1596.

Yang, W., and Suo, Z. (1996). Global view of microstructural evolution: Energetics, kinetics and dynamical systems. *Acta Mech. Sin.* **12**, 144–157.

Yang, W., Wang, W.-Q., and Suo, Z. (1994). Cavity and dislocation instability under electric current. *J. Mech. Phys. Solids* **42**, 897–911.

ADVANCES IN APPLIED MECHANICS, VOLUME 33

Strain Gradient Plasticity

N. A. FLECK

Engineering Department, Cambridge University
Cambridge, England

and

J. W. HUTCHINSON

Division of Applied Sciences, Harvard University
Cambridge, MA

I. Introduction 296

II. Survey of Strain Gradient Plasticity: Formulations and Phenomena . . . 301
A. Rotation Gradients: Couple Stress Theory 304
B. Rotation and Stretch Gradients: Toupin-Mindlin Theory 305
C. Phenomena Influenced by Plastic Strain Gradients 309

III. The Framework for Strain Gradient Theory 333
A. Toupin-Mindlin Theory 333
B. Connection with Couple Stress Theory 337
C. The Incompressible Limit 339

IV. Flow Theory 341
A. Summary of Elastic-Plastic Constitutive Relations 346
B. Minimum Principles 347

V. Single-Crystal Plasticity Theory 349
A. Kinematics 349
B. Stress Measures for Activating Slip 354

Appendix: J_2 Deformation Theory and Associated Minimum Principles 355

Acknowledgments 358

References 358

0065-2165/97 $25.00